On-line Monitoring and Oscillatory Stability Margin Prediction in Power Systems Based on System Identification

by

Hassan Ghasemi

A thesis

presented to the University of Waterloo

in fulfilment of the

thesis requirement for the degree of

Doctor of Philosophy

in

Electrical and Computer Engineering

Waterloo, Ontario, Canada, 2006

I hereby declare that I am the sole author of this thesis. This is a true copy of the thesis, including any required final revisions, as accepted by my examiners.

I understand that my thesis may be made electronically available to the public.

Abstract

Poorly damped electromechanical modes detection in a power system and corresponding stability margins prediction are very important in power system planning and operation, and can provide significant help to power system operators with preventing stability problems.

Stochastic subspace identification is proposed in this thesis as a technique to extract the critical mode(s) from the measured ambient noise without requiring artificial disturbances (e.g. a line outage), allowing these critical modes to be used as an on-line index, which is referred here to as System Identification Stability Indices (SISI) to predict the closest oscillatory instability. The SISI is not only independent of system models and truly representative of the actual system, but also computationally efficient. In addition, readily available signals in a power system and several identification methods are categorized, and merits and pitfalls of each one are addressed in this work.

The damping torque of linearized models of power systems is studied in this thesis as another possible on-line security index. This index is estimated by means of proper system identification techniques applied to both power system transient response and ambient noise. The damping torque index is shown to address some of drawbacks of the SISI.

This thesis also demonstrates the connection between the second order statistical properties, including confidence intervals, of the estimated electromechanical modes and the variance of model parameters. These analyses show that Monte-Carlo type of experiments or simulations can be avoided, hence resulting in a significant reduction in the number of samples.

In these types of studies, the models available in simulation packages are ex-

tremely important due to their unquestionable impact on modal analysis results. Hence, in this thesis, the validity of generator subtransient model and a typical STATCOM transient stability (TS) model are also investigated by means of system identification, illustrating that under certain conditions the STATCOM TS model can yield results that are too optimistic, which can lead to errors in power system planning and operation.

In addition to several small test systems used throughout this thesis, the feasibility of the proposed indices are tested on a realistic system with 14,000 buses, demonstrating their usefulness in practice.

Acknowledgments

I would like to express my sincere gratitude to Prof. Claudio A. Cañizares. I cannot say enough about his constant support, continuous encouragement and priceless guidance throughout my PhD study. In short, it was a great honor to work with him.

I am deeply indebted to Dr. Gordon Savage from System Design Engineering Department for fruitful, enlightening discussions. His remarkable skills and expertise were always beneficial to completing different parts of this thesis. Sincere thanks to Dr. Mehrdad Kazerani for providing technical support for parts of the research related to FACTS controllers. I will always remember the discussions and help of Dr. Hamid Sheikhzadeh on signal processing issues.

Warmest thanks to my colleagues in the Powerlab at the University of Waterloo: Mithulan, Sameh, Federico, Valery, Hong, Hamidreza, Warren, Rafael, Ismael, and Amirhossein.

The valuable remarks and suggestions from Powertech Labs' personnel is greatly appreciated. Special thanks to Dr. Prabha Kundur for providing an internship opportunity in Powertech Labs, which gave me great experience and a chance to meet wonderful people.

Very special thanks to my parents for their love and hardships during all years of my studies. The support and continuous encouragement of my brothers and sister are greatly acknowledged.

Last but not least, I would like to express my utmost thanks to my dear wife, Salimeh, for her unwavering support and truly pure love during sunny and cloudy days.

This thesis is dedicated to my wife and our lovely daughter, Hanyeh.

Contents

List of Figures

List of Tables

List of Terms

Acronyms:

ACF	:	Auto Correlation Function
AIC	:	Akaike Information Criterion
AR	:	Auto-Regressive
ARMA	:	Auto-Regressive Moving-Average
AVR	:	Automatic Voltage Regulator
COI	:	Center of Inertia
CPF	:	Continuation Power Flow
CVA	:	Canonical Variate Algorithm
DAE	:	Differential-Algebraic Equations
DLM	:	Dynamic Loading Margin
EVI	:	Eigenvalue Index
FACTS	:	Flexible AC Transmission Systems
FPE	:	Final Prediction Error
GLS	:	Generalized Least Square
HB	:	Hopf Bifurcation
IEEE	:	Institute of Electrical and Electronics Engineers
IV	:	Instrumental Variable
LIB	:	Limit-induced Bifurcation
LM	:	Linearized Model
LSMYW	:	Least Square Modified Yule-Walker
MA	:	Moving Average
MYW	:	Modified Yule-Walker
ODE	:	Ordinary Differential Equation

OLS	:	Ordinary Least Square
PEM	:	Prediction Error Method
PRBS	:	Pseudo-Random Binary Signal
PSAPAC	:	Power System Analysis Package
PSAT	:	Power Flow and Short-circuit Analysis Tool
PSS	:	Power System Stabilizer
PST	:	Power System Toolbox
PWM	:	Pulse Width Modulation
RFBW	:	Robust Fitting with Bisquare Weights
RHP	:	Right Half Plane
SLIB	:	Saddle-limit-induced Bifurcation
SLM	:	Static Loading Margin
SNB	:	Static-Node Bifurcation
SNR	:	Signal to Noise Ratio
SSAT	:	Small Signal Analysis Tool
SSSC	:	Static Synchronous Series Compensator
STATCOM	:	Static Synchronous Compensator
SVC	:	Static Var Compensator
SVD	:	Singular Value Decomposition
TCSC	:	Thyristor Controlled Series Compensator
TS	:	Transient Stability
TSAT	:	Transient Stability Assessment Tool
UWPFLOW	:	University of Waterloo Power Flow
VSC	:	Voltage Source Converter
WECC	:	Western Electricity Coordinating Council
WLS	:	Weighted Least Square

WSCC	:	Western System Coordinating Council
YW	:	Yule-Walker

Chapter 1

Introduction

1.1 Research Motivation

Power systems around the world are faced with challenging issues concerning overall system security, reliability and stability because of the unprecedented increase in electricity demand, lack of transmission expansion, and the fact that new power plants are not being built close to population centers because of environmental and economic constraints. Several major blackouts (e.g. August 2003 North-East blackout [2], September 2003 Italy blackout [3], September 2003 Sweden-Denmark blackout [4], August 1996 WSCC blackout [5]) are testimonies to these issues. Deregulation of electricity markets is further adding to this problem, since the main objective is to transfer power from generation surplus areas to generation deficit points, thus leading to increased transmission congestion problems.

Power system operators are constantly dealing with the challenge of operating their systems in a secure manner, while taking into account the uncertainty in demand and supply and the availability of enough security margins. Thus, off-line

system studies are performed to ensure the overall system security ahead of time. These studies are mainly classified into voltage stability analysis and angle stability analysis, based on short-, mid- and long-term stability studies. These off-line system studies are, however, based on power system models that are represented by differential-algebraic equations (DAEs). These DAE models are based on approximate system representation and data, since obtaining models and data for a system (e.g. system controllers) with several thousand buses is rather cumbersome. Therefore, during the last two decades, there has been a trend to use identification techniques based on the real-time response of the power system in order to analyze its behavior. Furthermore, these on-line tools and techniques can also provide useful information for system operators regarding readily available security margins, and can further assist operators in taking proper actions to avoid possible system problems.

This thesis studies various issues regarding on-line monitoring of oscillatory behavior of a power system, i.e. small-disturbance stability analysis, which are associated with phenomena that may lead to significant problems in power systems (e.g. the August 1996 WSCC blackout was mainly triggered by an oscillatory instability). In order to extract stability information from on-line measurements, several identification tools for different kinds of tests and signals are discussed and proposed. The possibility of predicting the corresponding stability margins using these system identification techniques is explored, as is the effect of using different system models on these oscillations.

1.2 Literature Review

Poorly damped electromechanical oscillations in power systems are related to lightly damped modes that arise from a number of factors, such as fast exciters, which are intended to enhance the synchronizing torque; long transmission lines; and improvements in the cooling system of turbo-alternators [6]. Upon a change in one of the system parameters such as loading level, these modes can become less damped, and eventually result in unstable oscillations, a phenomenon previously observed in power systems, with major consequences (e.g. August 1996 WSCC blackout [5]). In fact, being able to predict such problems would be extremely helpful in preventing them. Hence, there have been significant efforts in developing techniques to identify, predict and control these stability problems.

1.2.1 Stability Limit Prediction

In general, voltage collapse and oscillatory phenomena have been directly associated with bifurcation theory in nonlinear systems. Saddle-node bifurcations (SNB) and limit-induced bifurcations (LIB) have been directly related to voltage stability [7]. On the other hand, electromechanical oscillations have been associated with Hopf bifurcations (HB), which are important, as they restrain the transfer capacity of the system [8]. All these are, however, off-line methods, based on DAE models, and are consequently dependent on approximate data and models.

A fair amount of research work has been conducted to detect and predict the stability limits associated with voltage collapse [7, 9]. When voltage collapse is associated with an SNB, it may be predictable by monitoring the minimum singular value of the power flow Jacobian; however, these types of indices encounter discontinuities, and have a nonlinear profile. Therefore, these indices are usually

"linearized" by dividing them by their derivatives. In [10], a test function is also used in an existent performance index for detection of proximity to a static voltage collapse point; it is then compared with known singular values and eigenvalues indices, and with other previously proposed test functions, showing some advantages and disadvantages. On the other hand, LIBs cannot be detected by monitoring the minimum singular value or eigenvalue; hence, other approaches, such as the distance to generator Var limit as proposed in [9], have been proposed.

Some research has also been carried out on characterizing oscillatory behavior in power systems as well as its detection, prediction and control [11, 12, 13, 14, 15]. In [11], it is shown that a power system may experience either an SNB or an HB depending on the value of the causal parameter; however, an HB, if exists, occurs prior to an SNB. In [8], an HB index that employs the state matrix and critical eigenvalues is proposed; then another index, which does not require computing the state matrix, and hence is faster, is suggested. However, both indices rely on a DAE model of the system under study.

1.2.2 Electromechanical Mode Detection

Various techniques have been recently developed based on wide area measurements (WAM) to provide on-line information of poorly damped modes, to identify causal factors using sensitivity analysis, and to propose actions for real-time operation and off-line studies to alleviate the problematic system oscillations [16, 17, 18]. However, these tools are not designed to provide predictions of the available stability limits when loading or other system parameters change.

The Prony method, for instance, is a well-known system identification technique that has been widely used in power systems to determine modal content, develop

equivalent linear models of power systems, and tune controllers using system measurements [19, 20, 21, 22]. Compared with modal analysis, this method is a close duplicate; however, it needs a high signal-to-noise ratio (SNR) in order to get accurate results. Thus, it cannot be readily applied to the response of a normally operated power system since it needs "large enough" perturbations (e.g. line or generator outages), which are usually not available.

There are linear time-invariant models, such as auto-regressive (AR); auto-regressive moving-average (ARMA); and stochastic state-space, which is a transformed representation of an ARMA, that can be employed to analyze the measured response of power systems under normal operating conditions. In these models, the input is white noise, and it can be interpreted as random load switching during the day, assuming that the system does not change, and remains at its equilibrium point [23, 24]. ARMA models are more general than AR models, but they are computationally expensive, as they require the solving of an optimization problem and do not provide guaranteed global minima. Although it is possible to use an AR model by removing the moving average term of an ARMA, the system order needed to model the signal would be high. In [23], the parameters of an ARMA model is estimated by means of a Least Square Modified Yule-Walker (LSMYW) equation so as to avoid the optimization problem. However, the accuracy of the detected mode in this case would be somewhat compromised.

1.2.3 Modeling Effect on Stability Limits

DAE models are vital in power system analysis, as choosing models with different degrees of complexity would yield different results; for instance, stability limits have been shown to change significantly for the same system with different load models

[25, 26, 27, 28]. Generator and exciter modeling also plays a significant role in the dynamic studies of a power system [8, 29, 30].

Since a power system usually consists of several thousand buses and machines, its analysis requires handling of extremely large matrices. Therefore, simplified models such as power flow and transient stability (TS) models have been proposed to enhance computational efficiency (e.g. larger integration time step and smaller state matrix); these models are typically used in power system analysis packages instead of more detailed models. To the knowledge of the author, these models were validated by using only time-domain simulations and comparing their response with the ones obtained from more detailed models. For instance, the TS model proposed for all the Flexible AC Transmission Systems (FACTS) controllers in [1] was validated only by inspection of the time-domain simulation results. Thus, these TS models need also to be validated from the viewpoint of small-disturbance analysis and their accuracy in terms of their impact on the system modes. This requirement becomes important when FACTS controllers are used to enhance both large-disturbance and small-disturbance stability [15, 31]. For instance, additional damping for the electromechanical modes may be obtained by adding a supplementary control to the main control of a FACTS controller [8, 32]. It is important that TS models when utilized in a small-disturbance analysis program, yield appropriate information about the real system behavior.

System identification techniques are powerful tools that are used in this thesis to validate TS models from the abovementioned perspective. These tools can also be used to obtain transfer functions for tuning purposes [19, 20, 21].

1.3 Objectives

Based on the review of the state-of-the-art of the areas mentioned before, the following areas of interest will be researched in this thesis, concentrating mostly on the use of system identification tools for detecting and predicting oscillatory stability limits in a power system:

1. Propose a computationally efficient identification method to detect the electromechanical modes in a power system without requiring any major disturbances.

2. Develop a simple index for on-line applications that is independent of approximate models and data, based on the critical modes of the system.

3. Develop an index that does not require surveillance of specific, undetected critical modes.

4. Propose a technique to estimate the uncertainty of the calculated electromechanical modes to avoid Monte-Carlo type of simulations and experiments.

5. Validate TS models of major power system components, such as synchronous generator and FACTS controllers, by means of system identification.

1.4 Outline of the Thesis

This thesis is structured as follows: Chapter 2 presents a background on review of the main concepts on power system stability used here. It also describes the tools, models and test cases used throughout this thesis in order to demonstrate the feasibility of the proposed methods.

Chapter 3 discusses and categorizes the types of signals that can be readily measured in a power system, as well as corresponding techniques to extract the modal content of the signals. It also explains the merits and pitfalls of each technique.

Chapter 4 describes the development of a proposed stability index, which is based on the critical eigenvalues of a power system, used to predict the closest oscillatory instability point. The results for several test cases are presented, including those of a real system.

Chapter 5 discusses formulating the analytical representation of the damping torque, and proposes another index, which is based on the damping torque concept. Several test cases and dispatch scenarios are used to examine the feasibility of employing this index in practice.

Chapter 6 first presents a brief background on estimating the covariance of parameters and then it discusses the procedure to calculate the variance of the identified electromechanical modes by means of a technique that is employed to establish a connection between the variance of parameters and variance of modes.

In Chapter 7, the generator subtransient model is validated by comparing its time-domain simulation results with those obtained from the generator detailed model; system identification is employed to study the impact of using each model on the electromechanical modes. The TS model of a shunt FACTS controller known as STATCOM is also compared, from the small-disturbance analysis point of view, with its detailed model; the validity of the TS model with a supplementary control is then investigated.

Finally, Chapter 8 summarizes the main content and contributions of this thesis, and suggests directions for possible future research work.

Chapter 2

Background Review

2.1 Introduction

In this chapter, a general overview of models, power system stability analysis tools and techniques, and the test cases used throughout the thesis is presented. A discussion of the critical points one needs to take into consideration in different system studies, such as continuation power flow or small-disturbance stability analysis, is also presented here.

2.2 Modeling

Models for power system components have to be selected according to the purpose of the system study, and hence, one must be aware of what models in terms of accuracy and complexity should be used for a certain type of system studies, while keeping the computational burden as low as possible. Selecting improper models for power system components may lead to erroneous conclusions. For example,

the author in [8] studied the effect of using various load models on the system stability margin, showing that for some case studies, when only load models are changed, different stability margins in terms of MWs are obtained. In the following sections, the main elements of power systems, for the purpose of this thesis, are briefly discussed, and the corresponding models are reviewed.

2.2.1 Generators

Generators are important in system stability studies, and are modeled in dissimilar ways depending on the objective of the study. For instance, in a power flow study, a generator is modeled as a PV bus (defined as a bus with fixed voltage and power). For other complex analyses, such as small-disturbance stability, it may be required to use either generator subtransient or transient stability models that are represented by means of DAEs.

The per unit stator voltage equations for generator detailed model in dq reference frame are typically written as [33]:

$$\begin{aligned} e_d &= p\psi_d - \psi_q\omega_r - R_a i_d \\ e_q &= p\psi_q + \psi_d\omega_r - R_a i_q \end{aligned} \tag{2.1}$$

where e_d and e_q are the instantaneous stator phase voltages; p is the differential operator d/dt; i_d and i_q are the instantaneous stator phase currents; ψ_d and ψ_q are the flux linkages; ω_r is the rotor electrical speed; and R_a is the armature resistance per phase.

The two most common simplifications in obtaining generator stability models are: First, neglect the stator transients, which are represented by the $p\psi_d$ and $p\psi_d$ terms in 2.1; these terms are associated with network transients, which decay

rapidly. Second, neglect the effect of speed variations on stator voltages, i.e. $\omega_r = 1$ in 2.1. In addition to the abovementioned simplifications, other assumptions, such as balanced voltages with slowly varying phase and angle, yield generator stability models represented by differential equations with orders ranging from II (classical model) to VI (subtransient model) [34]. For instance, a generator subtransient model is obtained assuming two q-axis and one d-axis damper windings on the rotor, and $X_d'' = X_q''$, where X_d'' and X_q'' are subtransient reactances. On the other hand, a generator classical model is obtained by modeling the generator as a constant voltage source behind a reactance, and hence, only two differential equations are used to represent the electromechanical swing equations.

A generator is normally equipped with an exciter for primary voltage control and a governor for frequency control. Fast exciters are known to enhance generator synchronizing torque, but may deteriorate the damping [35], and hence, for some generators, a Power System Stabilizer (PSS) is installed to improve the damping. Several types of exciters, governors and PSSs are readily available (for more details, please refer to [33]), and are incorporated in most small-disturbance stability and transient stability analysis programs, such as the Power System Toolbox (PST) [36]. These models are not typically modeled in a power flow study; however, they have to be adequately represented in an eigenvalue analysis (small-disturbance analysis) or a transient stability analysis.

2.2.2 Loads

Load models are categorized as static and dynamic. Dynamic load models are more complicated, and are used mainly for transient stability analysis. On the other hand, static models are better suited for power flow and small-disturbance

stability analysis. The three main static load models are known as constant PQ (or MVA), constant current and constant impedance; all of them can be mathematically expressed by

$$P = P_0 \left(\frac{V}{V_0}\right)^a \tag{2.2}$$

$$Q = Q_0 \left(\frac{V}{V_0}\right)^b \tag{2.3}$$

$$\tag{2.4}$$

where P_0 and Q_0 are the active and reactive power consumed at voltage V_0, respectively. The type of the load model depends on exponents a and b, i.e. constant PQ for $a = b = 0$, constant current for $a = b = 1$, and constant impedance for $a = b = 2$.

2.2.3 Synchronous STATic COMpensator (STATCOM)

Shunt compensators are primarily used to regulate the voltage in a bus by providing or absorbing reactive power. They are also known to be effective in damping electromechanical oscillations [15, 31]. Different kinds of shunt compensators are currently being used in power systems, of which the most popular ones are Static Var Compensator (SVC) and Synchronous STATic COMpensator (STATCOM) [37]; however, in this research, only the STATCOM, which has a more complicated topology, is explained and studied. SVCs and STATCOMs are thyristor based and GTO based FACTS controllers, respectively. A thyristor has only turn-on capability, thus cannot be used in switch mode applications. Advanced devices such as Gate Turn-Off Thyristors (GTO) and Integrated Gate Bipolar Transistors (IGBT) have both turn-on and turn-off capabilities; hence, it is possible to use them in switched mode applications such as Voltage-Source Converters (VSC) in power

systems.

A VSC generates a synchronous voltage of fundamental frequency and controllable magnitude and phase angle. If a VSC is connected to a system via a coupling transformer as shown in Figure 2.1, the resulting STATCOM [37, 38, 39] can inject or absorb reactive power to or from the bus to which it is connected. The main advantage of a STATCOM over an SVC is its reduced size, which results from the elimination of ac capacitor banks and reactors. Moreover, a STATCOM response is 10 times faster than that of an SVC due to turn-on and turn-off control of the STATCOM.

The active and reactive power exchange between the VSC and the system are the function of the converter output voltage denoted as V_{out} in Figure 2.1, i.e.

$$P = \frac{V_{out}\, V}{X} \sin \alpha_{conv} \tag{2.5}$$

$$Q = \frac{V_{out}^2 - V_{out} V \cos \alpha_{conv}}{X} \tag{2.6}$$

where α_{conv} is the angle between the ac system voltage V and V_{out}.

Two control strategies may be used for a STATCOM; namely, Phase Control and PWM Control. In phase control, the DC bus voltage V_{dc} is regulated by changing α_{conv}, i.e. charging and discharging the DC capacitor, which ultimately controls V_{out}, as this voltage is proportional to V_{dc}; the block diagram of a phase control is shown in Figure 2.2. On the other hand, in the PWM control, both angle and magnitude of the converter output voltage are regulated as shown in Figure 2.3. Although less low frequency harmonics are produced by a STATCOM with a PWM control, the high switching losses due to the high switching frequency are the main constraints for its application in transmission systems.

The maximum and minimum operating points of a STATCOM are independent

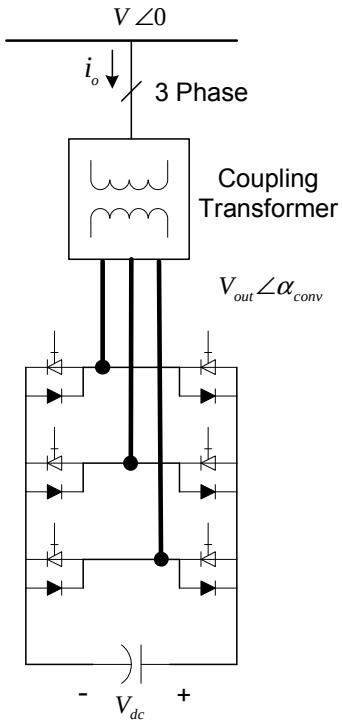

Figure 2.1: Basic structure of STATCOM.

from the system voltage as opposed to an SVC. The V-I characteristic of a STATCOM is limited only by the maximum voltage and current rating as depicted in Figure 2.4. This controller can be operated over its full output current range even at very low voltages (typically 0.2 p.u.).

STATCOM Transient Stability (TS) Model

For the case that the output voltage of the STATCOM is balanced and harmonic free, a TS model has been proposed, which does not include converter switching phenomena [1, 32]. The STATCOM TS model replaces the detailed model with a variable voltage source as shown in Figure 2.5, in which the magnitude of capacitor voltage is determined by a differential equation derived based on the power exchange

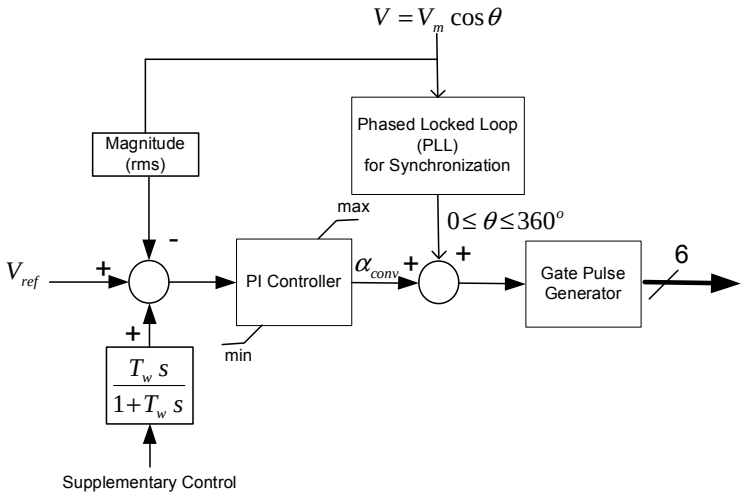

Figure 2.2: STATCOM control block diagram with phase control.

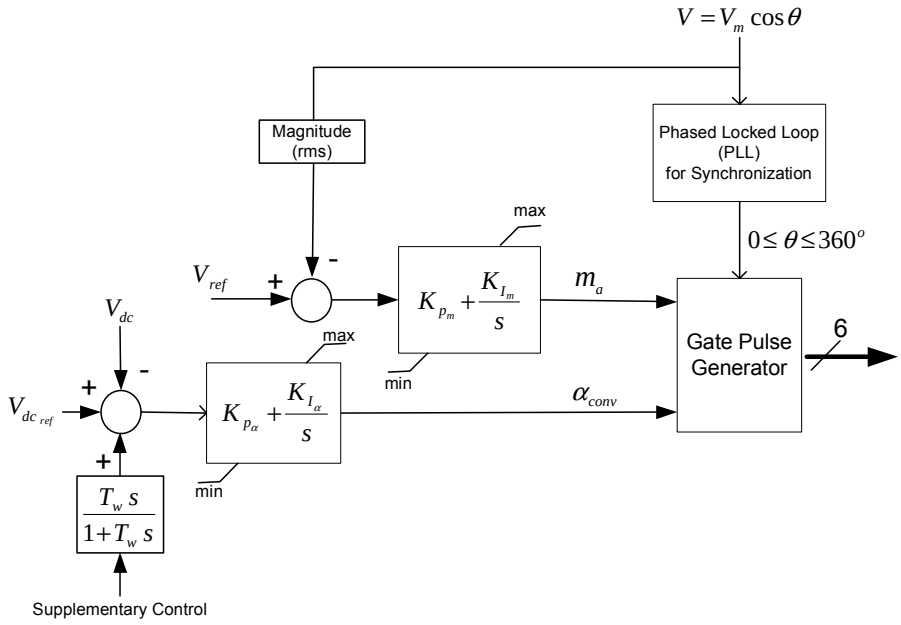

Figure 2.3: STATCOM control block diagram with PWM control.

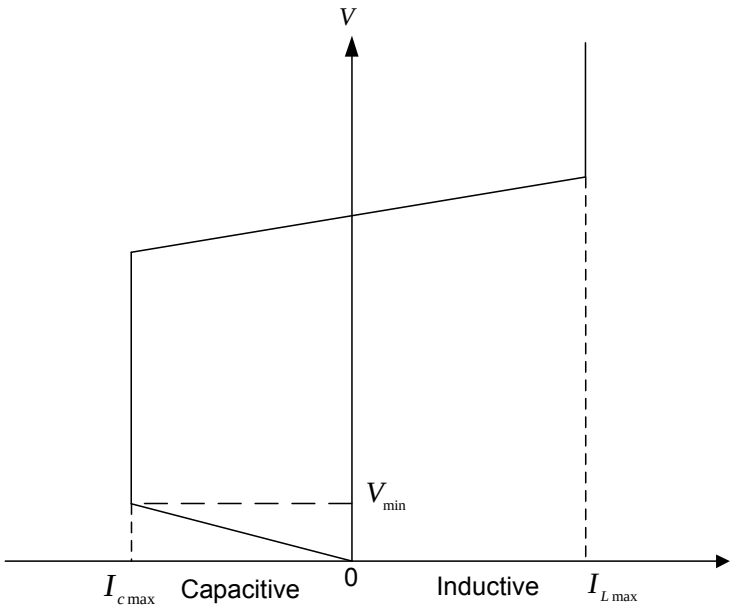

Figure 2.4: Voltage-Current characteristic of a STATCOM.

between the STATCOM and the network [1, 40]:

$$\frac{dV_{dc}}{dt} = \frac{3\ a\ k\ V}{CX}\ sin\ \alpha_{conv} - \frac{V_{dc}}{R_c\ C} \tag{2.7}$$

where a stands for the transformer ratio, and the resistance R_c represents the converter losses, which can be significant, depending on the number of switches and the switching frequency. All the blocks in Figure 2.5 are the same as the STATCOM detailed model in Figure 2.3, except that the converter and the blocks related to the switches are replaced by a voltage source $kV_{dc}\angle\theta$; the coefficient k is proportional to the modulation index m_a, which for a two-level inverter is $\frac{m_a}{2\sqrt{2}}$. It has been shown by means of time-domain simulation results that the TS model response is reasonably close to that obtained with the detailed model when the transients are small [1].

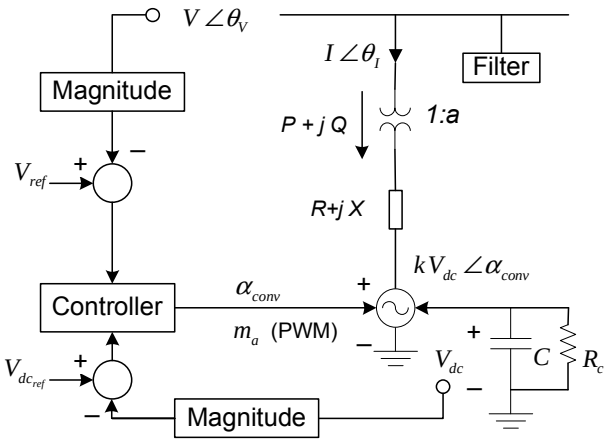

Figure 2.5: STATCOM transient stability model and its control [1].

2.3 Power System Stability

From the aforementioned models, a power system model can be represented using a DAE model, such as :

$$\begin{aligned} \dot{x} &= f(x,\ z,\ \lambda,\ \rho) \\ 0 &= g(x,\ z,\ \lambda,\ \rho) \\ y &= h(x,\ z,\ \lambda,\ \rho) \end{aligned} \tag{2.8}$$

where $x \in \Re^n$ is a vector of state variables that represents the state variables of generators, loads and other system controllers; $z \in \Re^m$ is a vector of steady state algebraic variables that result from neglecting fast dynamics in some load phasor voltage magnitudes and angles; $\lambda \in \Re^\ell$ is a set of uncontrollable parameters such as active and reactive power load variations; $\rho \in \Re^a$ is a set of controllable parameters such as tap or AVR set points; and $y \in \Re^l$ is a vector of output variables such as power through the lines and generator output power. The nonlinear functions $f : \Re^n \times \Re^m \times \Re^\ell \times \Re^a \mapsto \Re^n$, $g : \Re^n \times \Re^m \times \Re^\ell \times \Re^a \mapsto \Re^m$, and $h : \Re^n \times \Re^m \times$

$\Re^{\ell} \times \Re^{a} \mapsto \Re^{l}$ stand for the differential equations, algebraic constraints and output variable measurements, respectively.

The DAE model in (2.8) can be linearized about an operating point (x_o, z_o, λ_o, ρ_o) to obtain the system state matrix A:

$$A = D_x f \mid_o - D_z f \mid_o D_z g \mid_o^{-1} D_x g \mid_o \tag{2.9}$$

For slowly varying parameters λ, the power system model (2.8) has been shown to present local bifurcations, on which most stability indices in the current literature are based [41].

2.3.1 Voltage Stability

In a power system, voltage stability is directly related to the voltage on the system buses, and is defined as the power system ability to maintain steady acceptable voltages at all buses under normal operating conditions and after a contingency [33]. Thus, if the bus voltage magnitude decreases as the reactive power injection at the same bus increases, the power system is voltage unstable. This may lead to voltage collapse, if generators or other reactive power sources do not provide enough reactive power support. Voltage collapse can be explained within the context of bifurcation theories applied to DAEs in nonlinear systems, namely, SNB and LIB [7, 9].

Saddle-node Bifurcations (SNB)

When the system state matrix A has a simple and unique zero eigenvalue with nonzero left and right eigenvectors, the equilibrium point (x_o, z_o, λ_o, ρ_o) is typically

referred to as SNB point (other transversality conditions must also be met). In power systems, this bifurcation point is associated with voltage stability problems due to the local merger and disappearance of equilibria (operating points) as λ changes.

Limit-induced Bifurcations (LIB)

LIBs occur at an equilibrium point where the eigen-system of A undergoes a discrete change due to the fact that system states or algebraic variables reach a limit. There are various types of LIBs, of which a saddle LIB (SLIB) can be associated in power systems with voltage stability problems due to the local merger and disappearance of equilibrium points as λ changes.

2.3.2 Angle Stability

Angle stability is defined as the ability of interconnected synchronous machines to remain in synchronism [33]. In general, the angle instability may happen in the form of steady increase in rotor angle or undamped rotor oscillations; these phenomena are due to insufficient synchronizing torque and lack of damping torque, respectively. This thesis concentrates on the latter. These oscillations are due to poorly damped or undamped modes that are classified into local modes, inter-area modes, control modes, and torsional modes. Power system oscillations can be studied by Hopf bifurcation (HB) theory, which describes the onset of an oscillatory problem in nonlinear systems.

Hopf Bifurcations (HB)

In this case, two complex conjugate eigenvalues of A cross the imaginary axis as λ changes. This results in limit cycles that may lead to oscillatory instabilities, as it has been observed in practice [5, 42].

2.4 Tools

As explained before, power system stability analyses are classified into static and dynamic studies. In general, voltage stability analysis requires only static data, such as power flow data and dispatching scenarios, and is investigated by tracing P-V curves, which are obtained my means of continuation power flow techniques or optimal power flows. On the other hand, angle stability analyses require both static and dynamic data (e.g. exciter data), and hence are computationally more demanding when compared to voltage stability studies. An overview of all the utilized techniques and tools in this thesis follows.

2.4.1 Continuation Power Flow

For given dispatch scenarios, the continuation power flow [43] technique is used to obtain P-V curves similar to the one depicted in Figure 2.6, and thus determine the static loading margin (SLM) of the system (nose point) associated with a voltage collapse point, which could be the result of an SNB or an LIB. Figure 2.6 also demonstrates the dynamic loading margin (DLM) of a system, which is associated with an angle instability happening before the nose point.

All the P-V curves in this work have been obtained with the University of Waterloo Power Flow (UWPFLOW) program, which is computationally efficient,

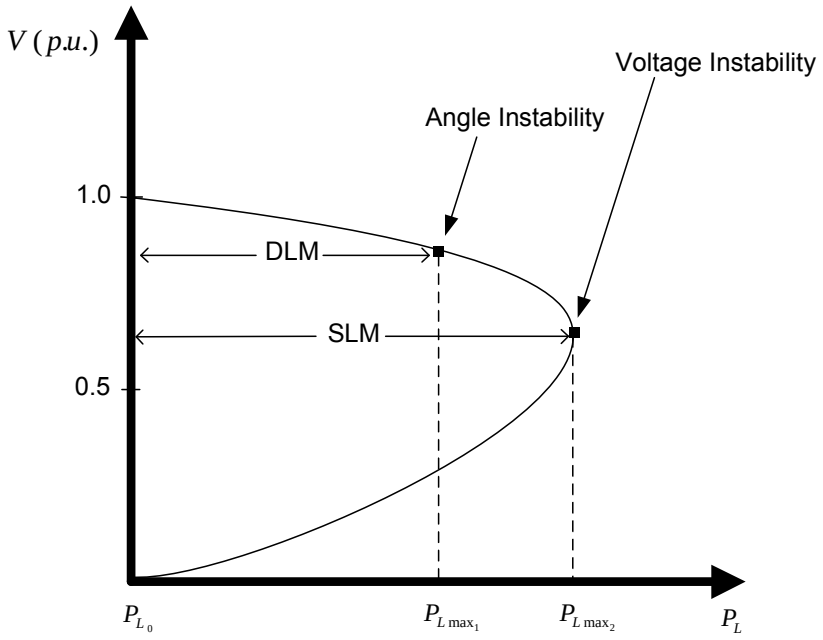

Figure 2.6: A typical PV curve and corresponding SLM and DLM.

as it has been developed in C and C++, and hence appropriate to study large systems. Furthermore, UWPFLOW provides other insightful information such the type of bifurcation and the corresponding right and left eigenvectors, plus power flow solutions and Jacobians.

2.4.2 Small-Disturbance Stability Analysis

As explained before, matrix A and its eigenvalues can provide valuable information about the system stability for small perturbations that may occur in the system. This is also referred to as small-disturbance stability analysis or eigenvalue analysis.

In this work, matrix A and its eigenvalues for the test cases have been obtained by means of the linearized transient stability models in the Power System Toolbox (PST) [36], which is a MATLAB based program. PST, when compared to

other programs, is user-friendly but slow, and hence inappropriate for large systems (more than 50 buses). Therefore, for large systems, the Small Signal Analysis Tool (SSAT) is used; as it is able to deal with systems made up of several thousand buses. It offers powerful features, such as complete eigenvalue analysis; Single-Machine-Infinite-Bus (SMIB) analysis; eigenvalue analysis within specified frequency and damping ranges; computation of modes closest to a specified frequency and damping; computation of modes related to a generator; sensitivity analysis; mode trace; etc.

2.4.3 Time-Domain Simulation

Time-domain simulation is mainly used for transient stability analysis of power systems following large perturbations, as it accounts for all the nonlinear effects by solving the complete set of DAEs by means of step-by-step trapezoidal or predictor-corrector integration [33]. However, in this thesis, this time-domain response of the power system is also used to obtain important small-disturbance stability information. Time-domain simulations of test cases were carried out by means of both the PST and the Transient Stability Analysis Tool (TSAT) [44]; however, the simulation of large systems was only feasible with the later. TSAT has two simulation engines: A conventional time-domain simulation engine that uses full numerical integration techniques and a fast time-domain simulation engine based on a quasi steady-state system model. It has several useful features for transient stability analysis, such as the possibility of running multi-contingency cases or multi-dispatch scenarios, obtaining a security index based on critical clearing time, etc. A wide range of dynamic models of power system components is available, and well-known formats, such as PTI PSS/E, GE PSLF, and BPA can be used as input data.

2.4.4 Identification

System identification is about building mathematical models of complex systems by using physical insights into the system and the measured input-output data. It is a useful tool, for a wide range of applications, including obtaining simplified models for large systems, model validation and controller tuning.

The advantage in studying power systems by means of system identification techniques is twofold: First, their studies take shorter time, when compared to analytical techniques that are based on DAE models of the power system, since the latter usually requires handling equations with several thousand states for a medium size power system; hence, identification techniques are of interest for on-line practical system monitoring. Second, these techniques rely on the actual response of the power system, as opposed to models that are based on approximate system representation and data.

Since the main objective of this research is to investigate the small-disturbance stability of the power system, linear parametric models have been used to study the indices proposed in this thesis. For the first proposed index, the prediction error method (PEM) and the stochastic subspace identification method are used to estimate the linear model parameters, and then use the model to extract the modal content of the time-domain response of the power system. For the second index, the PEM is used to estimate damping torque coefficients of individual generators, which in turn provides useful information about the current stability conditions and margins of the system under study.

The System Identification Toolbox [45] in MATLAB and ad-hoc coding are the basic tools used to perform these studies.

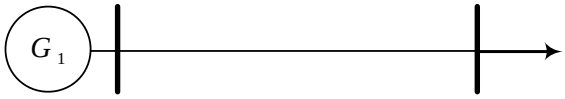

Figure 2.7: Single-Machine-Infinite-Bus (SMIB).

2.5 Test Systems

A variety of test cases, ranging from a Single-Machine-Infinite-Bus (SMIB) to a real power system with 14,000 buses, were used to test the feasibility of the proposed stability indices and system identification techniques. In some cases, several dispatch scenarios were considered in order to emulate the operation of a real power system. The general characteristics of these test cases are briefly reviewed in this section.

2.5.1 Single-Machine-Infinite-Bus (SMIB)

This is the simplest but the most widely used test case, as it consists of only a generator, a transmission line and a load as depicted in Figure 2.7. The load bus is modeled as an infinite bus, which is normally used to replace a stiff large system with a constant voltage magnitude and angle. This system can be used to investigate the behavior of a generator or group of generators, labeled as G_1 in Figure 2.7, with respect to the infinite bus.

2.5.2 IEEE 3-bus System

This corresponds to a case where two areas are connected through a long transmission line (weak connection); hence, power oscillations are observed in the tie-line.

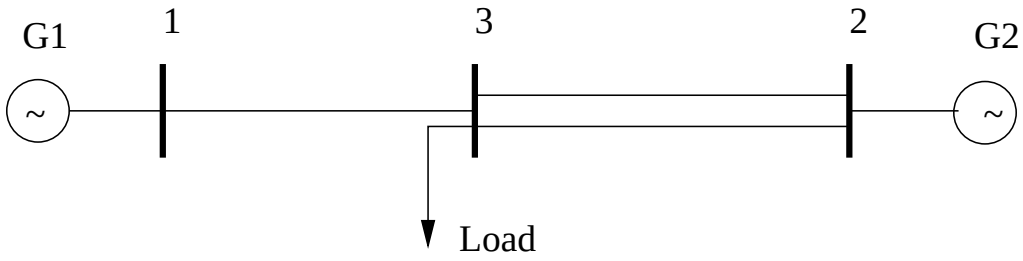

Figure 2.8: IEEE 3-bus test system.

A single-line diagram of the test system is shown in Figure 2.8 [8]. The base load used at Bus 3 is a 900 MW and 300 MVar load, and is modeled as a constant PQ. Each machine has a simple exciter, and a simple governor is used for the machine at Bus 1. The generators are modeled in detail by means of subtransient models. The corresponding static and dynamic data is presented in Appendix A.1.

2.5.3 IEEE 14-bus System

This test system is shown in Figure 2.9, and has 5 generators; two of them are providing both active and reactive power at Buses 1 and 2, and the generators at Buses 3, 6 and 8 are basically synchronous condensers [46]. The generators are modeled by means of subtransient models and equipped with DC exciters (type 1), and the loads are represented as constant impedances. The base total loading level of the system is 259 MW and 81.3 MVar. The corresponding static and dynamic data is presented in Appendix A.2.

2.5.4 Two-area Benchmark System

A single-line diagram of this system is shown in Figure 2.10 [33]. This is similar to the IEEE 3-bus test system in the sense that two areas are connected through

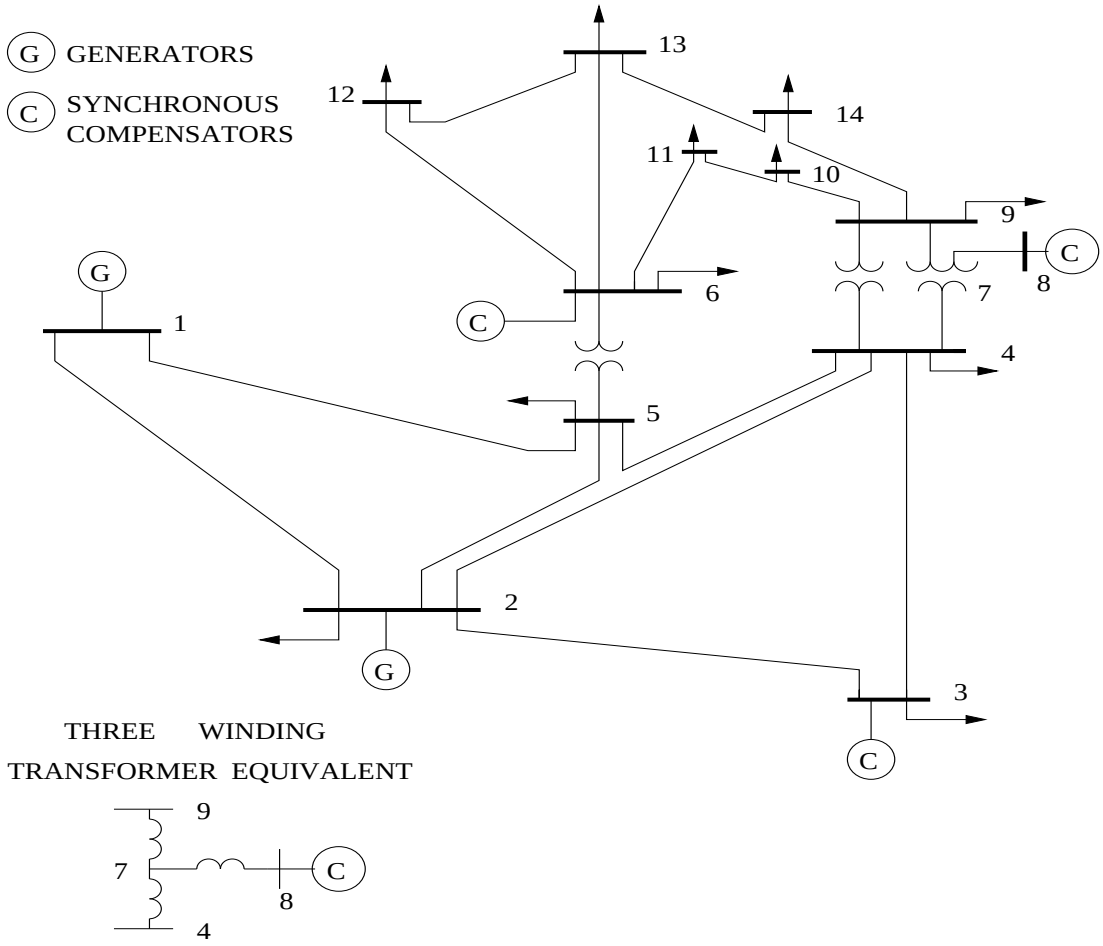

Figure 2.9: IEEE 14-bus test system.

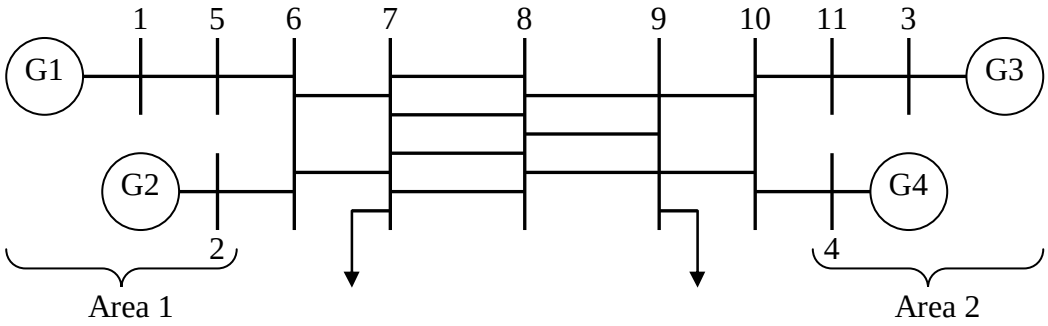

Figure 2.10: Two-area benchmark system.

tie-lines, hence resulting in an inter-area mode with a frequency of about 0.7 Hz. However, the individual machines in each area also contribute to a local mode in the same area with a frequency of about 1.3 Hz. Therefore, an inter-area rotor angle mode and two local modes are observed for this test case.

The generators were modeled using subtransient models and their exciters are simple exciters equipped with PSSs. The corresponding static and dynamic data is given in Appendix A.3. The total base loading level is 2734 MW and 200 MVar.

2.5.5 Real 14,000-bus System

This system consists of around 2,000 generators, 11,000 lines, 6,000 transformers, 22 areas and 6,500 loads (the details of the system are confidential); the total loading level of the system is 38.6 GW. Due to the extremely large size of the system, all the system studies such as power flow, continuation power flow, small-disturbance stability analysis, and time-domain simulations were carried on PSAT [47], VSAT [48], SSAT [49], and TSAT [44], respectively.

2.6 Summary

A brief explanation of some of the key power system components used in this thesis, such as loads and generators, is presented in this chapter. Also discussed in this chapter is the importance of selecting the right models for different kinds of analyses. Power system stability concepts and the analysis techniques and tools used throughout this thesis, such as voltage and angle stability, continuation power flow and system identification are briefly explained.

Chapter 3

System Identification Techniques

3.1 Introduction

Real-time signals measured in power systems represent the true response of these systems, as opposed to those obtained through simulation. These signals may be analyzed by means of signal processing techniques to obtain useful information, such as stability conditions, about the system. However, these techniques must be selected properly to ensure that the analysis results are both accurate and dependable. In order to capture the dynamic response of a power system, first it must be excited, a process that is based on either an external test (ringdown test), such as line/load tripping, or the existing random load switching happening throughout a day. A "proper" identification technique is then required to analyze the measurements.

This chapter discusses and categorizes the types of signals that can be readily measured in a power system, and the corresponding techniques used to extract the modal content of the signals. This modal content, in turn, provides useful informa-

tion about the system stability conditions. Depending on the kind of excitations that are present in the system, one can categorize the measured signals as deterministic ringdown data and stochastic ambient data. Thus, each type of data is explained here thoroughly, as are the corresponding appropriate techniques; the merits and disadvantages of the techniques are also discussed. A computationally efficient identification method is then proposed to overcome the shortcomings of previously used methods.

3.2 Ringdown Data

A power system may be excited by large perturbations (e.g. adding/removing large loads, generator tripping, severe short circuits), resulting in a transient response that can be easily observed and distinguished from ambient noise. These transients usually consist of one or several damped sinusoidal signals. Many techniques can be deployed to extract the modal content of these transients. Linear techniques are based mainly on the Prony method [50] and the Matrix Pencil method [51]. The Prony method is explained below, since it has been widely used in power systems in order to extract modal content and tune power system controllers such as power system stabilizers (PSSs) [21, 52, 53, 54].

3.2.1 Prony Method

The Prony method, proposed in 1795 by Gaspard Riche, Baron de Prony, is a viable technique to model a linear sum of damped exponentials. It was first used to explain the laws governing the expansion of various gases, and is closely related to the least square linear prediction algorithms used for AR parameter estimation. However,

the Prony method is used to fit a deterministic exponential model to evenly sampled data, as opposed to the AR and ARMA methods, which are based on a random model. Several versions of the original Prony method, such as the total least square Prony method and the singular value decomposition (SVD) Prony method, have improved its performance.

A measured signal $y(t)$ can be represented in continuous and discrete time, respectively, as a sum of n damped complex sinusoids:

$$y(t) \;=\; \sum_{i=1}^{n} \bar{R}_i \, e^{\lambda_i t} = \sum_{i=1}^{n/2} A_i \, e^{\alpha_i t} \, cos(\beta_i t + \phi_i) \tag{3.1}$$

$$y[k] \;=\; \sum_{i=1}^{n} \bar{R}_i \, Z_i^k \tag{3.2}$$

where $\bar{R}_i$ is an output residue corresponding to the mode $\lambda_i = \alpha_i + j\beta_i$; $Z_i = e^{\lambda_i T_s}$; T_s is the sampling time; $A_i = 2\left|\bar{R}_i\right|$; and k is integer time.

The original Prony method calculates λ_i and $\bar{R}_i$ as follows:

1. Consider that (3.1) is the solution to a difference equation with order n:

$$y[k] = -a_1 \, y[k-1] - a_2 \, y[k-2] - \ldots - a_n \, y[k-n] \tag{3.3}$$

This can be written in a matrix form:

$$Y \;=\; D \, \theta \tag{3.4}$$

where

$$Y = [y_{k+n} \; y_{k+n+1} \; y_{k+n+2} \; \cdots \; y_{k+N}]^T_{N-n+1} \tag{3.5}$$

$$\theta = [-a_1 \; -a_2 \; \ldots \; -a_n]^T \tag{3.6}$$

$$D = \begin{bmatrix} y_{k+n-1} & y_{k+n-2} & \cdots & y_k \\ y_{k+n} & y_{k+n-1} & \cdots & y_{k+1} \\ \vdots & & & \\ y_{k+N-1} & y_{k+N-2} & \cdots & y_{k+N-n} \end{bmatrix}_{(N-n+1)\times n} \tag{3.7}$$

where N is the number of samples. The least square method can be used to compute θ.

2. The vector θ leads to the eigenvalues $Z_i's$ of the system, which are the roots of the system characteristic equation:

$$Z^n + a_1 Z^{n-1} + a_2 Z^{n-2} + \ldots + a_n = 0 \tag{3.8}$$

3. One may write (3.2) in a matrix form similar to (3.4) using the calculated Z_i's, and solve for the residues $\bar{R}_i$'s.

The order of the system n is usually unknown. In [20], the "rule-of-thumb" of an initial guess for $n = N/6$ is proposed. Once the roots of the system characteristic equation are obtained, the poles corresponding to high frequencies, which are known not to be present in power systems, are discarded. This technique, however, may lead to results that depend heavily on the user. Furthermore, order underestimation results in inaccurate results; on the other hand, higher orders lead to accurate poles estimation as well as extraneous poles, since the model seeks to fit the noise corrupting the signal.

A better technique for choosing n is proposed in [55] for communication systems. This method is based on monitoring the singular values of matrix D for $n = N/2$. Although the maximum possible order, which can be chosen for the system, is $N/2$, the practical order of a matrix is equal to the number of its largest singular values. Thus, for $\sigma_1 \geq \sigma_2 \geq \ldots \geq \sigma_n \geq \ldots \geq \sigma_{N/2}$, if $\sigma_{n+1} \approx \sigma_{n+2} \approx ... \approx \sigma_{N/2} \approx 0$, then $n < N/2$ is the order of the matrix D.

When SNR is low, the Prony method is known to behave poorly, and yields biased and sensitive results since (3.3) no longer holds [56]. Its performance and problems in the presence of noise have been investigated in [57]. In this paper, the Prony method is shown to be unable to extract the true poles of the signal if the SNR is below a certain level; however, this level is higher for signals containing more modes. For instance, in the case of a single mode comprising the entire signal, a minimum SNR in the range of 10 to 20 db is required. Furthermore, it is mentioned that the real part of the mode is more sensitive to noise than its frequency. Hence, the Prony method is recommended as an appropriate tool to analyze the measured transient response of power systems with large disturbances, such as major contingencies or artificially added and removed loads, i.e. ringdown test.

3.3 Ambient Data

The load switching throughout the day, which is random in nature, are persistently exciting the power system. Hence, the response of the power system contains information about the dynamic behavior of the system, and it can be employed for on-line system stability monitoring. However, these perturbations normally appear as noise with very small magnitudes on ambient data, and therefore, cannot be easily distinguished from measurement noise. Due to the randomness of the perturbations, in order to model the measured signals, a stochastic framework has to be employed. Well-known linear models such as AR or ARMA have been used for this purpose; the underlying assumption in this case is that the system input is noise and so is the output. The input noise is assumed to be white in the frequency range of interest (0.1 Hz - 2 Hz). The output signal, however, would be a colored

noise, since its power spectrum density (PSD) is proportional to the system transfer function, i.e.

$$S_{output}(f) = |G_s(f)|^2 S_{input}(f) \tag{3.9}$$

where $G_s(f)$ is the system transfer function, f is the frequency, and $S_{input}(f)$ is the input signal PSD, which is assumed to be flat in the frequency range of interest. Thus, output signal in this case can provide insightful information about the system transfer function. The PSD of a discrete signal such as $x[k]$ is the Fourier transform of its autocorrelation function (ACF) $r_{xx}[k]$, which is defined as:

$$r_{xx}[\tau] = E\left[x^*[k]x[k+\tau]\right] \tag{3.10}$$

where τ is the lag time between the two samples, and E denotes the expectation operator. In this work, it is assumed that the process is wide-sense stationary. That is, the mean and the ACF do not depend on time, i.e. the ACF in (3.10) only depends on the lag time τ.

3.3.1 ARMA Model

The power system linearized model may be represented as a time series or a rational transfer function. That is, the output $y[k]$ and input noise $e[k]$, which represents the load switching throughout the day, are related in a linear difference form,

$$y[k] = -\sum_{i=1}^{p} a_i\, y[k-i] \; + \; \sum_{i=0}^{d} b_i\, e[k-i] \tag{3.11}$$

where a_i's and b_i's represent the coefficients related to the AR and MA terms, respectively, and p and d denote the order of the AR and MA terms, respectively. This is known as an ARMA(p,d) model. It is important to mention that the input noise or process noise is different from the measurement or observation noise.

The system transfer function $G_s(q)$ between the output and the input is defined as:

$$\begin{aligned} G_s(q) &= \frac{B(q)}{A(q)} \\ A(q) &= \sum_{i=0}^{p} a_i \, q^{-i} \,, \qquad a_0 = 1 \\ B(q) &= \sum_{i=0}^{d} b_i \, q^{-i} \end{aligned} \tag{3.12}$$

where q is the shifting operator defined by $q^{-1}y[k] = y[k-1]$. The roots of polynomial $A(q)$ yield the poles of the system. Thus, from (3.9), the relationship between the input and the output PSDs is,

$$S_y(f) \;=\; \sigma^2 \; \left| \frac{B(f)}{A(f)} \right|^2 \tag{3.13}$$

$e[k]$ is assumed to be white noise with variance σ^2.

The ARMA(p,d) is a strictly autoregressive model AR(p) if all b_k except b_0 vanish, and a strictly moving average model MA(d) if all a_k except a_0 are zero.

According to the Wold decomposition theorem and the Kolmogorov theorem [56], any ARMA or AR process can be represented by a unique MA process of infinite order and vice versa. This is important since, if one fails to choose a correct model structure and a right order for a system, it would still be possible to obtain a reasonable approximation by choosing an order higher than the true order.

3.3.2 Parameter Estimation

There are different approaches to estimating the parameters of any structure such as an ARMA model and a state-space model associated with the power system. They

mainly fall into the three following categories: Prediction error methods (PEM), correlation methods and subspace methods; each one providing potential gains as well as potential pitfalls. Each method is described briefly below [58, 59]:

- *Prediction Error Methods:* These methods are basically based on performing an optimization routine to obtain the unknown parameters θ. For instance, for the ARMA(p,d) model described in (3.11), $\theta = [a_1 \ ... \ a_p \ b_1 \ ... \ b_d]^T$ may be computed by minimizing an objective function such as

$$\begin{aligned} Min \quad V(\theta) &= \frac{1}{N}\sum_{k=1}^{N}\frac{1}{2}\epsilon^2[k] \\ s.t. \quad \epsilon[k] &= y[k] - \hat{y}[k] \end{aligned} \tag{3.14}$$

  where $\epsilon[k]$ is the prediction error and $\hat{y}[k]$ is the one-step-ahead prediction of $y[k]$, and can be mathematically expressed as

$$\hat{y}[k] = \left[1 - \left(\frac{B(q)}{A(q)}\right)^{-1}\right] y[k] \tag{3.15}$$

  This requires an iterative search for θ that yields the minimum of loss function $V(\theta)$. The optimization is a nonlinear optimization, and thus may lead to local minima as well as high computational burden. In this work, however, only the coefficients of polynomial $A(q)$ are of interest, since it is aimed at extracting the modal content of the signal, which are the roots of $A(q)$. Hence, one may consider applying other techniques such as the Yule-Walker (YW) method that only estimates the parameters of $A(q)$, thus employing more simplified and robust numerical techniques. It is also possible to model $y[k]$ in (3.11) with a high-order AR rather than using an ARMA as a result of Kolmogorov theorem. This leads to an objective function that can be solved by means of well-known least square method; thus, the least square used for an AR model

would be identical to that of the Prony method. A high-order AR, however, leads to extraneous poles close to the system poles, which could be difficult to distinguish between the true and extraneous modes. Furthermore, an AR model may result in biased estimates if residuals are not white. As previously mentioned for the Prony method, when the SNR is low, the model structure is an ARMA rather than a pure AR.

- *Correlation Methods:* The fundamental idea behind correlation methods is that, for a good model, the prediction error at time k should be independent of past data up to time $k-1$, i.e. if the errors are correlated with past data, then there was more information available in past data about $y[k]$ than picked by $\hat{y}[k]$. Normally, similar to the PEM, correlation methods require an iterative search technique to solve a nonlinear equation. However, Instrumental variable (IV) methods as an application of the correlation methods result in a linear regression. A special case of IV methods are shown to be the YW method [60] (a set of linear equations that can be solved by means of fast and efficient algorithms such as Levinson's). More details about the fundamentals of the original YW method and, different versions of YW such as modified YW (MYW) and least square modified YW (LSMYW) are presented in Section 3.3.3.

- *Subspace Methods:* Subspace methods have become popular because of their numerical simplicity, robustness of the techniques that are used in the algorithms, and their state-space form which is convenient for control purposes [61]. However, subspace methods are suboptimal, as they are not based on the minimization of a criterion. Some of the main advantages of these methods over previously mentioned identification methods are:

1. *Model order selection*: For PEM, different criteria have been proposed in order to select the best order of the model, such as Akaike Information Criterion (AIC) and Final Prediction Error (FPE) [58]. These techniques are defined based on prediction error variance. For instance, to choose the orders p and d of an ARMA(p,d) model, first a range is selected for p and d, then, for each (p,d) pair, the parameters of the model are estimated; the pair obtaining the lowest value of AIC or FPE criterion is selected as the best estimate of the model order. This approach results in high computational costs since, in order to obtain the prediction error variance, all the possible models in the selected range have to be first estimated. On the other hand, in subspace methods, there is the possibility to estimate the model order without having to estimate the parameters of a variety of different models. Order estimation in this case is one step of the algorithm, and only requires a SVD.
2. *Handling large data*: When the amounts of data are large, order selection with PEM based techniques is just not feasible [62]. This is the case of the application being considered in this thesis, which requires long "blocks" of data in order to truly estimate the power system mode(s).
3. *On-line application*: If for any reason, the system dynamics change, the model needs to be updated. The subspace methods are a better choice in this case, due to the superiority of subspace over other methods from a computational point of view [62].

The state-space matrices are identified in this case by using measured outputs and robust numerical techniques such as QR-factorization, least square and SVD without the need to calculate correlations, i.e. it is data driven instead of covariance driven. Therefore, these types of techniques are computationally

more efficient.

3.3.3 AR Parameter Estimation

Several approaches can be utilized to estimate the parameters of the coefficients of the polynomial $A(q)$ in an AR or ARMA model. They all result in a set of linear equations that relates the parameters with the help of the ACF. The basic YW equation is explained, and the variations of YW to overcome its shortcomings are then presented.

Yule - Walker (YW)

For a strictly AR process, equations (3.11) is rewritten as:

$$y[k] = -\sum_{i=1}^{p} a_i \, y[k-i] + b_0 \, e[k] \tag{3.16}$$

Multiplying both sides of (3.16) by $y[k-j]$ and taking the expectation yields:

$$r_{yy}[j] = \begin{cases} -\sum\limits_{i=1}^{p} a_i \quad r_{yy}[j-i] & \text{for} \quad j \geq 1 \\ \\ -\sum\limits_{i=1}^{p} a_i \quad r_{yy}[-i] \; + \; b_0 \, \sigma^2 & \text{for} \quad j = 0 \end{cases} \tag{3.17}$$

This equation is known as YW equation, and defines a relationship between the ACF and parameters of an AR(p) process. By solving the following set of linear equations, one can determine the parameters of an AR(p):

$$\underbrace{\begin{bmatrix} r_{yy}[0] & r_{yy}[-1] & \cdots & r_{yy}[-(p-1)] \\ r_{yy}[1] & r_{yy}[0] & \cdots & r_{yy}[-(p-2)] \\ \vdots & \vdots & \ddots & \vdots \\ r_{yy}[p-1] & r_{yy}[p-2] & \cdots & r_{yy}[0] \end{bmatrix}}_{R_{yy}} \begin{bmatrix} a_1 \\ a_2 \\ \vdots \\ a_p \end{bmatrix} = - \begin{bmatrix} r_{yy}[1] \\ r_{yy}[2] \\ \vdots \\ r_{yy}[p] \end{bmatrix} \tag{3.18}$$

The autocorrelation matrix R_{yy} is hermitant ($R_{yy}^H = R_{yy}$), and Toeplitz since the diagonal elements (top-left to lower-right) are the same. The model in this case yields stable poles [56]. Equation (3.18) may be solved by means of an efficient algorithm such as Levinson's, and it depends on the ACF. A reasonable approximation is to calculate the elements of R_{yy} from the limited available data.

Modified Yule - Walker (MYW)

A similar procedure previously used to derive the YW equation can be applied to an ARMA(p,d) model, leading to the following set of linear equations:

$$\underbrace{\begin{bmatrix} r_{yy}[d] & r_{yy}[d-1] & \cdots & r_{yy}[d-p+1] \\ r_{yy}[d+1] & r_{yy}[d] & \cdots & r_{yy}[d-p+2] \\ \vdots & \vdots & \ddots & \vdots \\ r_{yy}[d+p-1] & r_{yy}[d+p-2] & \cdots & r_{yy}[d] \end{bmatrix}}_{R'_{yy}} \begin{bmatrix} a_1 \\ a_2 \\ \vdots \\ a_p \end{bmatrix} = - \begin{bmatrix} r_{yy}[d+1] \\ r_{yy}[d+2] \\ \vdots \\ r_{yy}[d+p] \end{bmatrix} \tag{3.19}$$

The matrix R'_{yy} is Toeplitz, although not hermitant. Hence, the stability of the poles of $A(q)$ is not guaranteed [56].

Least Square Modified Yule - Walker (LSMYW)

Equation (3.19) could also be rewritten as:

$$r_{yy}[k] = -\sum_{i=1}^{p} a_i \, r_{yy}[k-i] \quad \text{for} \quad k \geq q+1 \tag{3.20}$$

Since there is information in the ACF with higher order lags, it is also possible to calculate the a_i's by incorporating these ACFs. Thus:

$$\underbrace{\begin{bmatrix} r_{yy}[d] & r_{yy}[d-1] & \cdots & r_{yy}[d-p+1] \\ r_{yy}[d+1] & r_{yy}[d] & \cdots & r_{yy}[d-p+2] \\ \vdots & \vdots & \ddots & \vdots \\ r_{yy}[M-1] & r_{yy}[M-2] & \cdots & r_{yy}[M-p] \end{bmatrix}}_{R''_{yy}} \begin{bmatrix} a_1 \\ a_2 \\ \vdots \\ a_p \end{bmatrix} = - \begin{bmatrix} r_{yy}[d+1] \\ r_{yy}[d+2] \\ \vdots \\ r_{yy}[M] \end{bmatrix} \tag{3.21}$$

In this case, $M - d \geq p$ and $R^{''} \in \Re^{(M-d)\times p}$ is a nonsquare matrix, as opposed to $R^{'} \in \Re^{p\times p}$; hence, the least square method has to be employed to calculate the a_i's.

It is stated in [56] that for large data records, the estimates obtained by solving LSMYW equations are asymptotically unbiased, and that its variance decreases as the number of equations $(M - d)$ increases, as long as $N \gg M - d$. In general, LSMYW offers better performance compared to MYW if the number of equations is not too large. As reported in [56], LSMYW yields the most accurate estimates when the poles are near the unit circle. This is usually the case in a power system with poorly damped oscillations, as the corresponding poorly damped modes are the ones with damping ratios less than 3%, i.e. the power system controllers (e.g. PSS) are well-tuned if the modes attain a minimum damping ratio of 3%.

Comparison

The previously explained YW method and its variations are compared here with the PEM based on estimating the parameters of an AR(10) or ARMA(10,5) for detection of an electromechanical mode. A two-minute recorded power signal P_{G_2} in the two-area benchmark system is used as the system output $y[k]$ (for more details regarding the test system, please refer to Chapter 2). The input is simulated as

random load switching, and 20 simulations with independent realizations of the noise yield the results depicted in Figure 3.1. The order of the system is selected to be 10 for the YW method. On the other hand, an ARMA(10,5) is assumed for both MYW and LSMYW methods, but the number of linear equations in (3.19) and (3.21) are different, i.e. 10 and 15, respectively. Observe that the YW method does the poorest job in estimating the electromechanical mode with a high variance, while providing stable poles, as mentioned in Section 3.3.3. However, some of poles estimated with the MYW and the LSMYW methods are unstable. The LSMYW performance is better than both the YW and the MYW methods, and comparable to the PEM results in terms of accuracy and variance. On the other hand, the long computational times needed by the optimization routine required in the PEM, and the associated numerical problems are drawbacks of using the PEM.

3.3.4 Stochastic Subspace Identification

Consider the discrete stochastic state-space model:

$$\begin{aligned} \Delta x[k+1] &= A_d\, \Delta x[k] + w[k], \quad A_d = e^{A\, T_s} \\ \Delta y[k] &= C\, \Delta x[k] + v[k] \end{aligned} \tag{3.22}$$

where $\Delta x[k+1]$ is the discrete time state vector; $w[k]$ and $v[k]$ are zero mean noise $E[w[k]] = E[v[k]] = 0$ representing the process noise and the measurement noise, respectively, and are independent from $\Delta x[k]$, i.e. $E[\Delta x[k].w^T[k]] = 0$, $E[\Delta x[k].v^T[k]] = 0$; and A and A_d denote the continuous and discrete time state matrices, respectively. The output measurements are put into a block Hankel ma-

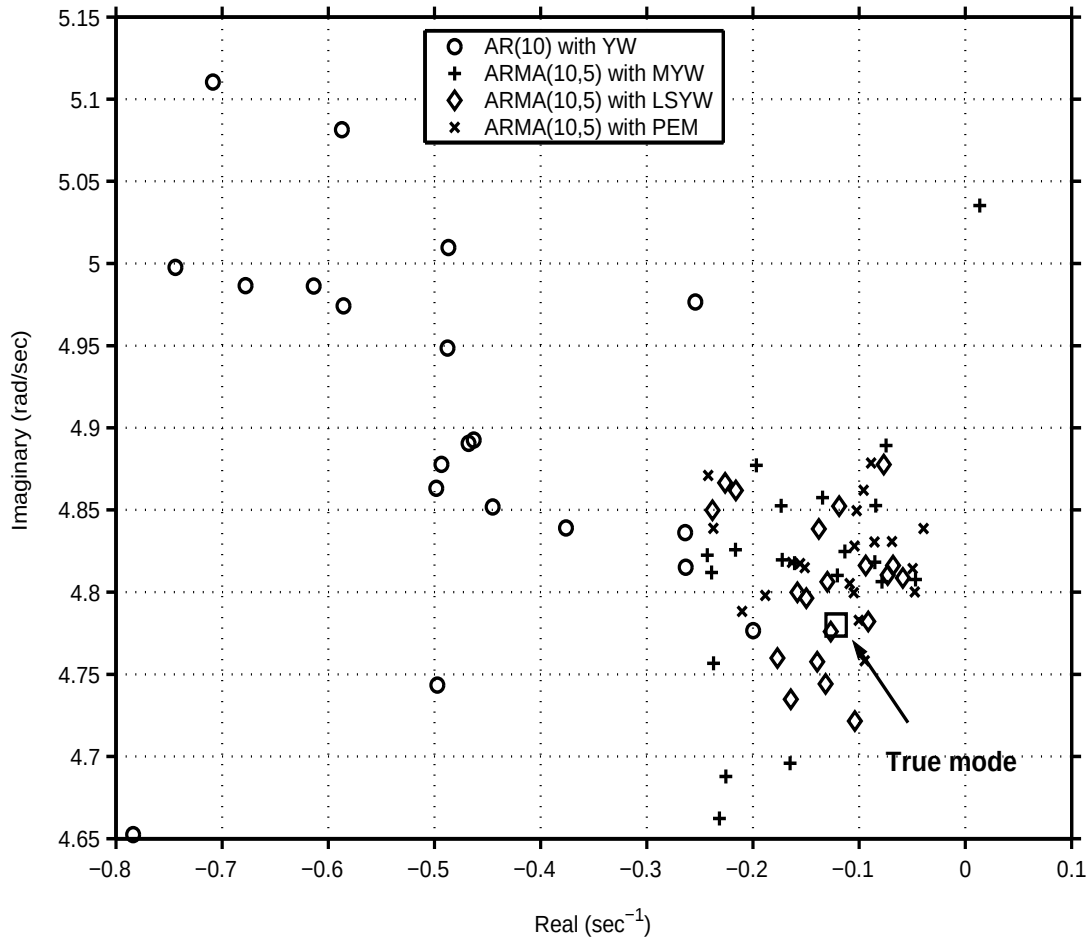

Figure 3.1: The performance of YW, MYW, LSMYW, and PEM in electromechanical mode estimation from ambient data.

trix, and divided into a past and future parts as follows:

$$
\begin{aligned}
Y_{0|2i-1} &= \left(\begin{array}{cccc}
\Delta y[0] & \Delta y[1] & \dots & \Delta y[j-1] \\
\Delta y[1] & \Delta y[2] & \dots & \Delta y[j] \\
\dots & \dots & \dots & \dots \\
\Delta y[i-1] & \Delta y[i] & \dots & \Delta y[i+j-2] \\
\hline
\Delta y[i] & \Delta y[i+1] & \dots & \Delta y[i+j-1] \\
\Delta y[i+1] & \Delta y[i+2] & \dots & \Delta y[i+j] \\
\dots & \dots & \dots & \dots \\
\Delta y[2i-1] & \Delta y[2i] & \dots & \Delta y[2i+j-2]
\end{array}\right) \\
&= \left(\frac{Y_{0|i-1}}{Y_{i|2i-1}}\right) = \frac{Y_p}{Y_f}
\end{aligned}
\tag{3.23}
$$

where i is typically equal to $2M/l$ [61], with M representing the "expected" maximal order of the system, and j is the number of samples of each measured output signal. The subscripts of $Y_{0|2i-1}$, $Y_{0|i-1}$ and $Y_{i|2i-1}$ are the first and last element in the first column of the block Hankel matrix. Matrices Y_p^+ and Y_f^- are defined by shifting the border between past and future data one row down in (3.23), i.e. $Y_p^+ = Y_{0|i}$, and $Y_f^- = Y_{i+1|2i-1}$.

There are different algorithms to calculate the system matrices A_d and C. The canonical variate algorithm (CVA) is used here as explained below.

Canonical Variate Algorithm [61]

Once the block Hankel matrix and its submatrices are formed, the following steps are taken:

1. Calculate the projection matrices $\mathcal{O}_i$ and $\mathcal{O}_{i-1}$:

$$\mathcal{O}_i = Y_f/Y_p \tag{3.24}$$

$$\mathcal{O}_{i-1} = Y_f^-/Y_p^+ \tag{3.25}$$

where Y_f/Y_p denotes a shorthand for the projection of the row space of the future matrix Y_f on the row space of past matrix Y_p, i.e. $Y_f Y_p^T (Y_p Y_p^T)^\dagger Y_p$ where the symbol † denotes the pseudo inverse of the matrix. Robust QR-factorization methods may be used to calculate the projection matrices.

2. Calculate the SVD of the weighted projection:

$$\begin{aligned} W_1 \mathcal{O}_i W_2 &= USV^T \\ &= (U_1 \;\; U_2) \begin{pmatrix} S_1 & 0 \\ 0 & 0 \end{pmatrix} \begin{pmatrix} V_1^T \\ V_2^T \end{pmatrix} \end{aligned} \tag{3.26}$$

where weighting matrices $W_1 = \left(\frac{1}{j} Y_f Y_f^T\right)^{-\frac{1}{2}}$, and $W_2 = I_j$ (identity matrix $j \times j$); and U and V are unitary matrices resulting from the SVD process. The order of the system n is determined by inspecting the singular values in S, i.e. determine the $n \times n$ submatrix S_1, which are the cosine of the principal angles between the row space of past outputs Y_p and future outputs Y_f. In practice, however, due to noise and rounding errors, the structure of S is not as shown in (3.26), i.e. the zero diagonal matrix is not really zero. In this case, a "large" reduction in the singular values of S are used to define S_1 (the system order n), as discussed in detail for the test systems in Chapter 4.

3. Determine the extended observability matrices Γ_i and Γ_{i-1} as follows:

$$\Gamma_i = W_1^{-1} U_1 S_1^{1/2} \tag{3.27}$$

$$\Gamma_{i-1} = \underline{\Gamma_i} \tag{3.28}$$

where $\underline{\Gamma_i}$ is obtained by removing the last l rows of Γ_i with l being the number of output signals.

4. Find the Kalman filter state sequences $\hat{X}_i$ and $\hat{X}_{i+1}$ as follows:

$$\hat{X}_i = \Gamma_i^{\dagger}\mathcal{O}_i \tag{3.29}$$

$$\hat{X}_{i+1} = \Gamma_{i-1}^{\dagger}\mathcal{O}_{i-1} \tag{3.30}$$

5. Then, A_d and C are determined from:

$$\begin{pmatrix} A_d \\ C \end{pmatrix} = \begin{pmatrix} \hat{X}_{i+1} \\ Y_{i|i} \end{pmatrix} \hat{X}_i^{\dagger} \tag{3.31}$$

Once A_d is calculated, the eigenvalues $Z_i = Z_{R_i} + jZ_{I_i}$ of matrix A_d can be transformed onto the s-plane $s_i = \lambda_{R_i} + j\lambda_{I_j}$ using a bilinear transformation, i.e. $s_i = \frac{2}{T_s}(Z_i - 1)/(Z_i + 1)$.

3.3.5 Computational Issues

One of the assumptions in stochastic subspace identification is that the $w[k]$ and $v[k]$ are independent of $\Delta x[k]$, i.e. $E[\Delta x[k].w^T[k]] = 0$, $E[\Delta x[k].v^T[k]] = 0$. It is typically assumed that the data blocks are long enough and ergodic, i.e. the underlying system model is not changing, so that the expectation operator E can be replaced with the average over one experiment run for infinite time. This is why subspace methods work well for long data blocks even in the presence of noise [61]. The asymptotic properties of the proposed subspace method are also discussed in [63], where it is shown that for a white noise input, the CVA and the PEM are asymptotically equivalent.

The effect of using different sizes of data blocks on the accuracy of the method was investigated for the 2-area benchmark system, and the asymptotic behavior

Table 3.1: CPU time in seconds for different methods and system orders

Method	MATLAB function	n=13	n=16	n=19	n=22
Subspace	`n4sid(n)`	0.63	0.83	1.00	1.16
ARMA	`armax(n,n)`	6.99	9.96	14.08	19.44
State-space	`pem(n)`	11.17	13.99	24.67	36.20

of the proposed subspace method was compared to an ARMA model and a state-space model whose parameters were estimated using the PEM. For this purpose, the following built in functions of MATLAB were used: function `n4sid()` for the subspace method; `armax()` for the ARMA model; and `pem()` for the state-space model. The data was generated for an inter-area mode $-0.1228 \pm j4.7824$ (damping 2.57% and frequency 0.7611 Hz). The standard deviation of the estimated real part and frequency of the mode for different size of data blocks are depicted in Figure 3.2 and Figure 3.3, respectively; these were obtained based on a Monte-Carlo type of simulation with 30 independent cases. Notice that for short data blocks, the ARMA and state-space models yield better performance. On the other hand, for long data blocks, as explained before, the proposed subspace method and ARMA and state-space models behave similarly.

From the computational burden point of view, the previously mentioned MATLAB built in functions were used to estimate the parameters of the corresponding models for the same 4-minute block data. Table 3.1 shows the CPU times obtained for each function as the system order n changes; observe that the subspace method is significantly faster than the others.

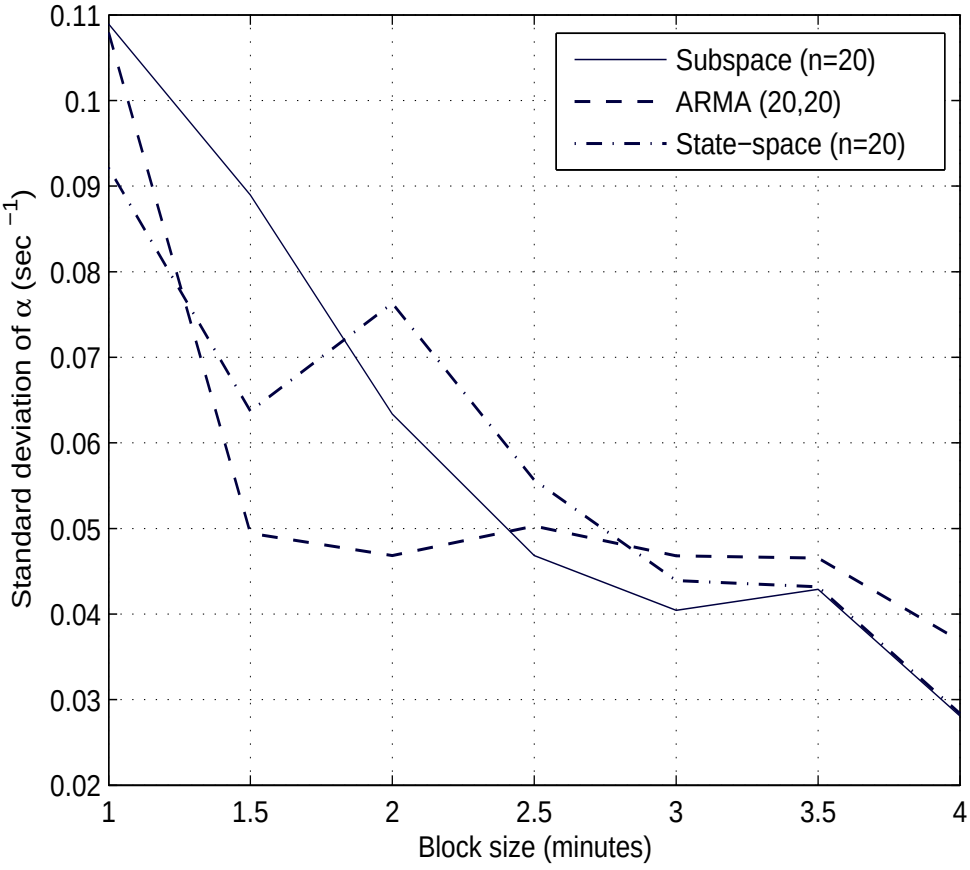

Figure 3.2: Standard deviation of the estimated real part α of the inter-area mode $-0.1228 \pm j4.7824$ for the 2-area benchmark system.

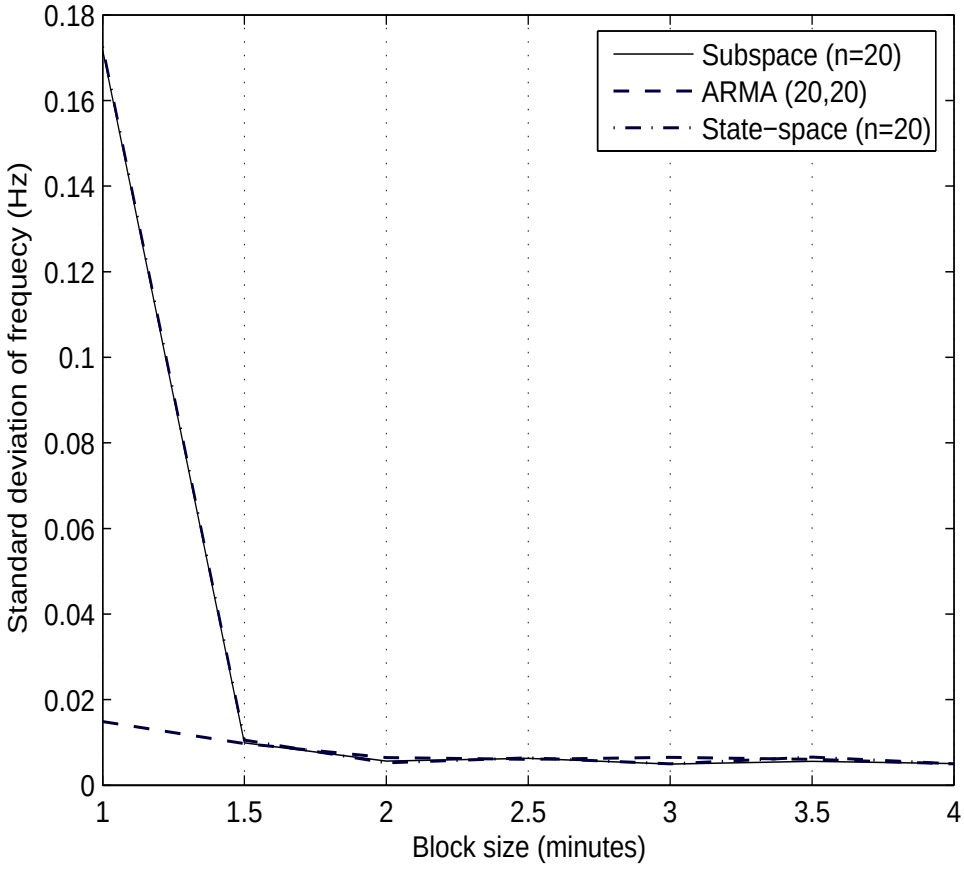

Figure 3.3: Standard deviation of the estimated frequency of the inter-area mode $-0.1228 \pm j4.7824$ for the 2-area benchmark system.

3.4 Summary

Different types of signals that can be readily measured in a power system are described as well as corresponding techniques to extract the modal content of the signals. This modal content, in turn, provides useful information about the system stability condition. Depending on the kind of excitations that are present in the system, appropriate techniques are recommended for both deterministic ringdown and stochastic ambient data, and the merits and pitfalls of each technique are discussed. Namely, the Prony method is suitable for the transient response with high SNR, while the LSMYW and the PEM are shown as proper techniques to analyze ambient noise.

The stochastic subspace identification method is proposed to capture the critical modes of a power system from ambient data; it uses robust numerical techniques, and is data driven instead of covariance driven, and hence is faster. The results demonstrate the accuracy and efficiency of the proposed method; therefore, it can be used as an on-line monitoring tool in power system surveillance and electromechanical mode detection. The asymptotic behavior of the proposed method was also investigated, and compared with the class of estimation methods known as PEM. It was shown that the methods are asymptotically equivalent; however, the proposed method is much easier to implement, and is computationally efficient.

Chapter 4

System Identification Stability Index

4.1 Introduction

The identification of stability limits associated with angle stability is of great interest to Independent System Operators (ISO). The availability of proper on-line monitoring tools can assist operators to determine the available security margins of the system, thus allowing them to take proper actions close to real time in the case of system contingencies.

In this chapter, a general overview is given regarding a previously proposed oscillatory stability index, which is calculated off-line and is used to predict oscillatory phenomena. A stability index to determine and predict the closest instability point in a power system with regards to the load change is then proposed and studied. This index is defined based on the critical eigenvalues of the system, i.e. the eigenvalues that eventually cross the imaginary axis, thus leading the system to

instability. Several test systems, including a real 14,000-bus system, are employed to test the effectiveness of the proposed index using both their transient response and ambient noise by means of the Prony method and the stochastic subspace identification method, respectively.

4.2 Proposed Oscillatory Stability Index

The index, referred in [13] as to Hopf bifurcation index (HBI), predicts the distance to the closest SNB or HB stability point, given a known load change direction. It is based on the system state matrix A and the "critical" eigenvalues $\mu_c = \alpha_c \pm j\beta_c$, i.e. the eigenvalues that eventually cross the imaginary axis at an SNB or HB point as λ changes. Thus, the HBI is defined as

$$\text{HBI}(A, \beta_c) = sv_{min}(A_m) \tag{4.1}$$

where sv_{min} is the minimum singular value of the modified state matrix A_m, which is defined as

$$A_m = \begin{bmatrix} A & +\beta_c I_n \\ -\beta_c I_n & A \end{bmatrix}_{2n} \tag{4.2}$$

At an SNB or HB point, sv_{min} becomes zero. In [13], the authors also compare the HBI to an eigenvalue index (EVI) which is defined as the real part of the critical eigenvalue. It is worth mentioning that almost in all test cases both HBI and EVI present a fairly linear behavior.

Computing the HBI in (4.1) requires making assumptions about the model, so that the matrix A can be explicitly determined. However, if the "output" deviations

$\Delta y(t) \in \Re^l$ of (2.8), i.e.

$$\begin{aligned} \Delta\dot{x}(t) &= A\,\Delta x(t) \\ \Delta y(t) &= C\,\Delta x(t) \end{aligned} \tag{4.3}$$

is measured, the modal content in the output signal $\Delta y(t)$ is the same as the modal content in matrix A if the system modes are excited; hence, these modes can be calculated using system identification techniques. If the eigenvalues $\mu_i(A) = \alpha_i + j\beta_i$ of the system can be identified, one may define a new diagonal state matrix $\Lambda = diag\{\mu_1, \mu_2, \ldots, \mu_n\}$, which can be used to define the following new modified state matrix:

$$\Lambda_m = \begin{bmatrix} \Lambda & +\beta_c I_n \\ -\beta_c I_n & \Lambda \end{bmatrix}_{2n} \tag{4.4}$$

In this case, using basic singular value decomposition concepts as shown in Appendix B, the sv_{min} for Λ_m can be calculated using:

$$sv_{min}(\Lambda_m) = \min_{i=1,n} \left\{ \sqrt{\alpha_i^2 + (\beta_c - \beta_i)^2} \right\} \tag{4.5}$$

If the closest eigenvalue to the imaginary axis is the critical one, then

$$sv_{min}(\Lambda_m) = |\alpha_c| \tag{4.6}$$

Since multiple eigenvalues can be readily determined using system identification tools applied to measured signals such as generator speed or power, and assuming that the critical eigenvalue can be monitored, a System Identification Stability Index (SISI) is hence defined here:

$$\text{SISI} = |\alpha_c| \tag{4.7}$$

Observe that this index does not require assumptions regarding the system modeling as the HBI would require. Furthermore, based on the observations in [13] regarding

the behavior of the HBI and EVI, one would expect this index to behave "linearly" close to an HB point.

In practice, several modes need to be monitored, i.e. an index value would be generated for each mode, so that the mode that eventually crosses the imaginary axis is properly captured. This can be accomplished by measuring signals in different parts of the system, where the modes of interest are best observed. However, in some cases, the critical mode is known from previous knowledge of the system (e.g. the 0.28 Hz mode in the WECC system which can be easily observed on transmission corridors between the north and south of the system), in which case, this is the mode used to define the SISI.

It is important to mention that the trend of the index, and more specifically its slope, may change when the system changes due to large disturbances as well as changes in loading and dispatching [13]. Figure 4.1 illustrates an example of a possible index profile for a real power system as system conditions vary. Notice that, as the system operating conditions change, the index changes as well; when this index reaches a predetermined threshold, which could be readily associated with a minimum system damping, a warning or emergency alarm would be triggered.

4.3 SISI from Transient Response

As previously explained in Chapter 3, depending on the type of the tests that are carried out on power systems, one needs to employ appropriate system identification techniques to obtain both reliable and accurate modal estimates. Hence, it was concluded that the measured transient response of the power system with a good quality, i.e. high SNR, as a result of a large disturbance or ringdown test, may be analyzed with the use of the well-known Prony method.

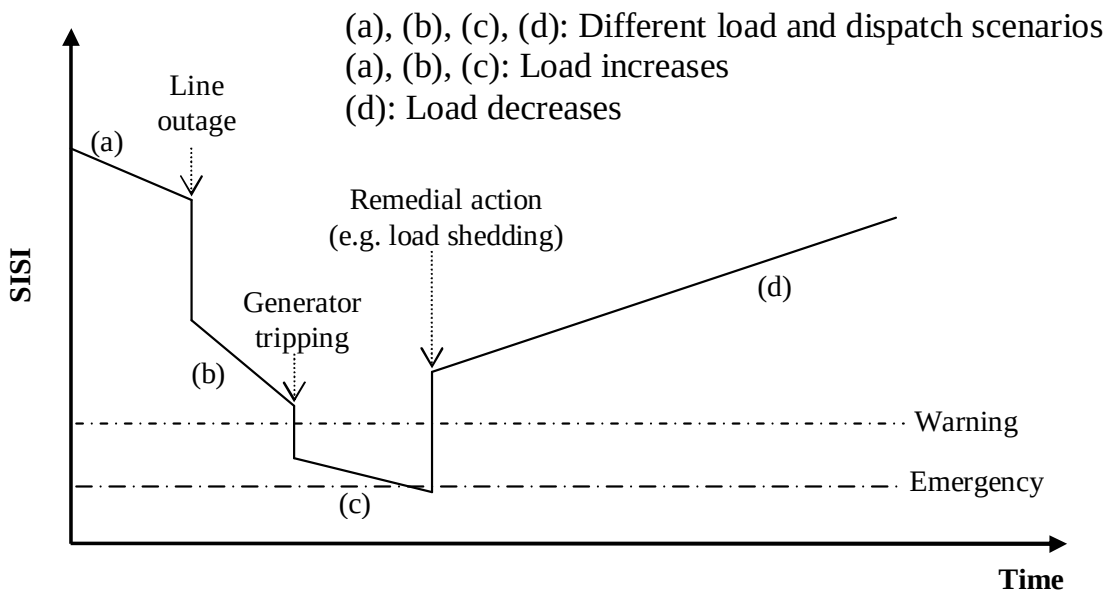

Figure 4.1: SISI profile for a real power system with varying operating conditions.

The response of the system to a large disturbance, such as a line outage or a three phase fault, is recorded such that it contains at least three periods of oscillations. Then, the measurement noise is removed with a Chebyshev low pass filter with a cut off frequency of 2 Hz, then re-sampling the signal at 10 Hz; the mean and low frequency trends of the measured signal have to be removed as well. The Prony method is then applied to the preprocessed signal to obtain the modal contents of the signal and thus the SISI. The behavior of the index, as the system loading changes, is depicted below for each test system, illustrating the application of the SISI to the prediction of the stability margin.

4.3.1 IEEE 3-bus System

The IEEE 3-bus system of Figure 2.8 is used here to test the application of the proposed index. The P-V curves for the base system and for a line 2-3 outage

are given in Figure 4.2; observe that these cases present HBs at certain loading conditions before the maximum SLM (nose point). The rotor speed of generator G_1 for a line 2-3 outage is shown in Figure 4.3 for two loading conditions; notice that at higher loading, the contingency results in unstable oscillations associated with the HB depicted in Figure 4.2. For a SNR of 30 db, the 8 largest singular values of the matrix D in (3.7) are {0.26568, 0.24935, 0.0089838, 0.0037355, 0.0000252, 0.0000228, 0.0000067, 0.0000006}; hence, the practical order of the system is $n = 2$, as there is a large drop from the second to the third singular value. Nevertheless, higher orders are examined as well. The characteristic equation can then be formulated, and the modal content of the signal is obtained using (3.8).

The small-disturbance stability program of the PST program [36] was also used to obtain the critical eigenvalues from a linearized model of the power system, and obtain the corresponding EVI of DAE Model. With the variation of the load at Bus 3, the eigenvalues of the base system and the system under a line 2-3 outage were computed using PST and the Prony method; the eigenvalue profiles obtained with PST with respect to load changes in the base system are illustrated in Figure 4.4. For each system, the stability indices (from the linearized DAE model and the mean value of 30 simulations) are depicted in Figures 4.5 and 4.6. Observe that all indices predict an HB at about 1500 MW for the base system and 1130 MW for a line 2-3 outage, with both EVI and SISI indices presenting a rather linear profile. The results for the Prony method when the SNR is 10 db are shown in Figure 4.7, demonstrating poor results compared with the case when SNR is 30 db, as expected and explained in Section 3.2.1.

Increasing the model order results in more accurate estimates of the critical modes, as shown in Figures 4.5, 4.6 and 4.7. However, the order cannot be increased without considering the following: First, the appearance of extraneous

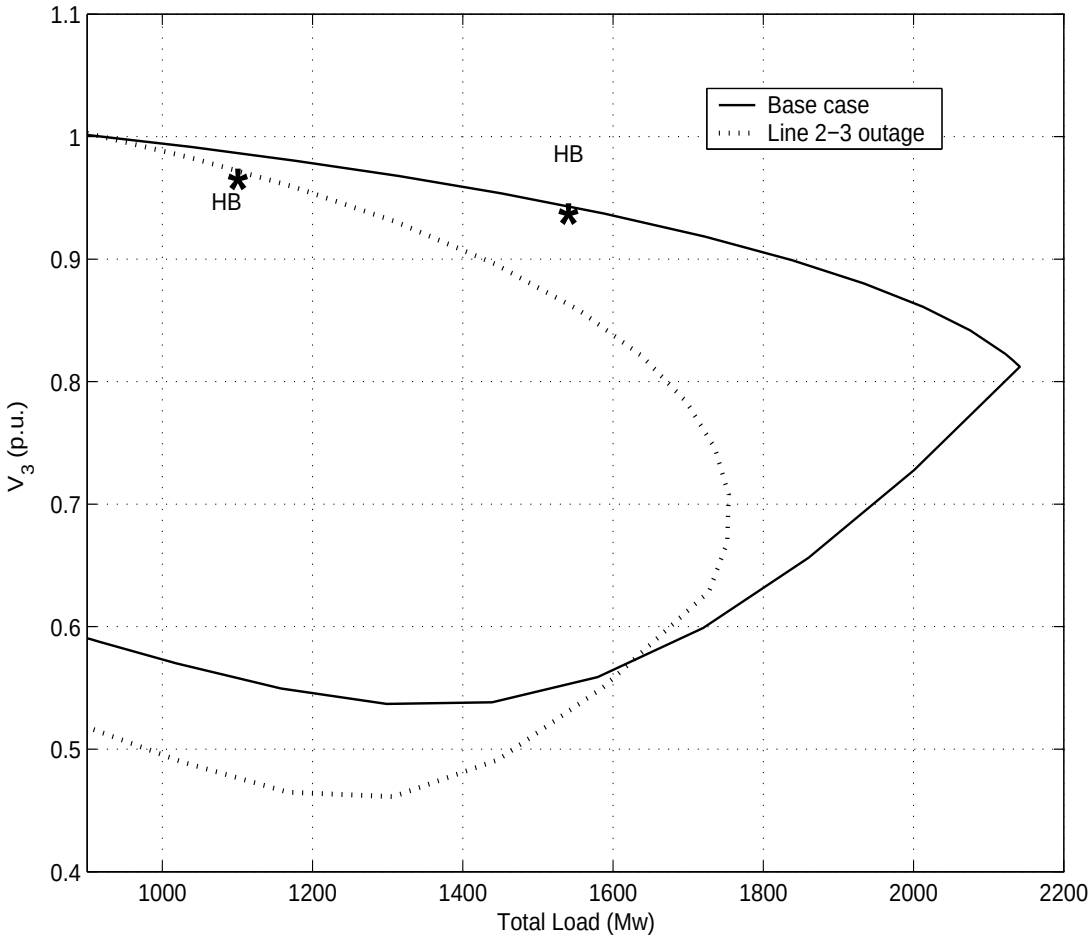

Figure 4.2: P-V curves at Bus 3 for the IEEE 3-bus system, for the base case and for a line 2-3 outage.

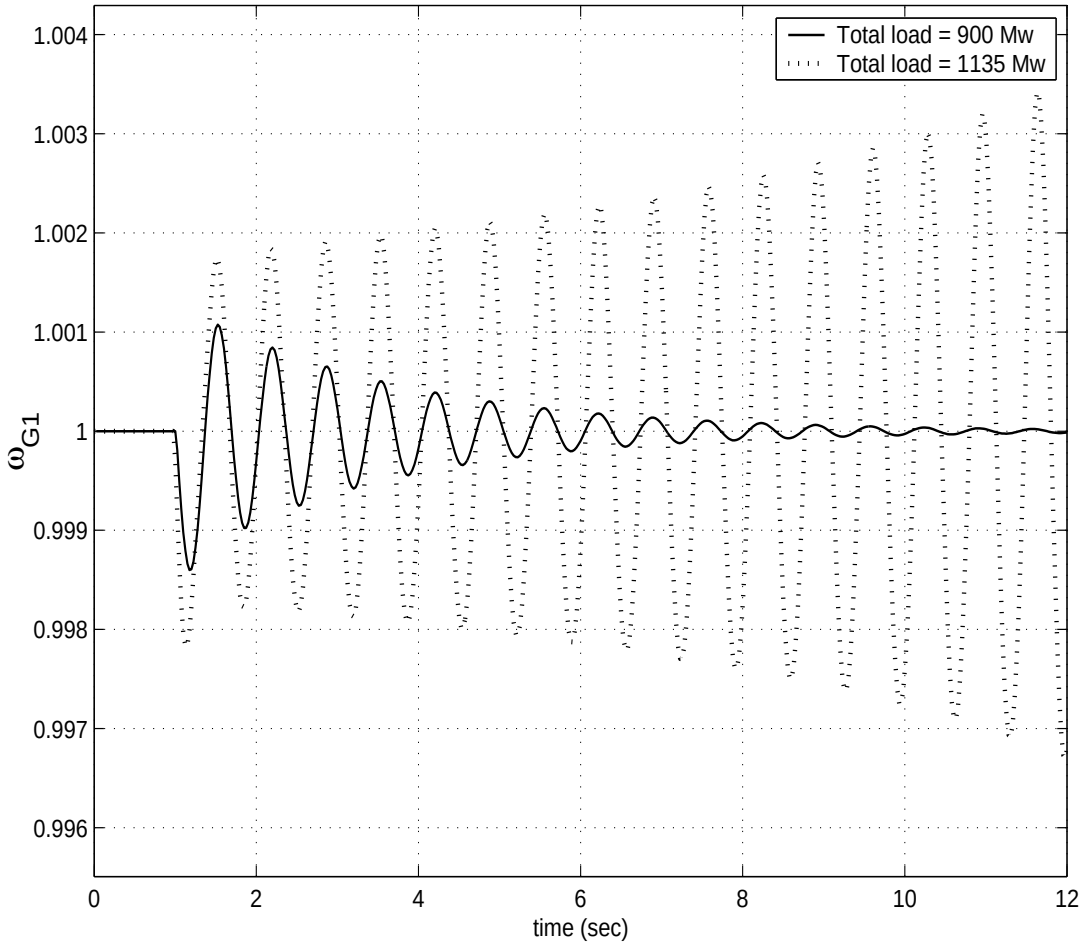

Figure 4.3: Generator G_1 speed following a line 2-3 outage in the IEEE 3-bus system.

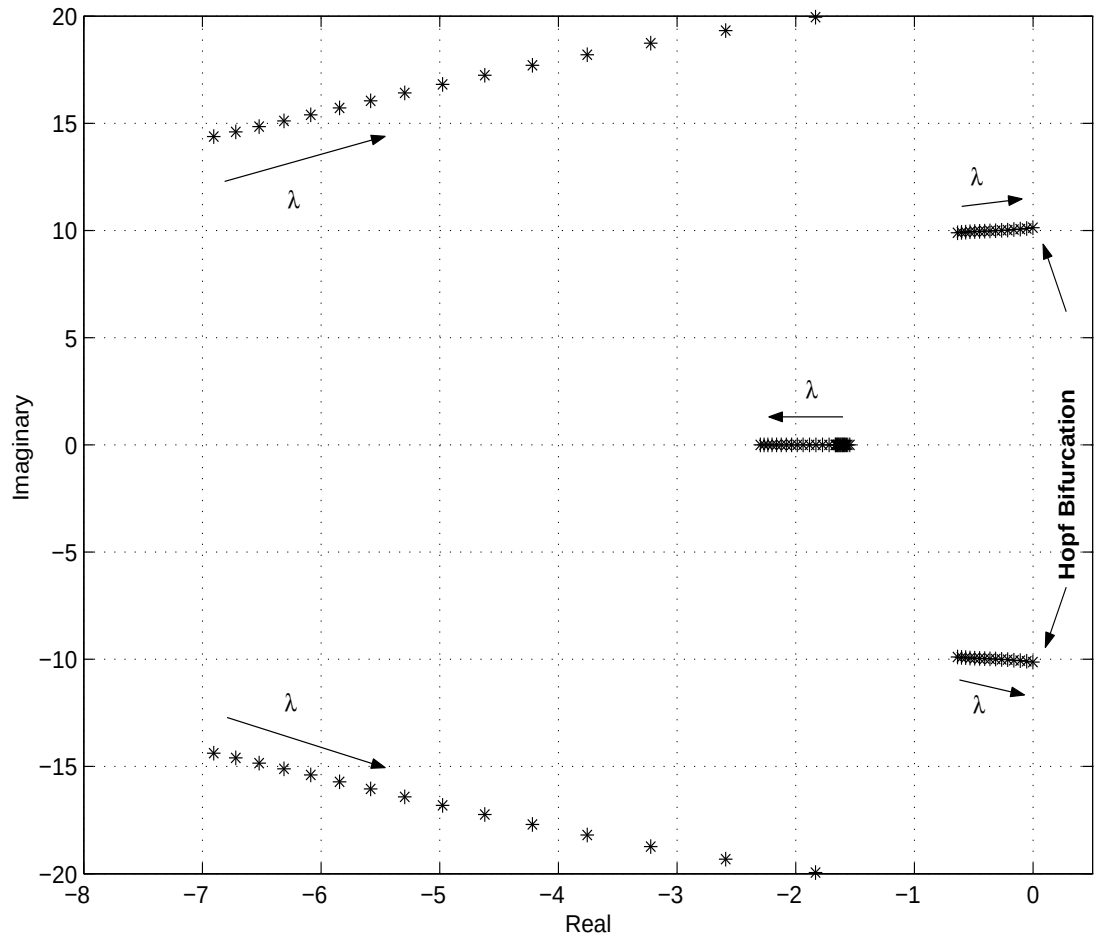

Figure 4.4: Eigenvalue profiles with respect to load changes in the IEEE 3-bus system.

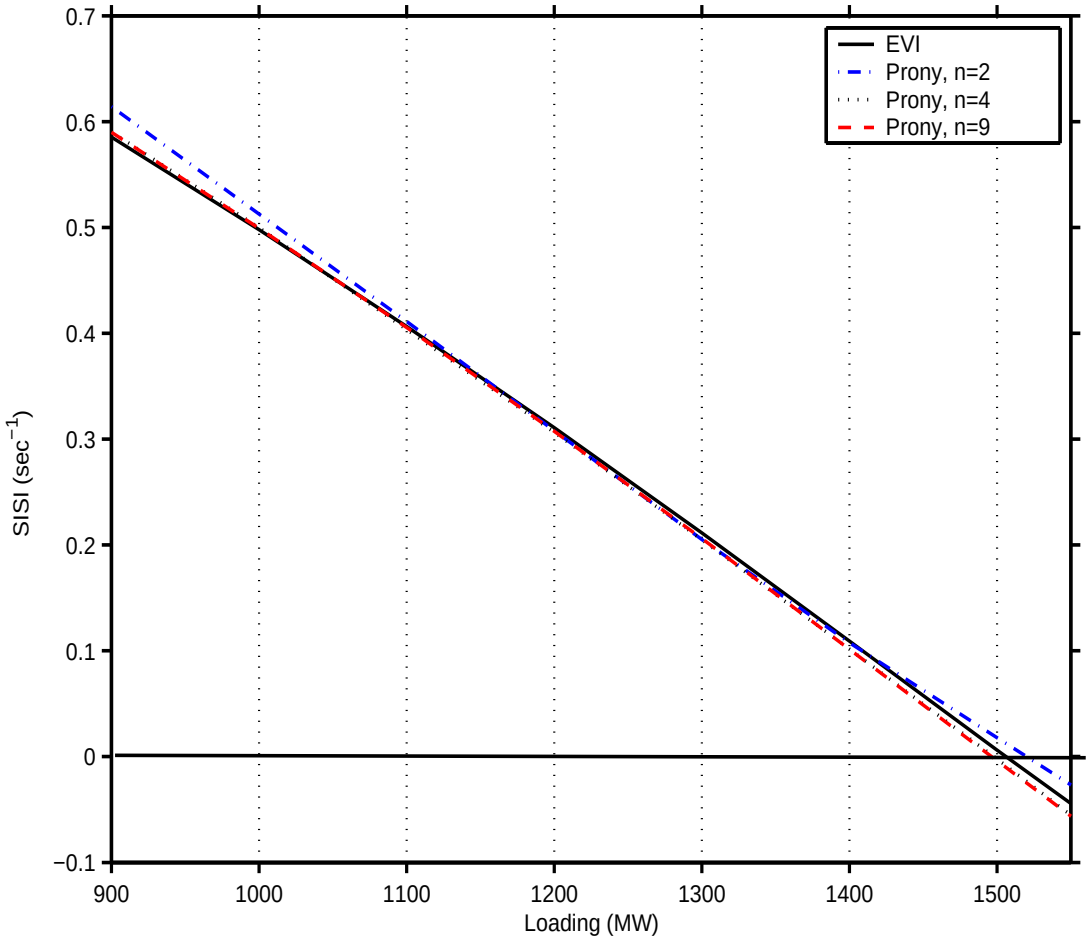

Figure 4.5: Stability index for the IEEE 3-bus system for SNR = 30 db; base system.

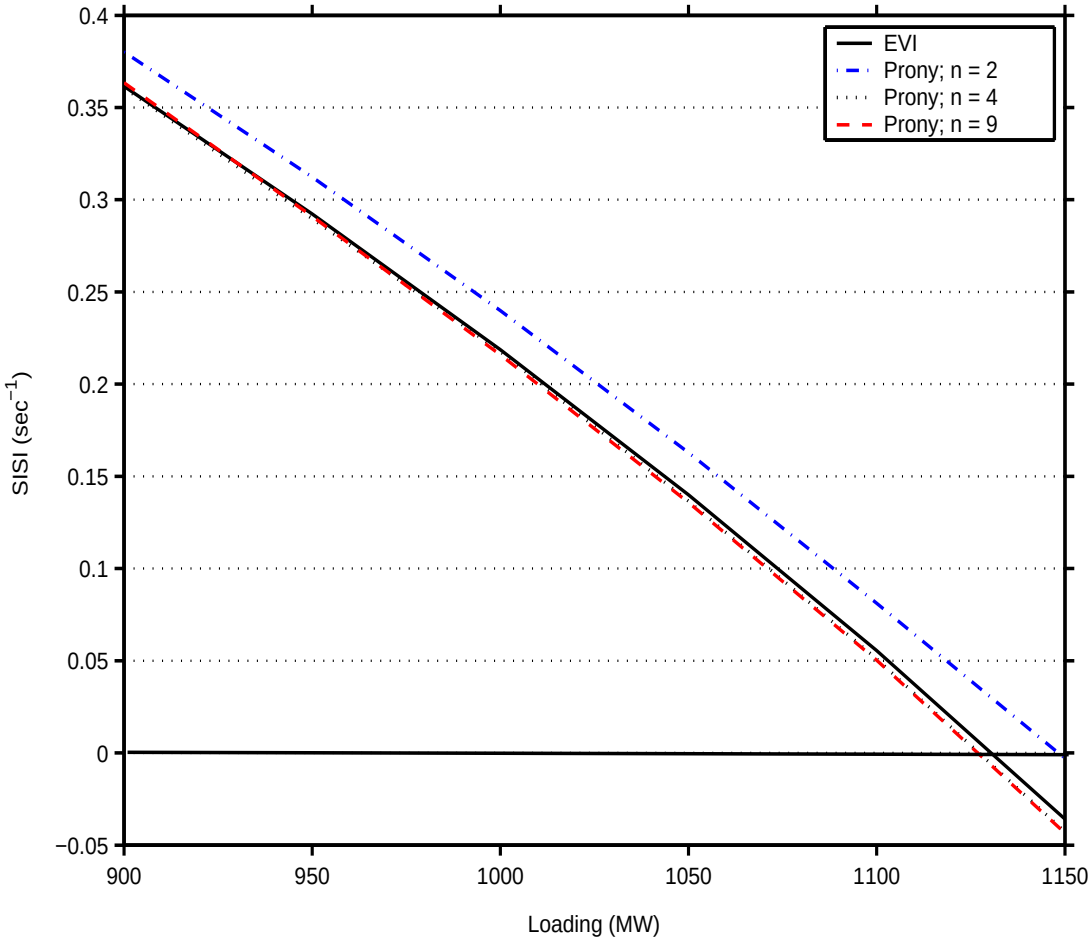

Figure 4.6: Stability index for the IEEE 3-bus system for SNR = 30 db; line 2-3 outage.

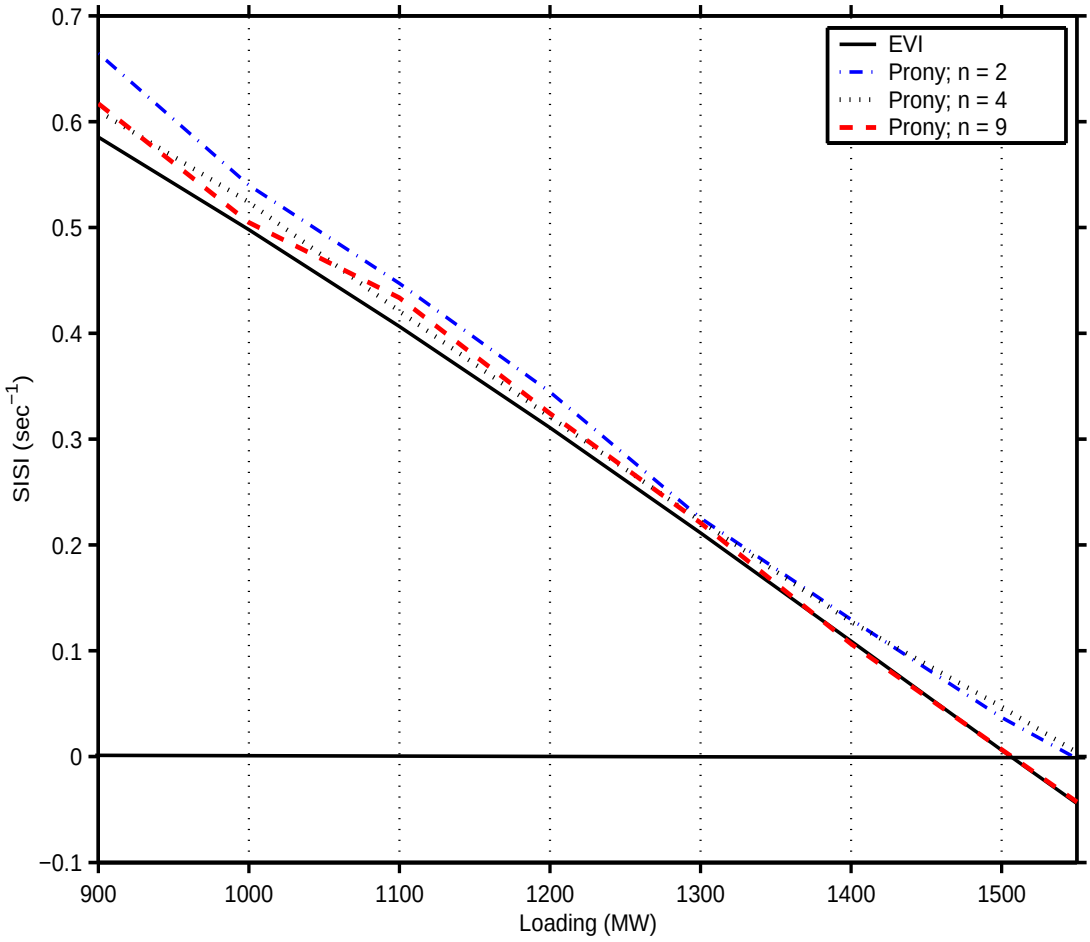

Figure 4.7: Stability index for the IEEE 3-bus system for SNR = 10 db; base system.

modes, which makes it difficult to distinguish between the true modes and spurious ones. Second, the variance of mode/pole estimates, which is directly related to the variance of the SISI.

One should make a distinction between the variance of the parameters θ, i.e. coefficients of the characteristic equation or coefficients of an AR(p), and the variance of mode/pole estimates that are the roots of the characteristic equation. There is a nonlinear relationship between them, and the theoretical background on the former is well understood and developed. Thus, the variance of the parameters θ is known to increase asymptotically, as the order increases [58]. Figure 4.8 illustrates this behavior; observe that when the order of the system increases from 2 to 4 and then 9, there is a significant increase in the variance of the parameters estimates. On the other hand, no clear conclusion can be reached regarding the variance of pole estimates when the order changes. This can be clearly observed in Figure 4.9, which shows the standard deviation of pole estimates, depicted with use of the standard deviation of both the SISI and the frequency.

4.3.2 IEEE 14-bus System

The IEEE 14-bus benchmark system shown in Figure 2.9 is used as a more realistic test system. There is an HB point for both the base system and for a line 2-4 outage before the "nose" point, as shown in the corresponding P-V curves depicted in Figure 4.10. The base system yields the critical eigenvalues $\mu_c = -0.21637 \pm j8.8298$ (1.4 Hz frequency and 2.45% damping ratio) at a 259 MW load; this is the eigenvalue that eventually crosses the imaginary axis at the HB point, as shown in the eigenvalue profiles depicted in Figure 4.11.

The stability indices for the base system and for a line 2-4 outage are depicted

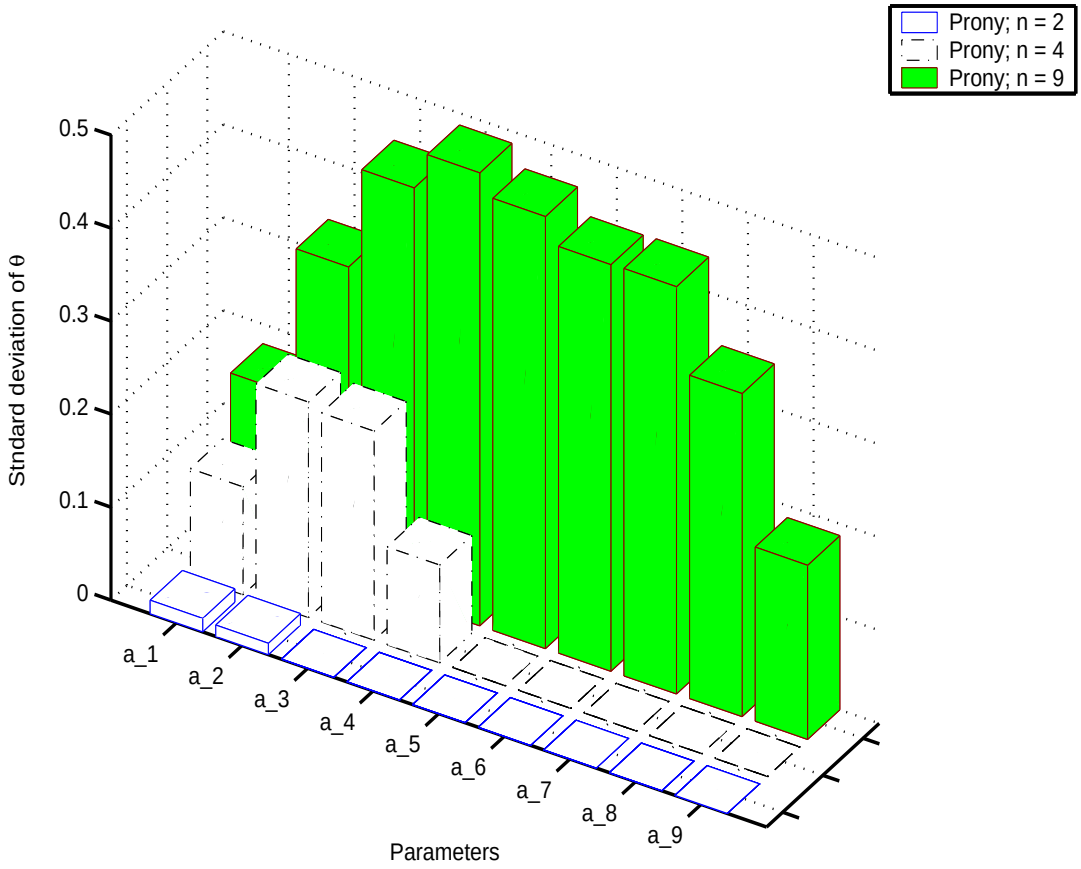

Figure 4.8: Standard deviation of parameter estimates for the IEEE 3-bus system; a_i's are the characteristic equation coefficients.

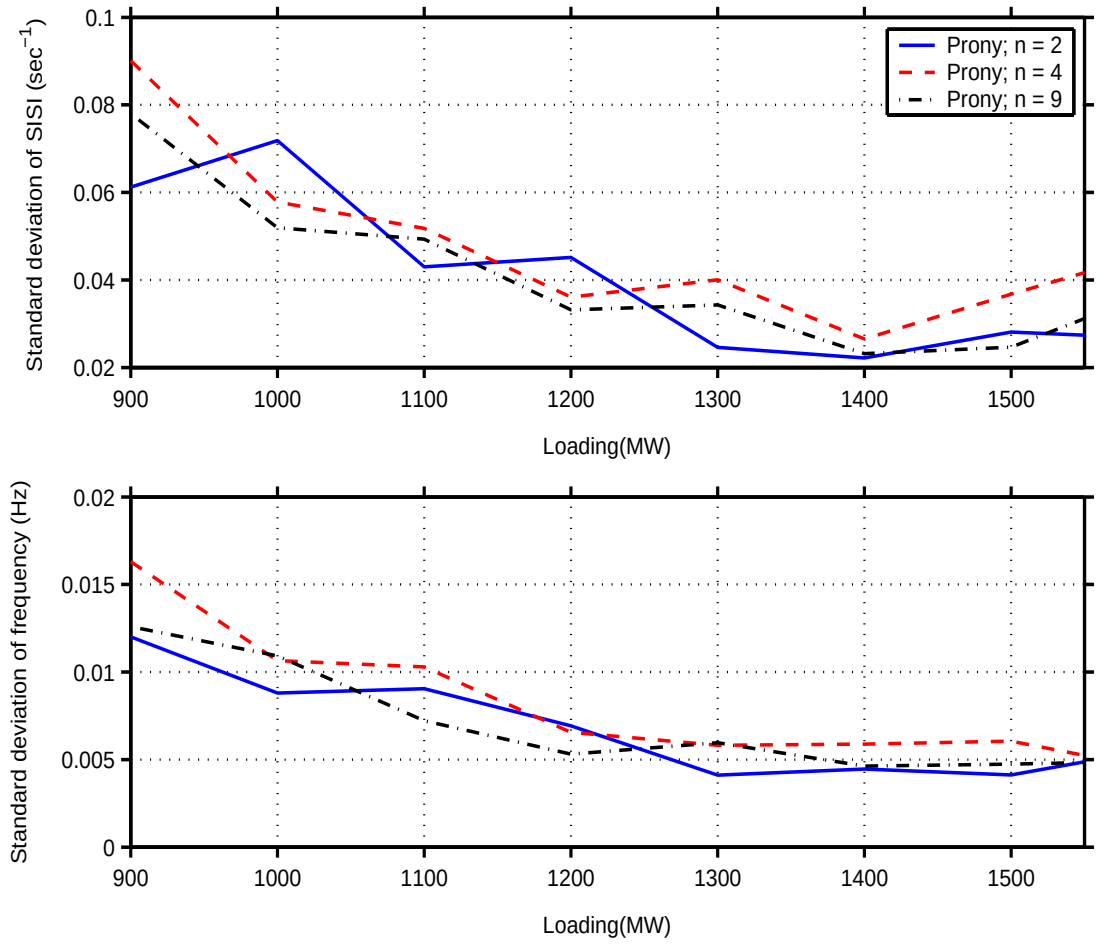

Figure 4.9: Standard deviation of the SISI and the critical mode's frequency for the IEEE 3-bus system.

in Figures 4.12 and 4.13, respectively. Observe that SISIs in this case are not as close to the EVI values as in case of the IEEE 3-bus system. This can be explained by looking at the time-domain response of the system as depicted in Figure 4.14. Note that the 1.4 Hz signal (fast) does not oscillate about the pre-contingency operating condition as opposed to Figure 4.3; hence, the identified indices, when compared with the IEEE 3-bus system results, deviate significantly from the EVI model values. This behavior is due to the fact that the type of load models used in the IEEE 3-bus and 14-bus systems are different; for the IEEE 3-bus system, the constant PQ load model makes the time-domain response oscillate about the pre-contingency conditions.

4.3.3 Real System (14,000 buses)

In order to investigate the shape of the proposed index for a real power system, a 14,000-bus system is studied. To move this system closer to an instability condition, several generator outages are modeled; thus, a low damped 0.33 Hz mode appears due to the simulated contingencies. The power transfer among some areas in the system is then increased until the appearance of an HB point associated with this mode at a 39.6 GW loading level, approximately. It is interesting to highlight the fact that this example is somewhat similar to the Western Electricity Coordinating Council (WECC), previously known as WSCC, 1996 blackout, where several contingencies triggered a 0.28 Hz mode that led the system to instability [5].

The system in this case is perturbed using two 50 MW load perturbations in different areas to obtain the desired signals and excite the desired mode. By analyzing the 0.33 Hz mode shape, two generators' output power signals in the main areas that oscillate against each other were selected to identify the mode.

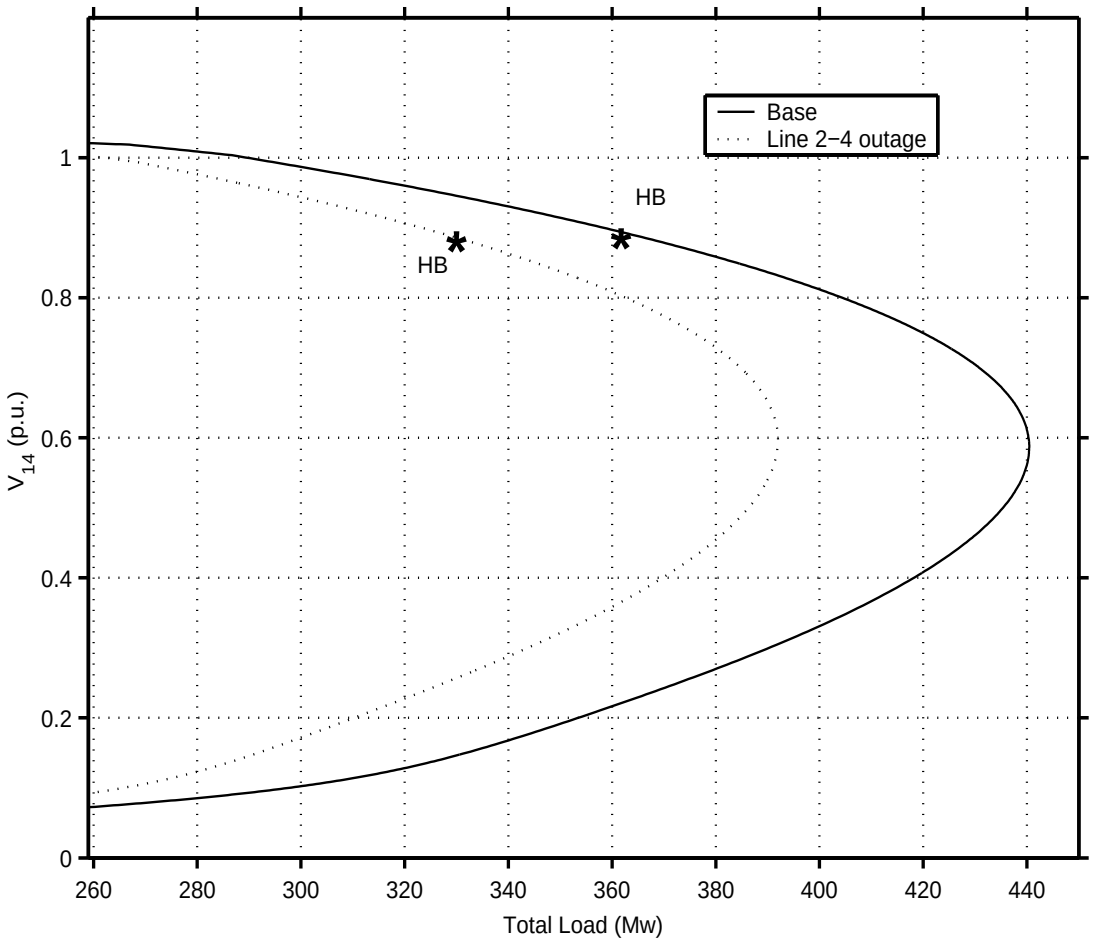

Figure 4.10: P-V curves for the IEEE 14-bus system at Bus 14, for the base case and for a line 2-4 outage.

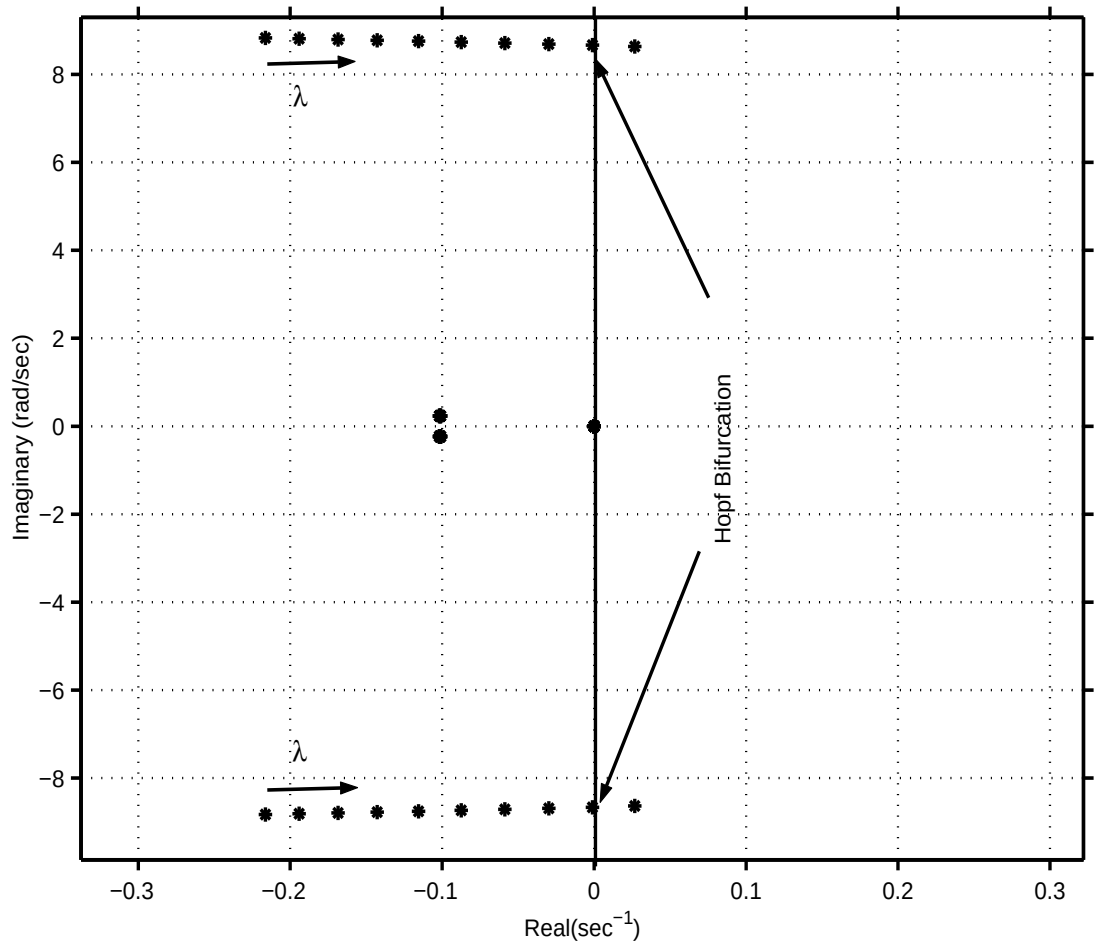

Figure 4.11: Eigenvalue profiles with respect to load changes in the IEEE 14-bus system.

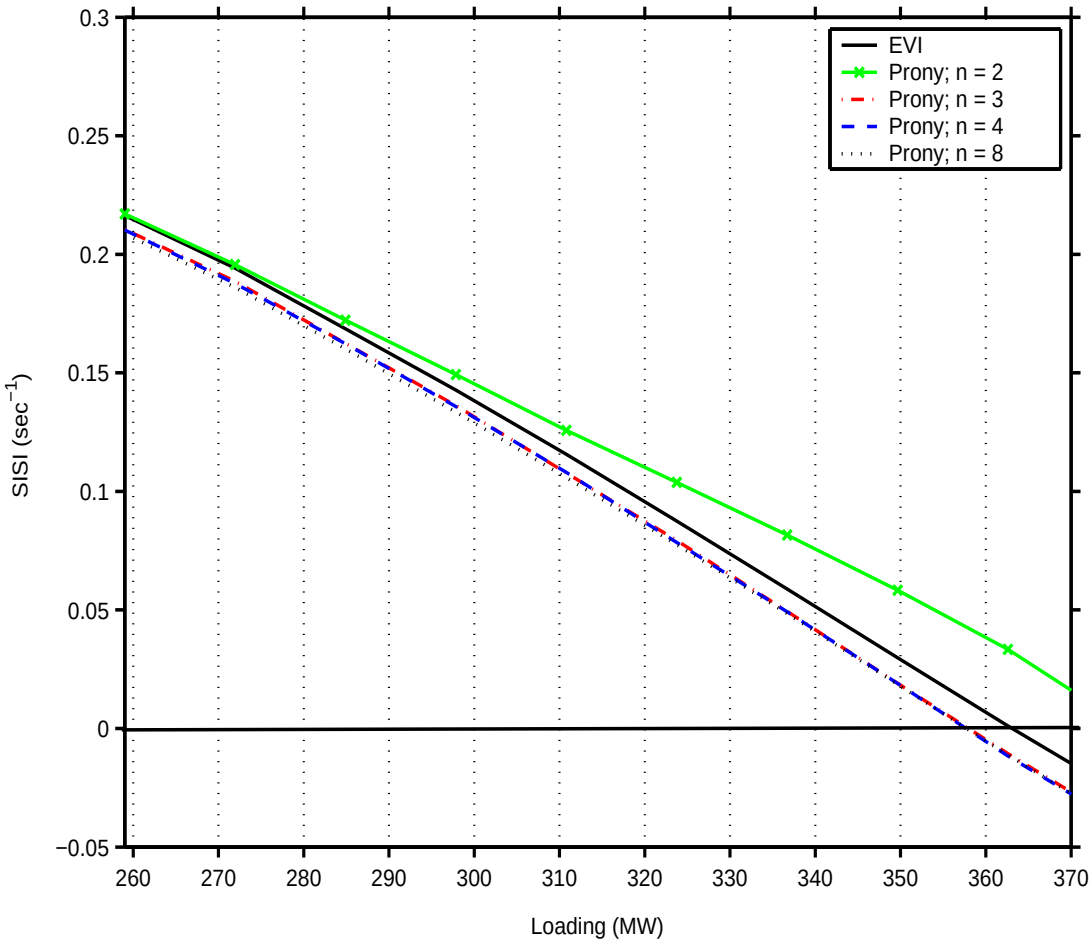

Figure 4.12: Stability index for the IEEE 14-bus system; base system.

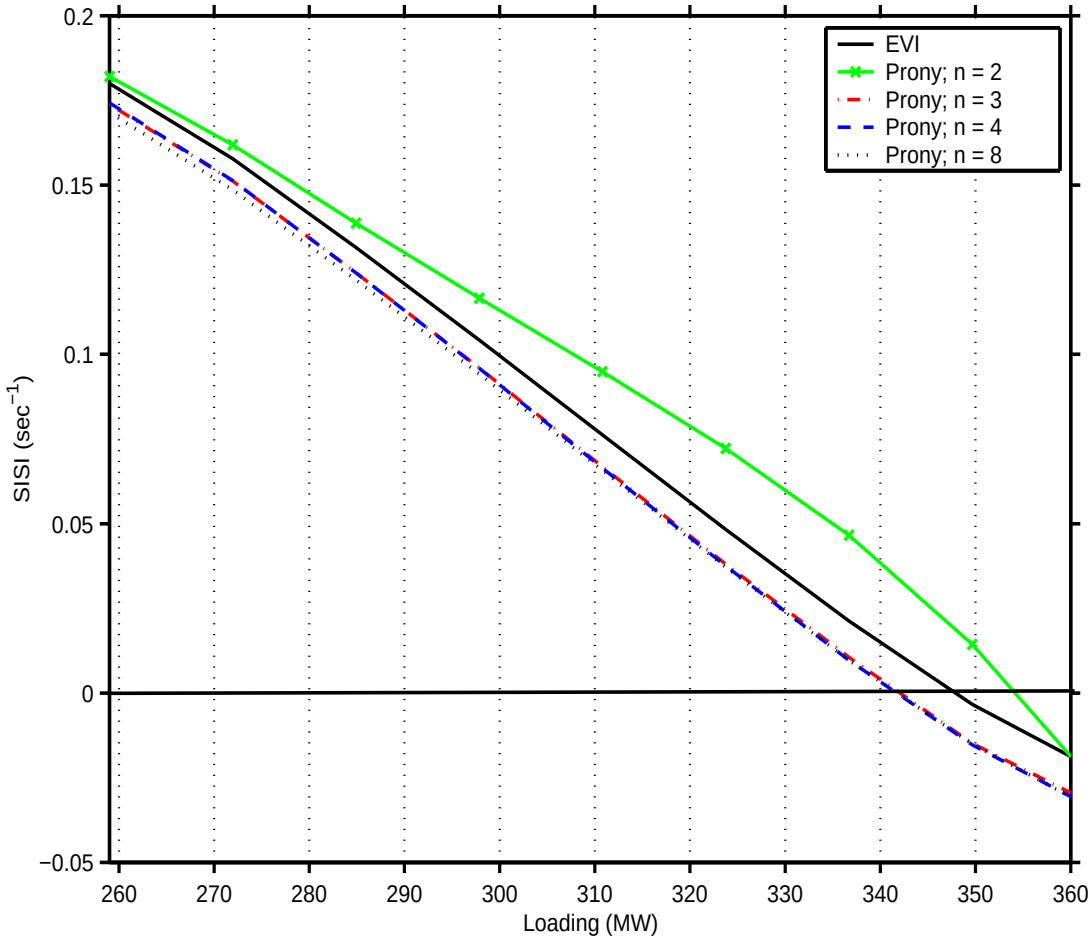

Figure 4.13: Stability index for the IEEE 14-bus system; line 2-4 outage.

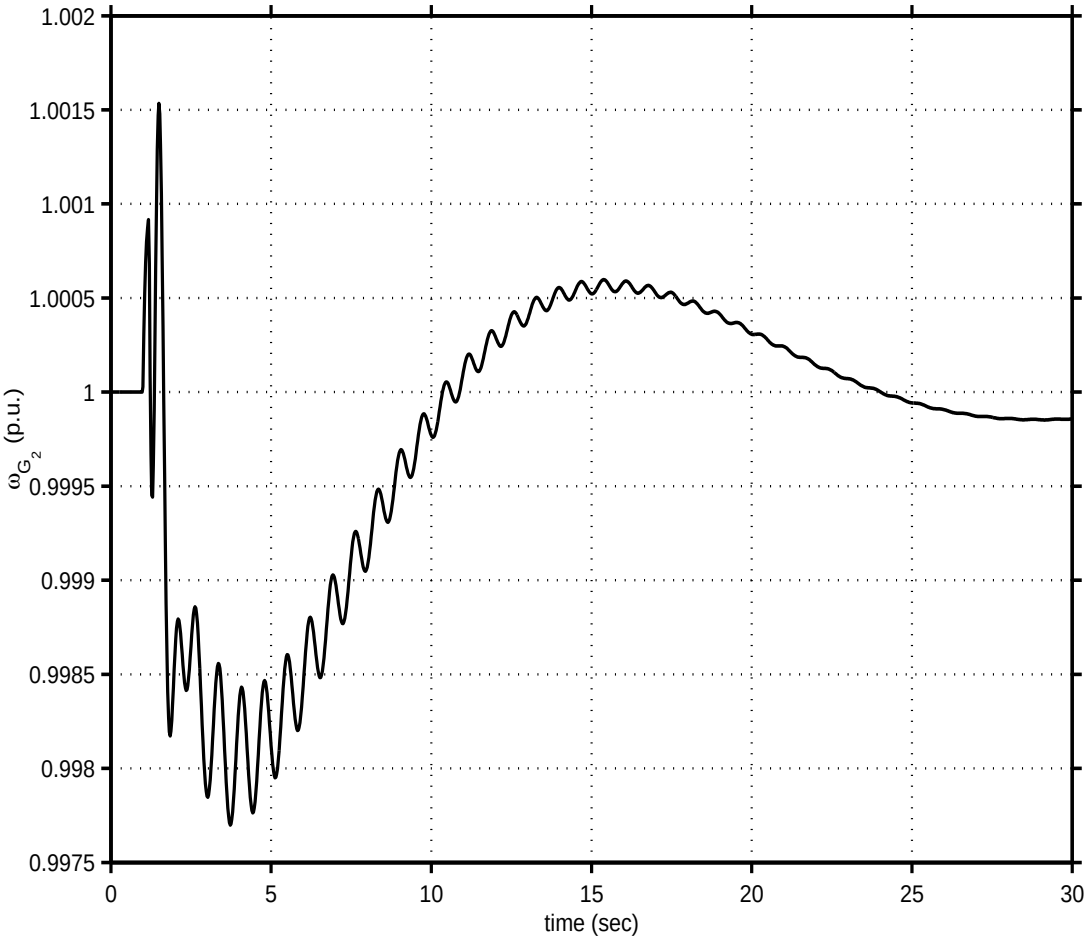

Figure 4.14: Generator G_2 speed following a three phase fault at Bus 4 in the IEEE 14-bus system.

The SISIs obtained from system identification and the linearized transient stability model are shown in Figure 4.15; the maximum error between the identified and modeled SISI is 0.0042 sec^{-1}. Notice that in this case, the index is not quite as linear as in the previous cases, and hence prediction of maximum loading margins at light loading levels are not that accurate; however, no discontinuity was observed while increasing the power transfer between areas, even though several generators reached their Var limits.

4.4 SISI from Ambient Data

Dealing with low quality random signals (ambient data) is more involved, since these have to be examined with random models (e.g. ARMA model), and their corresponding parameters have to be estimated with the more complicated techniques described in Chapter 3.

In this case, it is assumed that the system is persistently being excited by random load switching, emulating the load switching in a real power system throughout the day. Several methods can be used to monitor the critical electromechanical mode of the system. The stochastic subspace identification method is used here due to its superiority over other methods from a computational point of view, as explained in Section 3.3.

The desired signals for various test cases are obtained with use of independent random load modulation with a magnitude of 1% of both active and reactive power at load buses; white Gaussian noise is added to the output signals as measurement noise v_k, so that the SNR is 20 db. A Monte-Carlo type of simulation is used to test the feasibility and accuracy of the identified modes by simulating 30 independent cases at each operating condition. The mean and the standard deviation σ of the

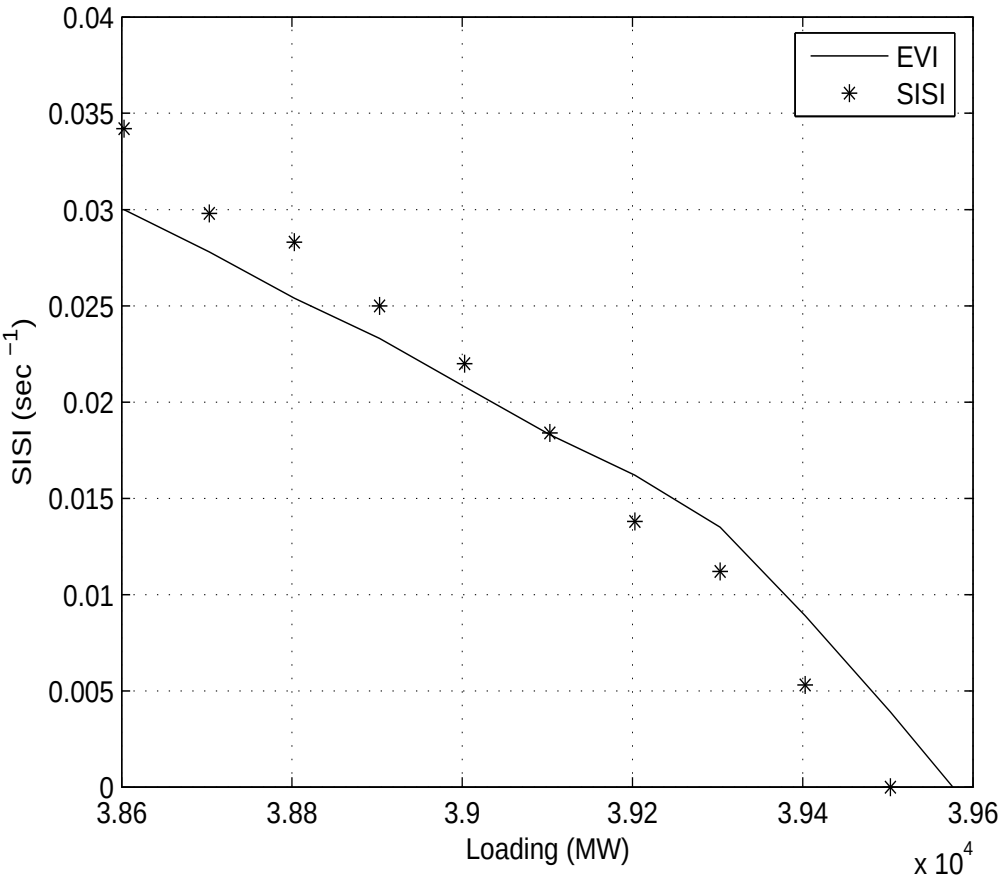

Figure 4.15: SISI for the 14,000-bus real system.

mode estimates do not change significantly when the number of simulations is more than 30, as it can be observed from Figures 4.16 and 4.17 for the 2-area benchmark system. Assuming a direction for the load change and the generation dispatch, critical modes and indices are computed at different operating conditions using both small-disturbance stability analysis of a linearized transient stability model and the proposed stochastic subspace identification method applied to signals generated by time-domain simulation.

The order of the system was determined by inspecting the singular values of S in (3.26), as explained in Section 3.3.4; thus, n is chosen based on a "large" reduction in these singular values. For the different test cases, Figure 4.18 shows the singular values obtained from simulations used in this case. Thus, from this figure, $n = 14$ for the IEEE 3-bus system, $n = 14$ for the IEEE 14-bus system, and $n = 13$ for the 2-area benchmark system. Experience has shown that order overspecification results in better estimates of modes; hence, n was selected to be 18, 20, and 16 for these three test cases, respectively.

4.4.1 IEEE 14-bus System

The SISI results of applying the proposed subspace method to 4-minute blocks of P_{G_1} and P_{G_2}, which are the output generator power signals for genertors 1 and 2, respectively, (a one-minute block of P_{G_2} is depicted in Figure 4.19), as the system loading changes are shown in Figure 4.20; this figure depicts the mean value and the confidence limit of one standard deviation σ of the SISI. Observe that as the critical mode moves towards the RHP, and hence becomes less damped, the standard deviation decreases; this has been previously observed for ARMA models as well in [23]. As loads are increased, some of the generators reach their maximum

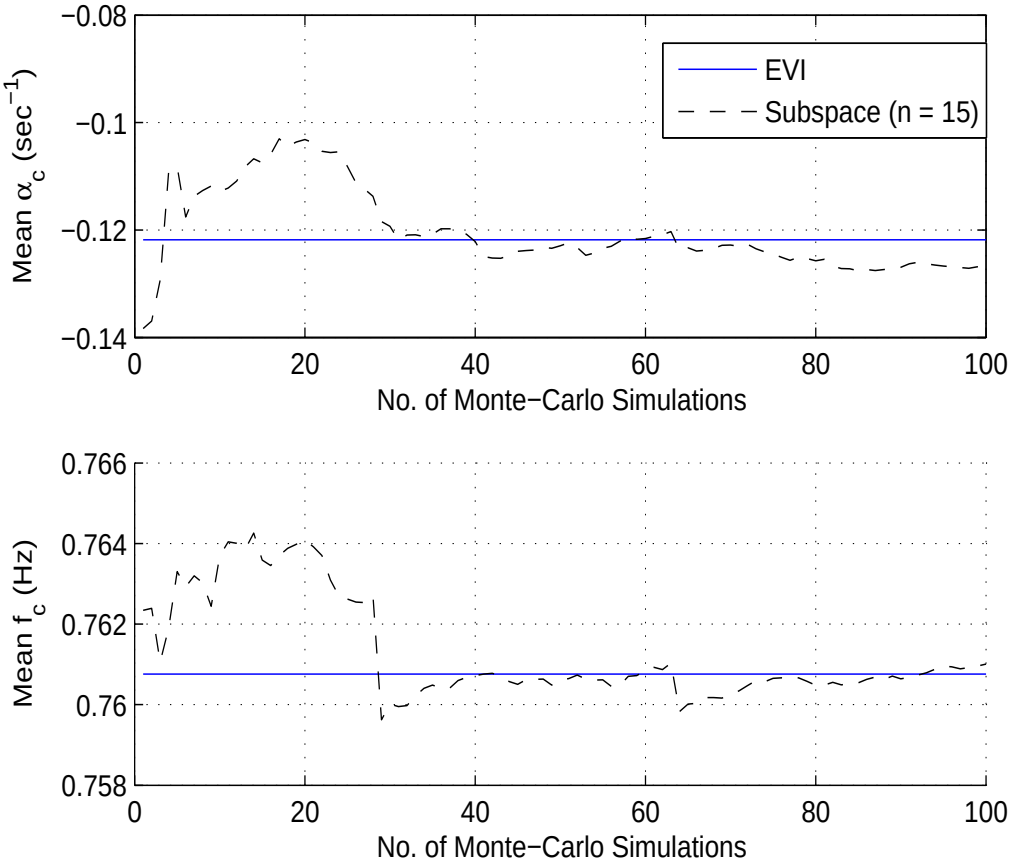

Figure 4.16: Mean of the real part and frequency of the identified critical mode $\mu_c = \alpha_c \pm \beta_c$.

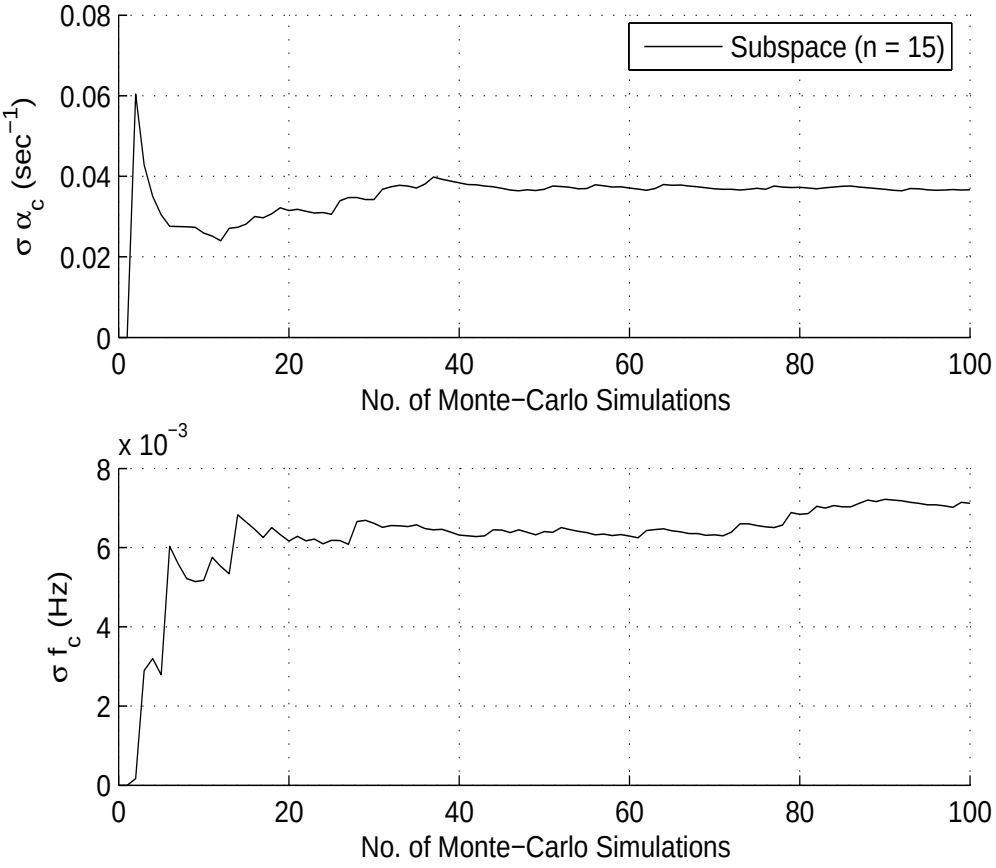

Figure 4.17: Standard deviation of the real part and frequency of the identified critical mode $\mu_c = \alpha_c \pm \beta_c$.

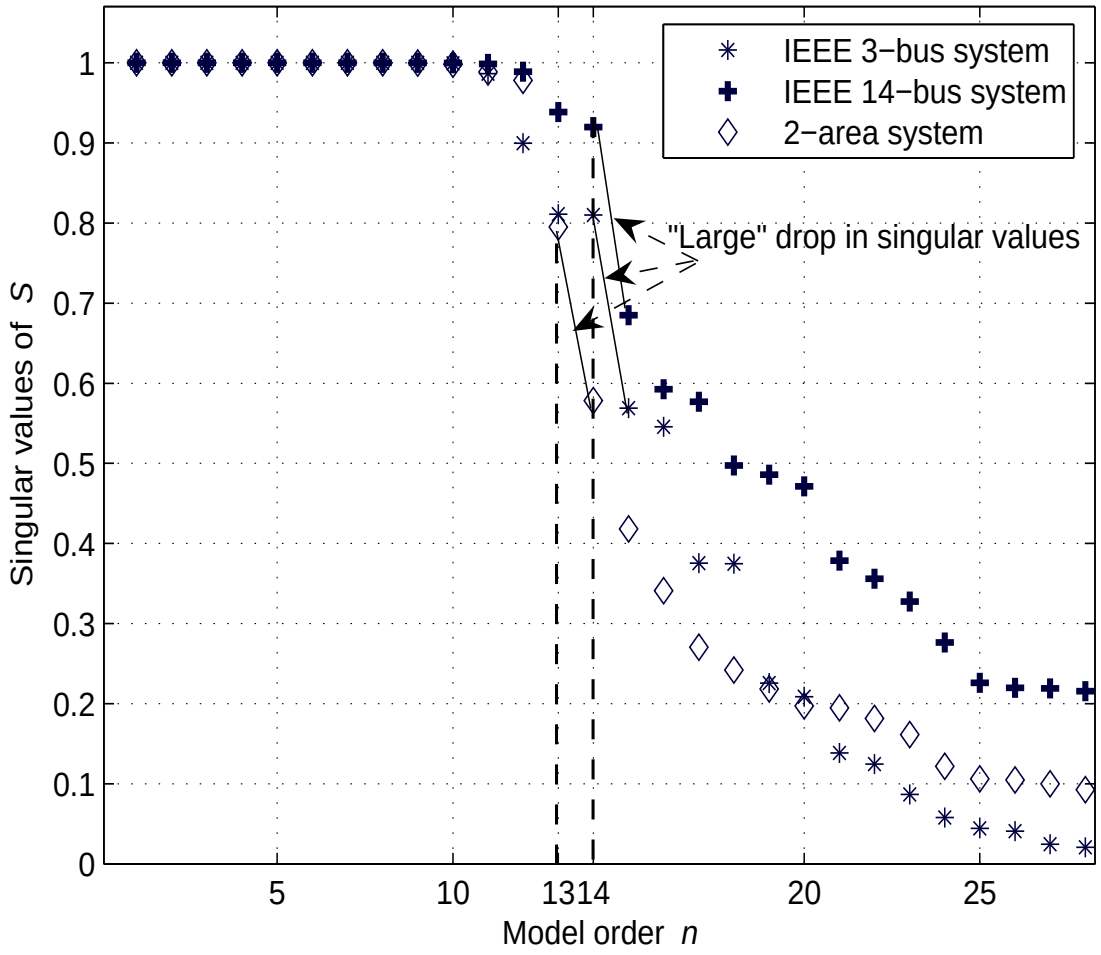

Figure 4.18: Singular values of weighted projection (3.26).

Var limit; notice that no discontinuity was observed in the index, as opposed to SNB indices that usually show discontinuities when control limits are reached [7]. The maximum error between the mean value of the identified and modeled SISI is 0.0121 sec^{-1}, which shows that the proposed identified SISI is a good measure of proximity to oscillatory instabilities.

4.4.2 Two-Area Benchmark System

There is an inter-area mode that eventually crosses the imaginary axis as loads are increased. Generators G_2 and G_3 are rescheduled proportionally to their base power to respond to load increases at Bus 7 and 9. There is an HB point before the nose point as shown in the corresponding P-V curve depicted in Figure 4.21. Loads are modeled as constant PQ loads and are increased with a constant power factor. The inter-area mode, $\mu_c = -0.4204 \pm j4.9123$ (damping 8.53% and frequency 0.7818 Hz), crosses the imaginary axis at about 3100 MW of total loading. The mean value and confidence limit of one standard deviation of the SISI obtained using the proposed identification technique, and the SISI using the linearized transient stability model associated with the inter-area mode are depicted in Figure 4.22; observe the relatively linear profile of these SISIs. As critical mode becomes less damped, it is more likely to capture it accurately, i.e. the method works better for less damped modes, since the oscillations die out slower once the mode is excited. The maximum error between the mean value of the identified and modeled SISI is 0.0462 sec^{-1}, showing the good accuracy of the proposed identification method.

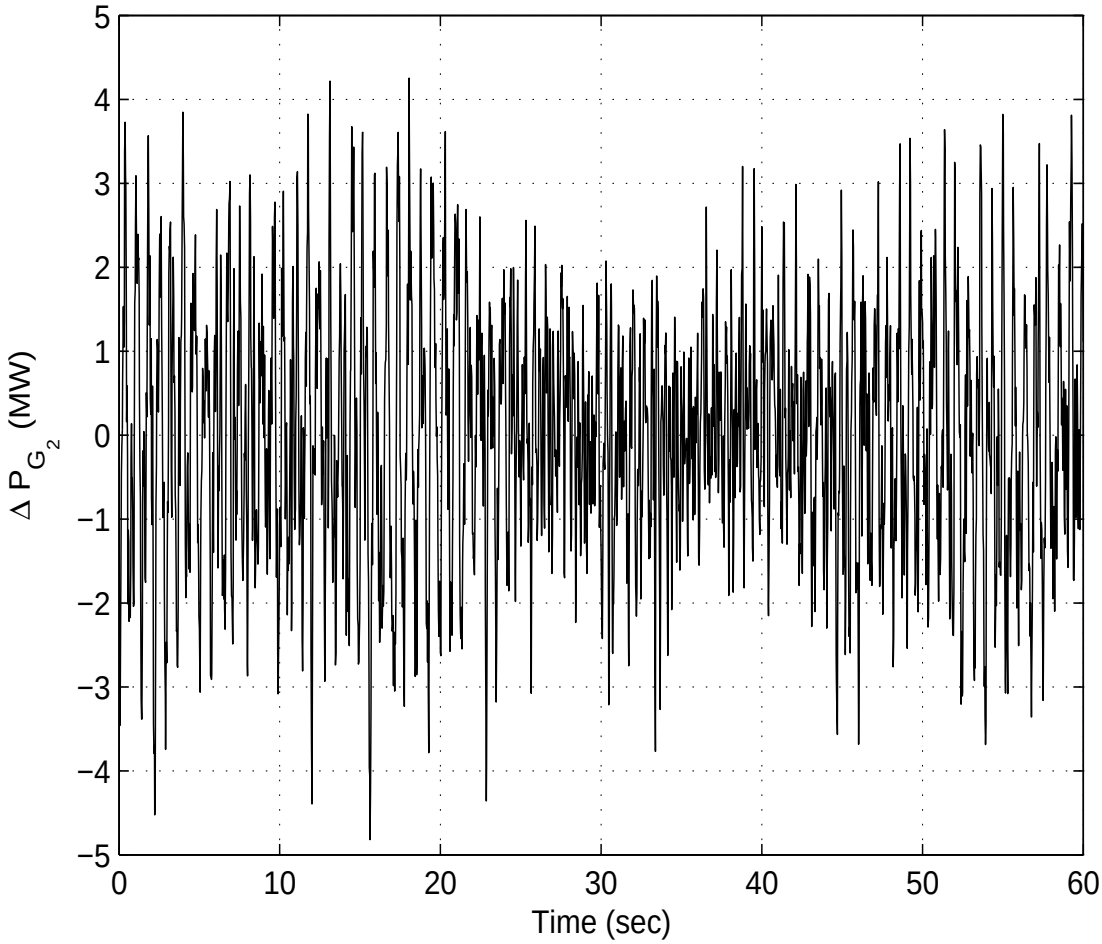

Figure 4.19: One-minute block measurement of the change in generator G_2's power at a 285 MW loading level.

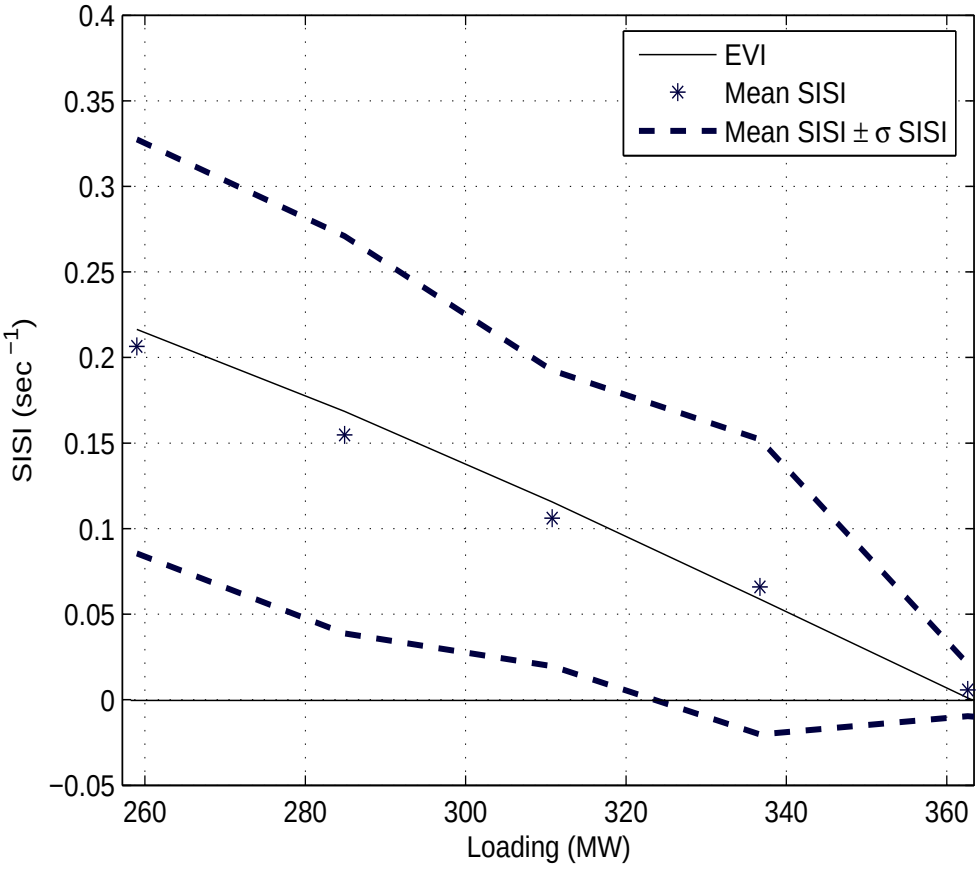

Figure 4.20: SISI for the IEEE 14-bus system obtained with the use of the subspace method.

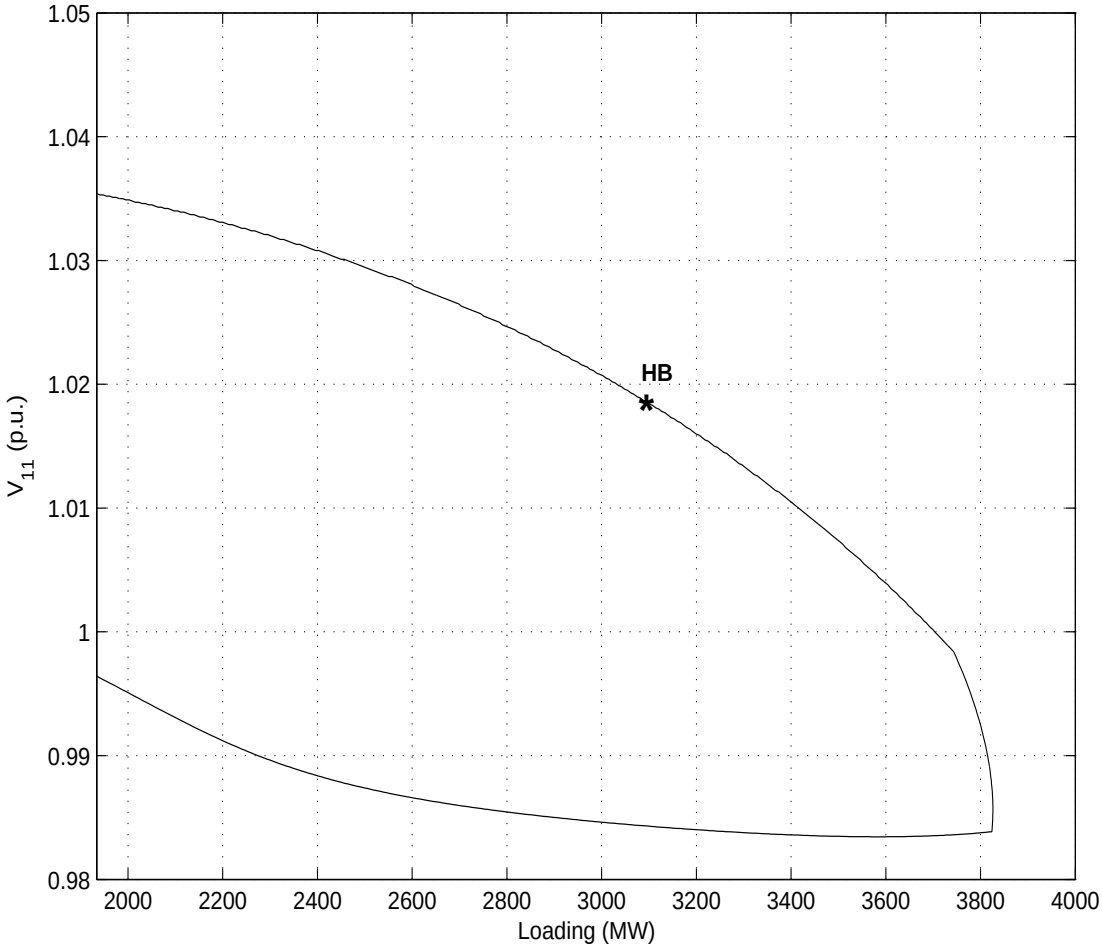

Figure 4.21: P-V curve at Bus 11 for the 2-area benchmark system.

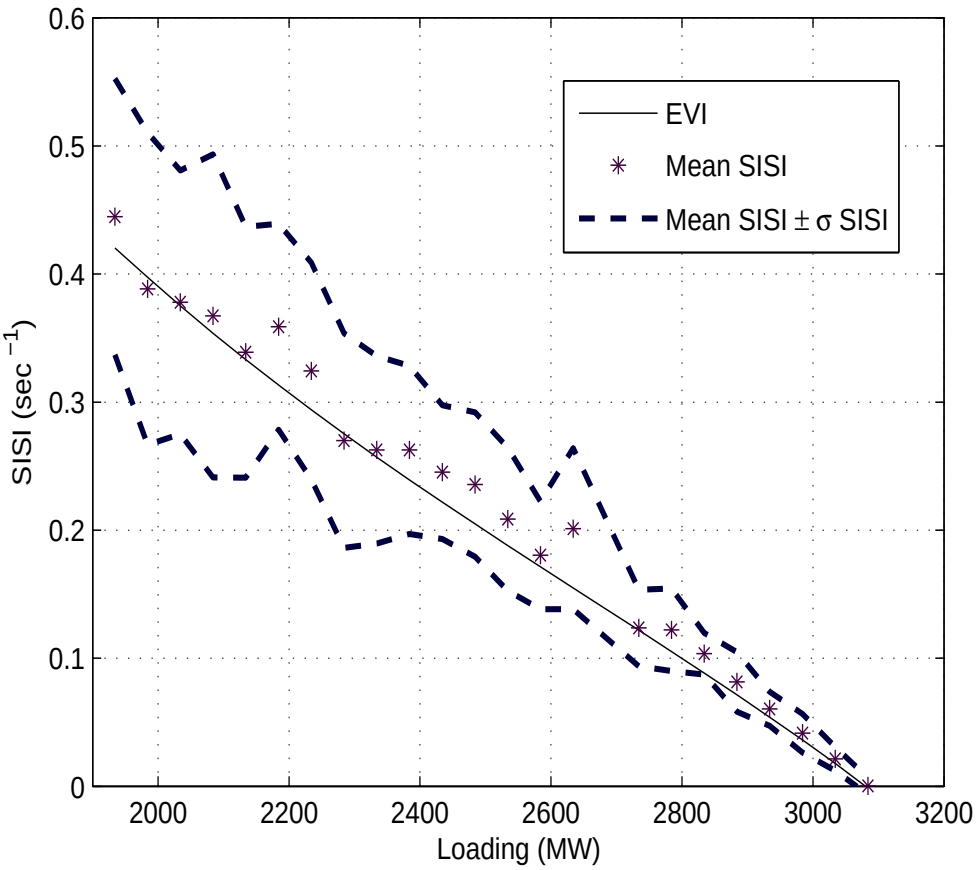

Figure 4.22: SISI for the 2-area benchmark system obtained with use of the subspace method.

4.5 Summary

The stability index proposed in this chapter can be used to determine and predict the closest instability point in a power system with regards to load changes. This index is defined based on the critical eigenvalues detected using system identification; hence, the proposed index is based on the actual response of the system. The feasibility of the index and the proposed identification methods is investigated on several test cases including a 14,000 bus real system, obtaining results which show that it can successfully capture and predict the impending oscillatory stability problems.

The results demonstrate the effect of load models on the identified critical modes, showing that for the system with constant PQ load models, the identified modes are relatively closer to those obtained from an eigenvalue analysis, when compared to the system with constant impedance load models.

Chapter 5

Damping Torque Index

5.1 Introduction

The main obstacle for the stability index SISI in the preceding chapter, as well as with similar off-line indices, is identifying the critical modes in advance, which is not an easy task in some systems. Therefore, in this chapter, another index is proposed, which is also based on the time-domain response, and hence of use in on-line stability monitoring. The new index is defined based on damping torque concepts for the individual generators.

The theoretical background on damping and synchronizing torques is first presented, and the procedure to derive the damping and synchronizing coefficients from a linearized model (LM) of the power system is described. Then, the identification techniques used to estimate the damping coefficient from the transient response of the system are explained. The results of applying the proposed identification methods to calculate the damping torque coefficient are also presented and discussed for a variety of test cases, focusing on the behavior of this coefficient as

a stability/security index. Finally, damping torque estimation from ambient data is discussed and an effective identification method is proposed.

5.2 Damping and Synchronizing Torque

The concept of damping and synchronizing torques for a single-machine-infinite-bus (SMIB) system was first introduced in [35]. Thus, electromechanical torque T_e deviations of a machine can be expressed in terms of its speed ω and angle δ deviations, known as damping and synchronizing torque, respectively. The damping and synchronizing torques are the in time phase components proportional to the speed and angle deviations [64], and are defined as:

$$\Delta T_e(t) \;=\; \underbrace{K_d\,\omega_0\,\Delta\omega(t)}_{\text{damping}} \;+\; \underbrace{K_s\,\Delta\delta(t)}_{\text{synchronizing}} \tag{5.1}$$

or in the frequency domain:

$$\Delta T_e(s) \;=\; (K_d \;+\; \frac{K_s}{s}\,)\,\omega_0\,\Delta\omega(s) \tag{5.2}$$

where K_d (p.u./rad/sec) and K_s (p.u.) are damping and synchronizing coefficients, respectively; and ω_0 (rad/sec) is the system angular frequency. The generator's angle and speed deviations in (5.1) are typically measured with respect to a center of inertia (COI), i.e. $\delta_i = \hat{\delta}_i - \delta_{COI}$ and $\omega_i = \hat{\omega}_i - \omega_{COI}$, where

$$\begin{aligned} \delta_{COI} &= \frac{1}{M_T}\sum_{i=1}^{g} M_i\hat{\delta}_i \\ \omega_{COI} &= \frac{1}{\omega_0}\frac{d\delta_{COI}}{dt} \end{aligned} \tag{5.3}$$

and $M_T = \sum_{i=1}^{g} M_i$ is the total inertia of the g generators.

Since $\omega_0 \Delta\omega(t) = d\Delta\delta(t)/dt$, or in discrete form $\omega_0 \Delta\omega[k] = (\Delta\delta[k] - \Delta\delta[k-1])/T_s$, where T_s is the sampling time, one can rewrite (5.1) as:

$$\Delta T_e[k] = \xi \, \Delta\delta[k-1] + \zeta \, \Delta\delta[k] \tag{5.4}$$

where $\xi = -K_d/T_s$ and $\zeta = K_d/T_s + K_s$. Equation (5.4) can be used to calculate ξ and ζ from sampled signals, thus yielding K_d and K_s. Using (5.4), which only requires two signals T_e and δ, as opposed to (5.1), which requires three signals T_e, ω and δ, reduces the errors due to mean value and low frequency trends in the measured signals, due to the effect of the governor's response.

For a single-machine-infinite-bus (SMIB) system, the synchronizing and damping coefficients correctly define the frequency and damping of the electromechanical mode. However, for a multi-machine power system, the electromechanical oscillations contain different modes, and hence a single mode cannot simply be assigned to a single machine [65], since the oscillations of each machine are a linear combination of all the modes. Hence, in this case, one must be aware that the damping coefficient of a given machine includes the effect of several modes.

5.2.1 Damping and Synchronizing Coefficients

In the linear model (4.3), let assume that only the i^{th} mode of the system $\lambda_i = \alpha_i + j\beta_i$ is excited by an initial condition x_0 in the direction of right eigenvector U_i associated with λ_i. Hence, any output $y_k(t)$ can be expressed as $y_k(t) = C_k U_i e^{\lambda_i t}$, or $y_k(s) = C_k U_i/(s - \lambda_i)$ where C_k is the k^{th} row of C. In this case, one may write the following relationship between the speed and electrical torque of machine j, defined as D_j:

$$D_j \;=\; \frac{\Delta T_{e_j}(t)}{\Delta\omega_j(t)} \;=\; \frac{\Delta T_{e_j}(s)}{\Delta\omega_j(s)} \;=\; \frac{C_{T_{e_j}} \, U_i}{C_{\omega_j} \, U_i} \tag{5.5}$$

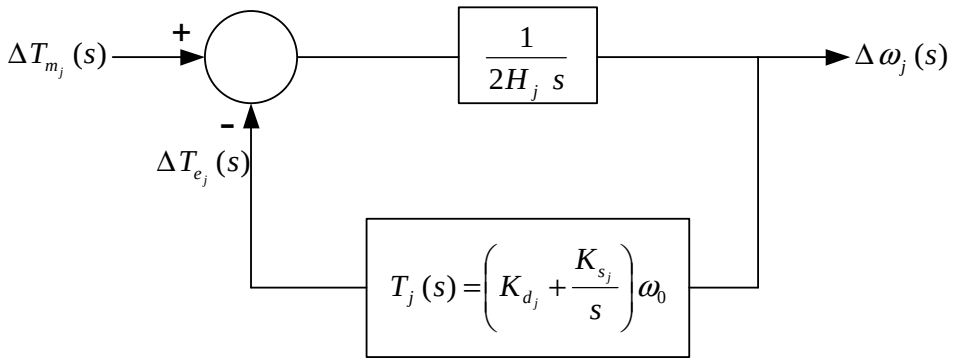

Figure 5.1: Torque-speed block diagram.

This ratio is a complex number, i.e. $D_j = D_{R_j} + jD_{I_j}$ and can be calculated using a state-space model. Thus, from (5.2) and (5.5),

$$\begin{aligned} K_{d_j} &= \frac{\left[\frac{\alpha_i\, D_{I_j}}{\beta_i} + D_{R_j}\right]}{\omega_0} \\ K_{s_j} &= \frac{-D_{I_j}\,|\lambda_i|^2}{\omega_0 \beta_i} \end{aligned} \tag{5.6}$$

This K_{d_j} and K_{s_j} coefficients may be used in the torque-speed block diagram for a given generator, as depicted in Figure 5.1. This system is stable if both K_{d_j} and K_{s_j} are positive, and becomes oscillatory instable at an operating condition where $K_d = 0$ (HB point). Hence, K_d may be used as an index to predict the closest oscillatory instability. In this work, K_d is referenced to as the damping torque index.

It is worth mentioning that the K_d and K_s coefficients presented here are different from the damping and synchronizing coefficients discussed in [6, 66], since in these references, these coefficients are defined by disabling the shaft dynamics in all generators, which is not the case here. This point is more clearly explained in Appendix C, which presents another approach to calculate (5.5).

5.2.2 Electromechanical Mode Estimation

The characteristic equation corresponding to the block diagram depicted in Figure 5.1 can be mathematically expressed as

$$\frac{2H_j}{\omega_0}\, s^2 + K_{d_j}\, s + K_{s_j} = 0 \tag{5.7}$$

The roots of the characteristic equation may be used to estimate the damping and the frequency of the electromechanical mode. Although this is true if oscillations consist of only one mode, it may still be used when several modes are present but one is more dominant. However, the estimates in this case will not be accurate due to under-parameterization of a system of order $n \geq 2$ when represented by a second order system. Thus, if several strong modes are dominant in the response, in order to correctly capture all of the modes, the linear parametric models, such as the ARMA model or the state-space model explained in Chapter 3, have to be employed instead.

The main application of using K_d, as explained before, is predicting the available stability margin without the need to monitor certain modes. However, it can also be used to provide information about the poorly damped local or sometimes inter-area modes, and hence re-tuning the controllers such as PSSs.

5.3 Techniques

5.3.1 Ordinary Least Square (OLS)

Damping and synchronizing coefficients in (5.1) can be estimated using an ordinary least square (OLS) method [64]. It is basically a fitting problem which can be

described as:

$$\begin{aligned} Y &= [\Omega \quad \Delta]\ K + \epsilon \\ &= X\ K + \epsilon \end{aligned} \tag{5.8}$$

where $Y = \left[T_e[1]\ T_e[2]...\ T_e[N]\right]^T \in \Re^N$; $\Omega = \omega_0 \left[\Delta\omega[1]\ \Delta\omega[2]...\ \Delta\omega[N]\ \right]^T \in \Re^N$; $\Delta = \left[\Delta\delta[1]\ \Delta\delta[2]...\ \Delta\delta[N]\right]^T \in \Re^N$; $\epsilon \in \Re^N$ represents "residuals" introduced to account for fitting errors and measurement noise; $K = [K_d\ K_s]^T$; and N is the number of samples. The ordinary least square estimate can be obtained as:

$$\hat{K}_{OLS} = (X^T X)^{-1} X^T Y. \tag{5.9}$$

Here, $\hat{K}_{OLS}$ is unbiased, efficient (or Markov estimate), and consistent when ϵ is white noise with zero mean [67]. Furthermore, it is also identical to the maximum likelihood estimator when ϵ is normally distributed. However, the condition of whiteness for the current application is not guaranteed, thus $\hat{K}$ might be biased. This will be clearly shown here in a number of case studies.

5.3.2 Generalized Least Square (GLS)

From the system identification point of view, (5.8) can be represented as follows:

$$y[k] = x[k]\ K + H(q)\ e[k] \tag{5.10}$$

where $e[k]$ is white noise, $H^{-1}(q)$ is a whitening filter, and q is the shifting operator defined by $q^{-1}y[k] = y[k-1]$.

Selecting a proper candidate model set in this case, which includes the true model, is an essential aspect to obtain accurate parameter estimates. On the other hand, over-parameterization can lead to high computational costs as well as numerical problems (e.g. convergence and local minima). Therefore, one should search

for a model set that includes the true model with as low number of parameters as possible. It is also important to consider that choosing a rather simple model, i.e. under-parameterization, might lead to inaccurate parameter estimates [59].

The candidate model (5.10) with $H(q) = 1$, which leads to (5.9), is not a general model and may not correctly represent the power system dynamics. For example, when the perturbations are large and hence the linearity assumption does not hold, the OLS estimates can lead to erroneous results. Experience shows that by adding a transfer function such as $H(q) = 1/(1 + h_1 q^{-1} + h_2 q^{-2} + ... + h_p q^{-p})$ with $p = 1$ or 2, good results can be obtained [67]. This method is also known as generalized least square (GLS) and can be used to correctly model the residuals or filter the nonlinear effects. In this case, K along with the parameters of the whitening filter are denoted as θ, and are estimated using PEMs. These methods are basically based on an optimization problem such as:

$$\begin{aligned} Min \quad V(\theta) &= \frac{1}{N}\sum_{k=1}^{N}\frac{1}{2}\epsilon^2[k] \\ s.t. \quad \epsilon[k] &= H^{-1}(q)\ \{y[k] - x[k]\ K\} \end{aligned} \tag{5.11}$$

5.3.3 Robust Fitting with Bisquare Weights (RFBW)

Robust fitting may also be employed as another remedial method for handling the nonlinear effects, which can occur due to large deviations from an operating point. This method is basically an iterative weighted least square (WLS) method, and is able to give different weights to each residues during the fitting process; data with lower quality are given less weight, since the part of the signal that is distorted due to the nonlinear effects is hard to fit, and hence should be less important in the estimation process. One may consider using small perturbations as a way to avoid

nonlinearities; however, in the current application, small disturbances may not be feasible, since the perturbations have to be large enough to be distinguished from measurement noise.

Robust fitting employs the following objective function, which assigns weights to different predicted errors:

$$Min \quad V \quad = \quad \frac{1}{N}\sum_{k=1}^{N} w_k \, \epsilon^2[k] \tag{5.12}$$

The estimated damping and synchronizing coefficients in this case are:

$$\hat{K}_{WLS} \quad = \quad (X^T \, W \, X)^{-1} X^T \, W \, Y. \tag{5.13}$$

where $W = diag\{w_1, w_2, \ ... \ , w_N\} \in \Re^{N \times N}$. There are different weights which can be utilized in the objective function (5.12) [68]; in this work, bisquare weights are used. This method has been previously used in economics to decrease the sensitivity of least square to "extreme" values called *outliers*.

5.4 Damping Torque Estimation from Transient Response

For various test cases, the damping torque index is calculated here by means of the previously mentioned techniques. Similar to the eigenvalue index SISI, the feasibility of using K_d for different types of signals known as ringdown data (transient response) or ambient data (noise) is addressed. The signals are recorded with the same specifications mentioned for the eigenvalue index SISI; however, in addition to the generator power signal, generator angle or speed have to be measured. The behavior of the index, as the system loading changes, is depicted for each case, illustrating its capability to predict the closest stability margin.

The electromechanical torque and generator angle of each generator following a large disturbance, such as a line outage or a three phase fault, are recorded so that it contains at least three periods of oscillations. Then, the measurement noise is removed with a Chebyshev low pass filter with a cut off frequency of 2 Hz, and then re-sampling the signal at 10 Hz. The mean and low frequency trends of the measured signal have to be also removed.

5.4.1 Single-Machine-Infinite-Bus (SMIB)

The generator in the simple test system depicted in Figure 2.7 was modeled using a subtransient model. There is an electromechanical mode, which moves toward the RHP, as the load increases from 100 MW to 700 MW, resulting in an increase in tie-line power as well as a gradual decrease in the generator's damping coefficient K_d. The results obtained for "theoretical" and estimated values of K_d are shown in Figure 5.2; observe that all the identification methods were able to correctly calculate K_d. However, for heavy loads, the different values for K_d obtained from the various methods used coincide, which is to be expected, since at light loading conditions the mode is well-damped. This is akin to the case when eigenvalues are to be identified using the time-domain response of the system, as reported in [23].

5.4.2 Two-area Benchmark System

The single line diagram of the two-area benchmark system used here is shown in Figure 2.10. There is an inter-area mode and two local modes that change as the loads are increased. Depending on the load and dispatch scenarios, one could expect to have different eigenvalue profiles. For instance, in this system, two dispatch scenarios, Schedules 1 and 2, result in fairly different eigenvalue profiles,

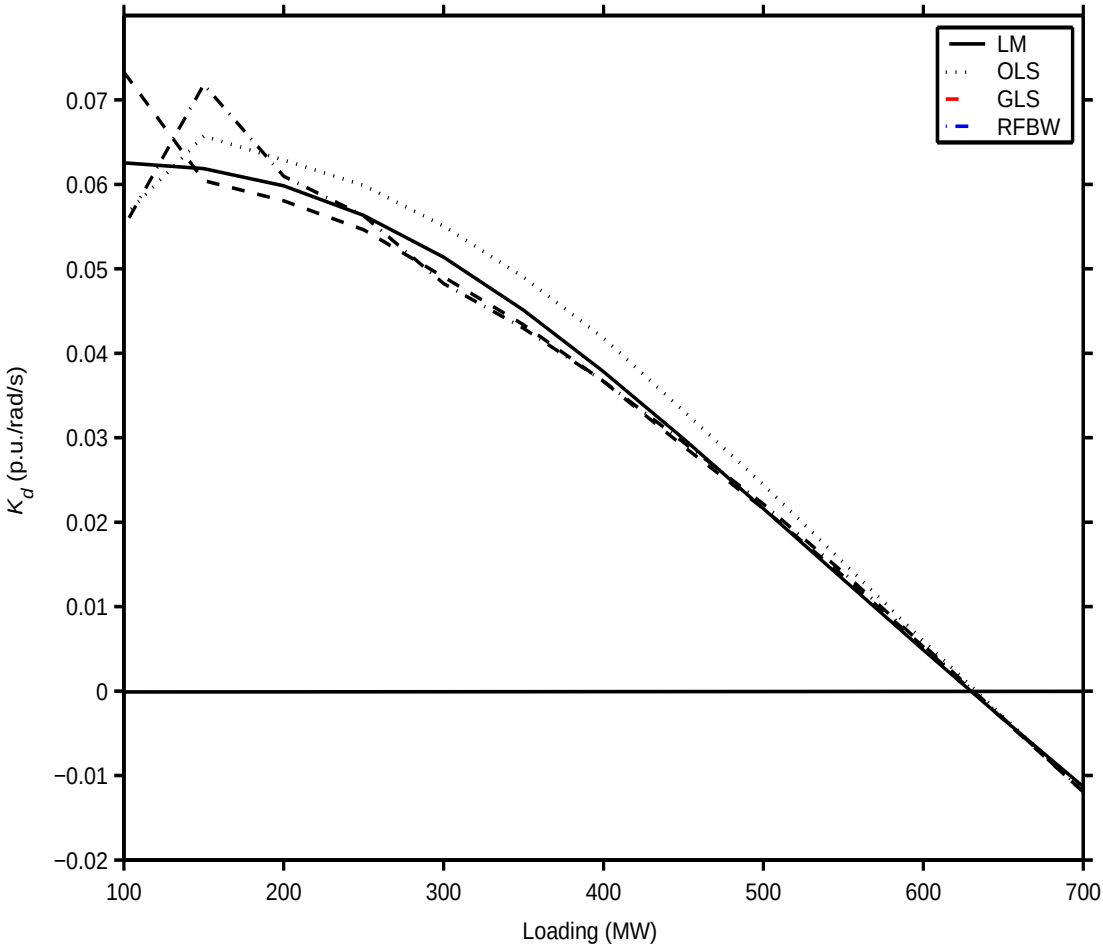

Figure 5.2: Damping coefficient K_d from transient response for the SMIB.

as depicted in Figure 5.3. There is an HB point before the nose point, as shown in the corresponding P-V curves depicted in Figure 5.4.

Schedule 1

This dispatch results in the inter-area mode becoming unstable as loading increases. In this case, generators G_2 and G_3 are dispatched proportionally to their base power as the loads at Bus 7 and 9 increase. Loads are modeled as constant PQ loads and are increased with a constant power factor. The inter-area mode becomes unstable at a loading level of about 3050 MW. This can also be observed clearly in Figure 5.5, which depicts the theoretical and estimated values of K_d for this case study. Observe that all the calculated K_d's tend to zero as the load increases; however, the GLS method offers superior performance in terms of predicting the HB point, since the estimates are fairly close to the theoretical values.

Schedule 2

Schedule 2 is an interesting dispatch scenario where the inter-area mode is primarily the critical one, until at certain loading level (3030 MW), the local mode in Area 2 becomes critical, crossing the imaginary axis and hence leading the system to oscillatory instability conditions at a loading level of about 3150 MW. In this case, the loads are increased as in Schedule 1; however, only Generator G_3 is dispatched to respond to the load change. This certainly stresses G_3 more, and thus the local mode in Area 2 becomes critical, as shown in Figure 5.3.

For this scenario, it is possible to compute two values of K_d using (5.6) which are associated with the inter-area mode and the local mode in Area 2, as depicted in Figure 5.6. Since both inter-area and local mode in Area 2 are dominant modes,

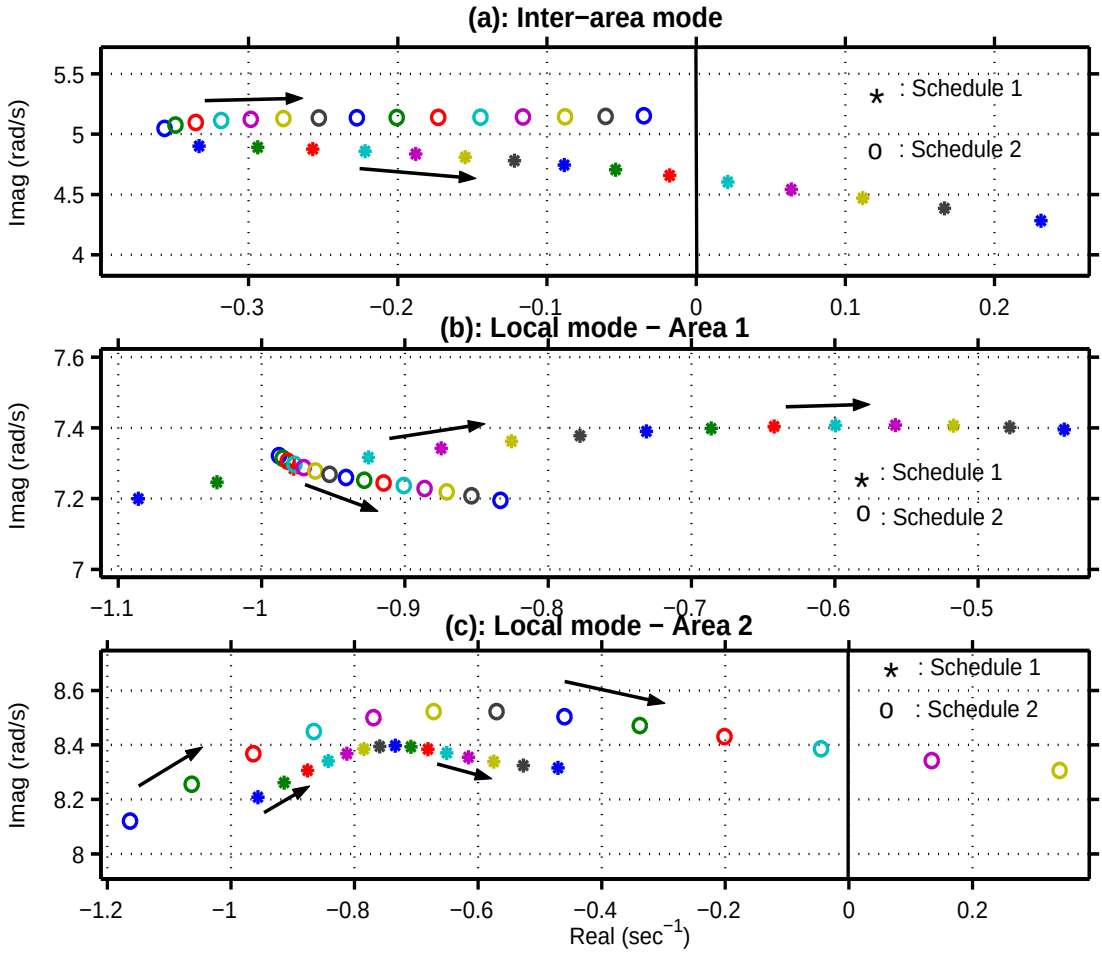

Figure 5.3: Eigenvalue profiles for different dispatch scenarios; Schedules 1 and 2.

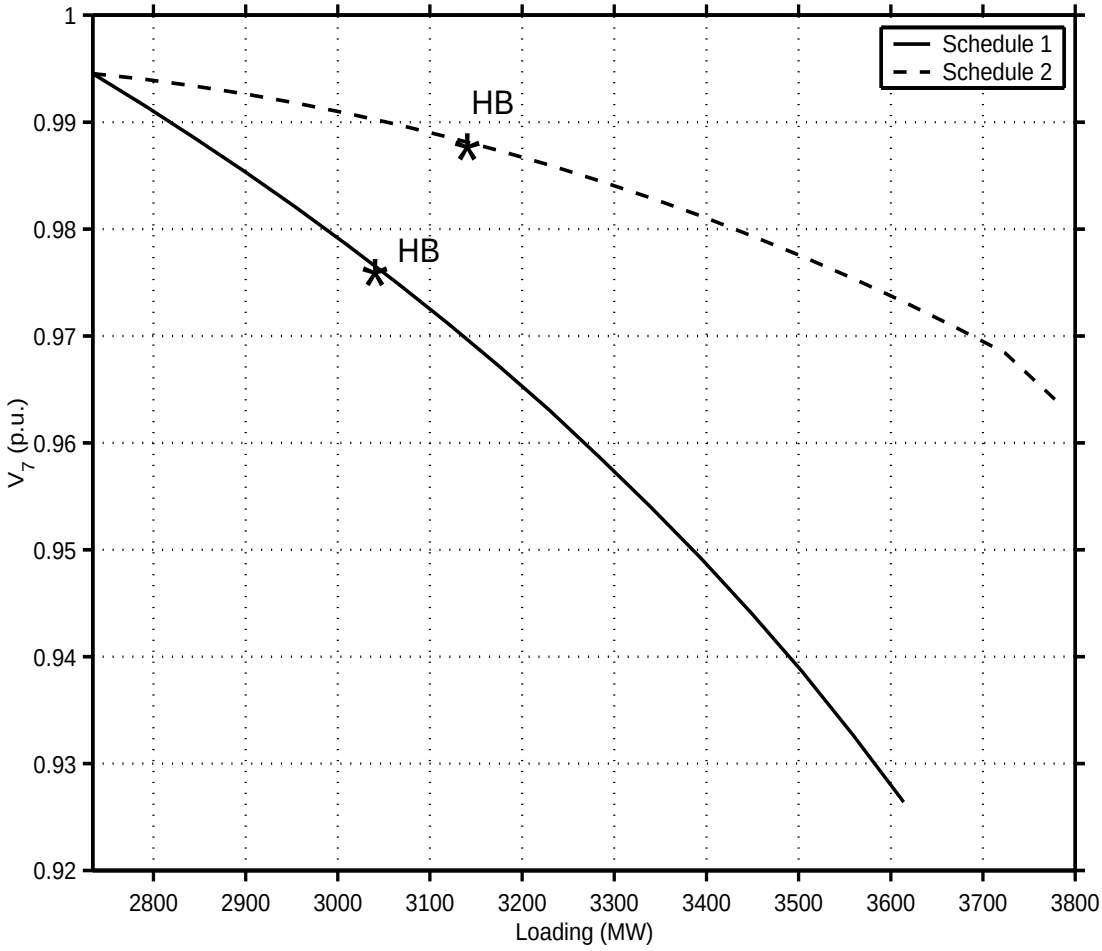

Figure 5.4: P-V curves at Bus 7 for the 2-area benchmark system.

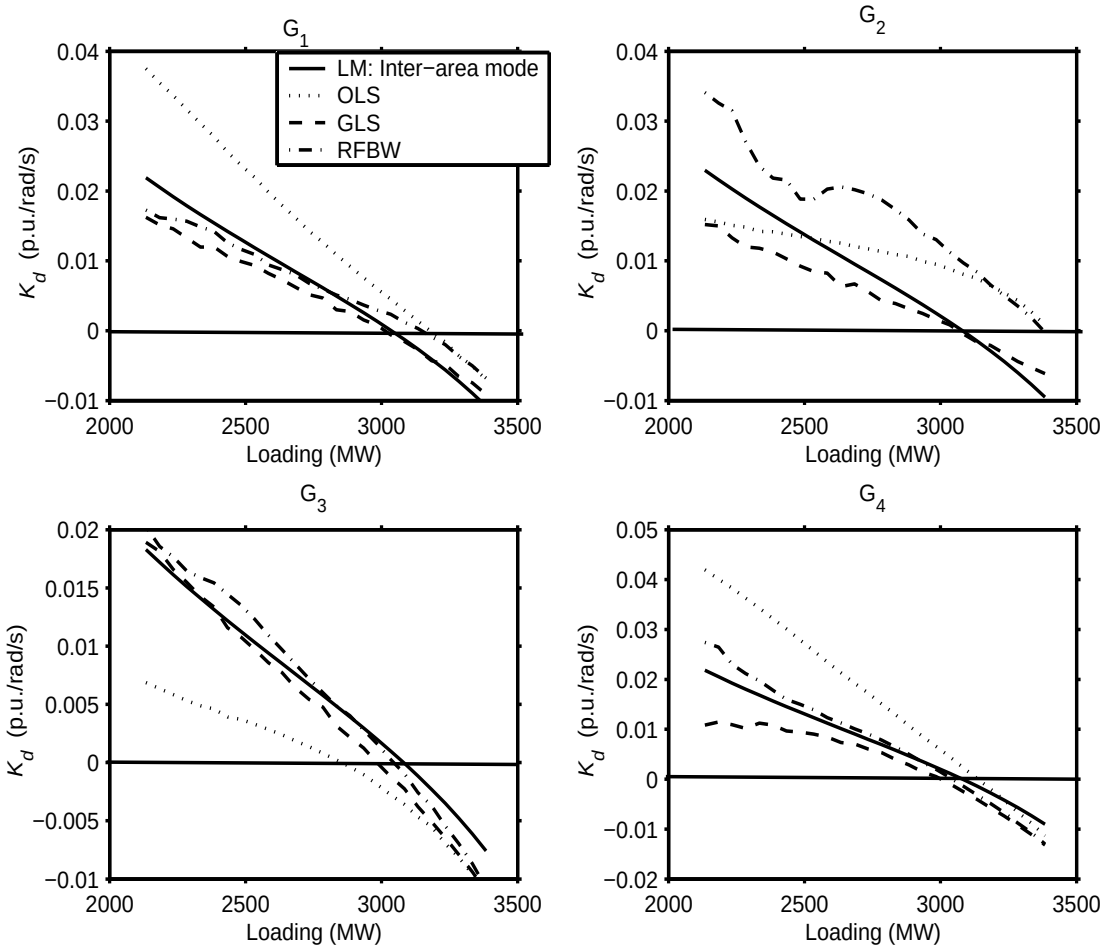

Figure 5.5: Damping coefficients of all generators obtained from transient response for the 2-area benchmark system for Schedule 1.

time-domain simulation results in this case would be influenced by both of them, and so would be the identified K_d's. Notice that in this case, the values obtained for K_d from OLS are not accurate; neither are the predicted stability margins. On the other hand, the K_d's obtained using GLS present the best results in terms of accuracy in estimation as well as prediction. The RFBW's accuracy is between the OLS and GLS, and from the computational point of view, it is slower than OLS and faster than the GLS. The advantage of using K_d, when compared to eigenvalue based indices, is that, in order to monitor system stability/security margin, the damping coefficient is able to provide accurate margins without the need for monitoring particular modes. This can be an issue for eigenvalue-based indices. For instance, the damping torque is able to capture the oscillatory phenomenon for both schedules; on the other hand, for Schedule 2, if only the inter-area mode were used as an index, it would yield inaccurate margins.

5.4.3 Real System (14,000 buses)

There are around 2000 generators and 22 areas in this system, and hence only the slack generators in some areas are monitored. The areas are selected by looking at the mode shape corresponding to the critical mode. The critical mode moves to the RHP with respect to load change, resulting in unstable oscillations triggered by a line outage as shown in Figure 5.7. Figure 5.8 depicts the K_d for the slack buses in four different areas where the critical mode is highly observable. Observe that only some of the generators are able to successfully predict the oscillatory phenomenon, indicating the importance of employing several monitoring units in different parts of the system.

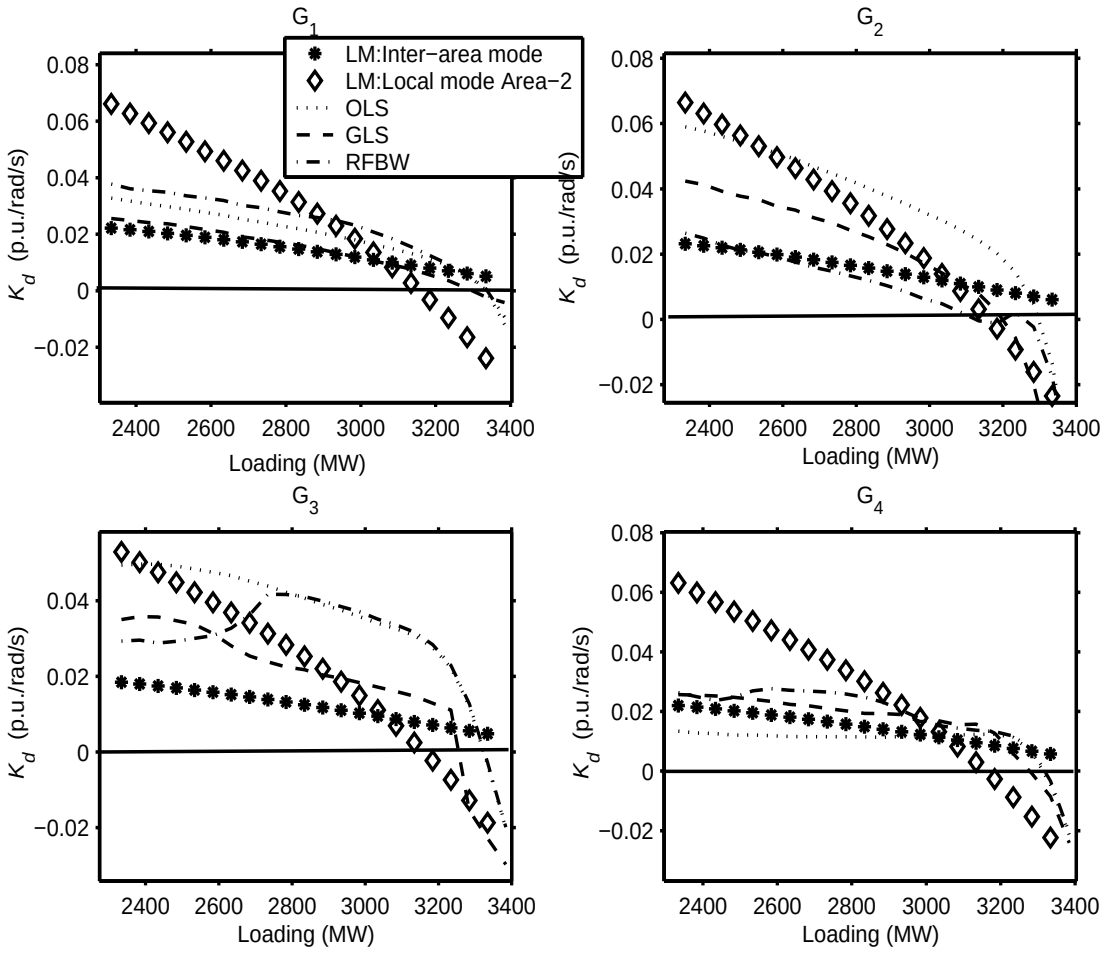

Figure 5.6: Damping coefficients of all generators obtained from transient response for the 2-area benchmark system for Schedule 2.

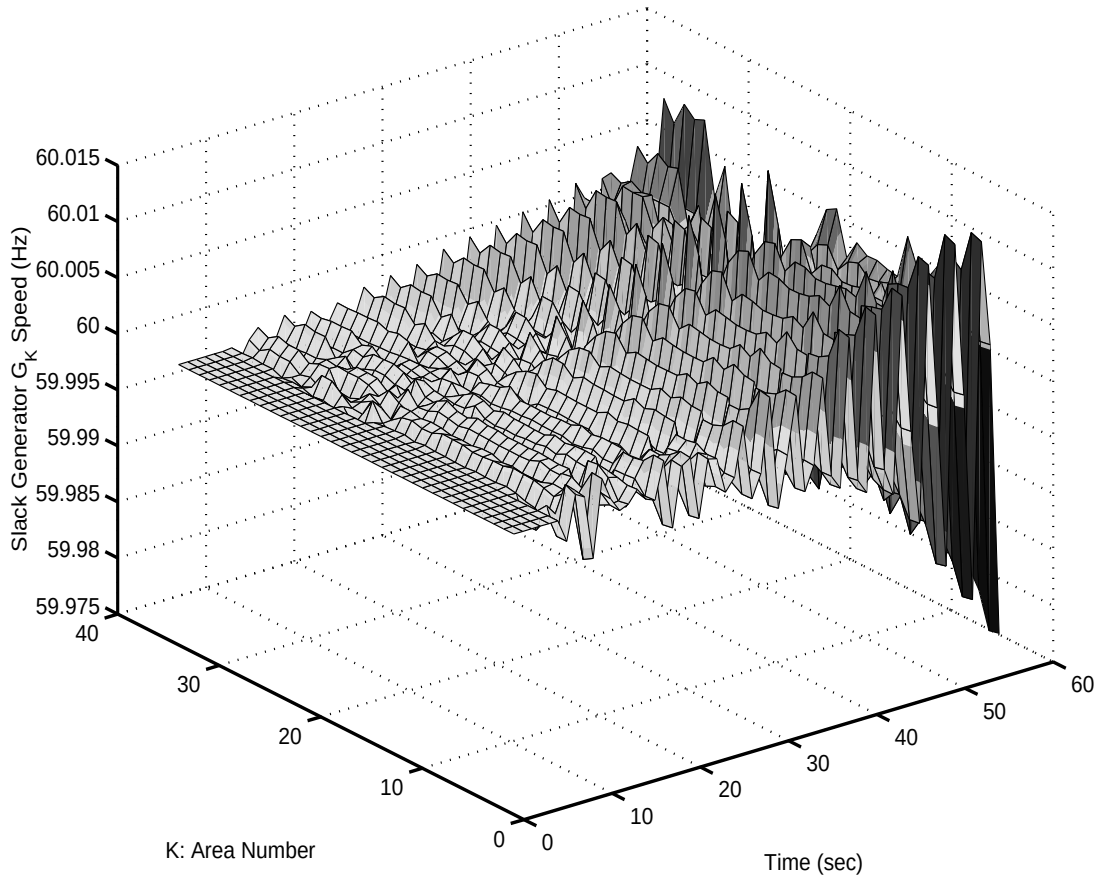

Figure 5.7: Generator speed oscillations due to the trigger of the unstable electromechanical mode in the 14,000-bus real system.

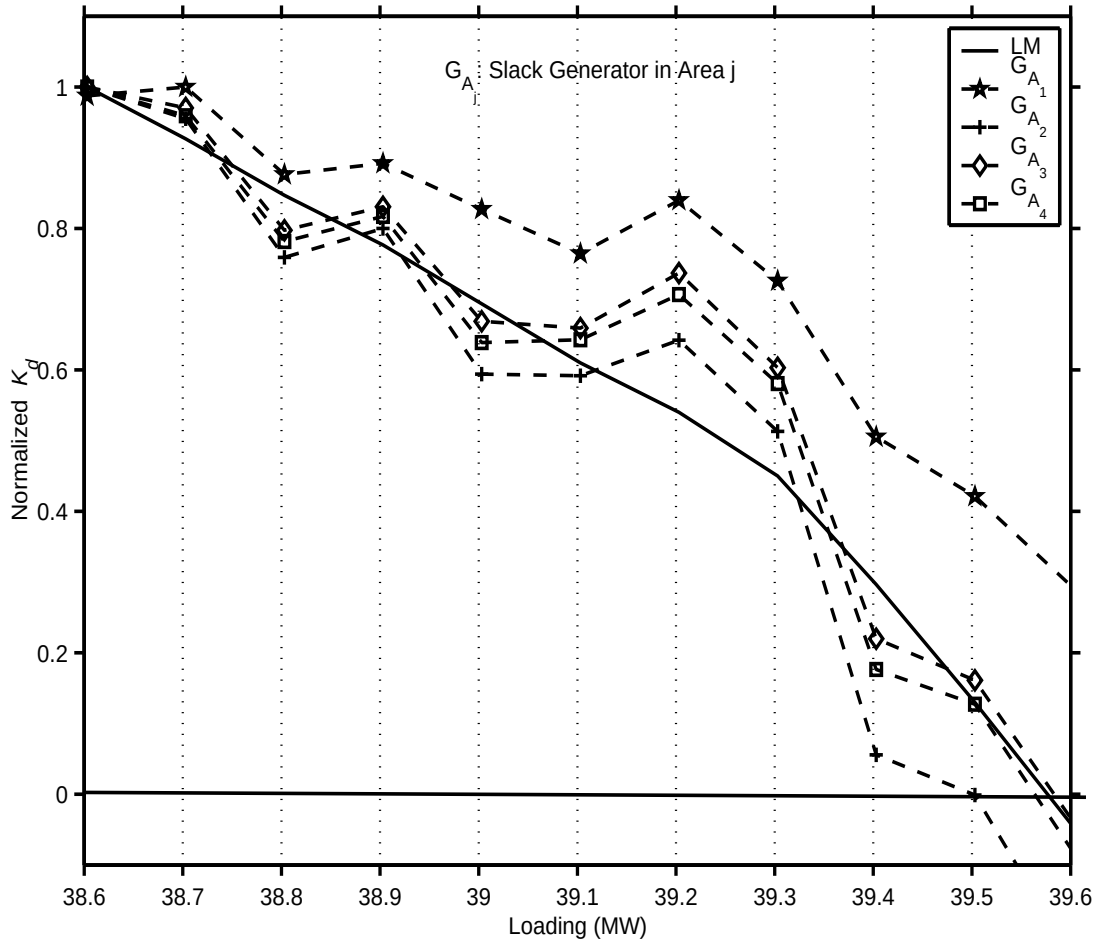

Figure 5.8: Damping coefficients of slack generators in different areas for the 14,000-bus real system.

5.5 Damping Torque Estimation from Ambient Data

For the following test cases, it is assumed that the system is persistently being excited by random load switching, and hence the measured signal of the system is a colored noise. The advantage of using this kind of signals is twofold: There is no need to carry on expensive, risky, intrusive tests; second, the linearity assumption due to the small magnitude of the perturbations holds.

5.5.1 Box-Jenkins Model

Experience shows that RFBW yields results similar to OLS, because the perturbations are small, and the problem of nonlinear effects does not show up in the measured response. However, due to the persistent excitation of different modes, the whitening filter in this case is more complicated.

As explained in Section 5.3.2, for the transient response of the system, GLS is used to model the correlated residuals; notice that the residuals were modeled by means of an AR(p). Since the objective is to obtain white $\epsilon[k]$, and considering the fact that the first term on the right side of (5.10) ($x[k]$ K) cannot be changed, it would be beneficial to use a Box-Jenkins model. This model provides a parametric model with errors being modeled separately from the first term that is related to the system dynamics. The error term properties are modeled by a rational transfer function $H(q)$ with both numerator and denominator; thus, (5.10) can be written

as:

$$y[k] = x[k]\ K + H(q)\ e[k] \tag{5.14}$$

$$H(q) = \frac{1 + c_1\ q^{-1} + c_2\ q^{-2} + \ldots + c_{n_c}\ q^{-n_c}}{1 + d_1\ q^{-1} + d_2\ q^{-2} + \ldots + d_{n_d}\ q^{-n_d}} \tag{5.15}$$

This model is known as a Box-Jenkins (BJ) model and is denoted by BJ(n_c,n_d). The BJ model in this case is indeed employing an ARMA(n_c,n_d) in order to correctly model the residuals. The orders n_c and n_d can be selected by means of AIC or FPE. For instance, the FPE can be computed as:

$$\text{FPE} = V(\theta)\ \frac{1 - \frac{\kappa}{N}}{1 + \frac{\kappa}{N}} \tag{5.16}$$

where $\theta = [K^T\ c_1\ c_2\ ...\ c_{n_c}\ d_1\ d_2\ ...\ d_{n_d}]^T$ and $\kappa = dim(\theta)$. It is worth mentioning that for large data blocks, i.e. $N \longrightarrow \infty$, the FPE is the same as the loss function $V(\theta)$, which is the case for ambient data; and therefore, $V(\theta)$ can be used instead of FPE.

5.5.2 Two-area Benchmark System-Schedules 1 and 2

For the 2-area benchmark system explained in detail in Section 5.4.2, two previously defined dispatch scenarios (Schedules 1 and 2) are investigated, where 1% of the loads at Buses 7 and 9 are being switched as driving noise. The BJ(n_c,n_d) model for each case is utilized to estimate the damping torque; the optimum order is selected by inspecting the loss function of models for a given range of n_c and n_d. First, a range is selected for n_c and n_d, thus resulting in models with different orders; for each case, the corresponding BJ model as well as the loss function $V(\theta)$ are then estimated. Usually, as the order is increased, after a certain point which is related to the optimum order, no significant reduction in $V(\theta)$ is achieved. The

parsimony principle [58] has to also be taken into consideration, which suggests selecting the simplest model of all the models that can accurately describe a system. Furthermore, from an optimization point of view, adding more MA terms results in more complexity and nonlinearity, as the corresponding regressor is not linear; thus, parameter estimation would be significantly easier for smaller n_c's.

For instance, Figures 5.9 and 5.10 suggest BJ(1,2) for Schedule 1, and BJ(2,5) for Schedule 2. Only an inter-area mode is dominant for Schedule 1, as opposed to Schedule 2; consequently, Schedule 1 needs a simpler model to describe the residuals.

The predicted errors $\epsilon[k]$ may also be examined to check the whiteness assumption, which in turn, leads to efficient estimates as explained in Section 5.3.1. The typical whiteness test is inspecting the sample autocorrelation function ACF ($r_\epsilon[\tau]$), i.e. for $\epsilon[k]$ to be white, $r_\epsilon[\tau] = 0$ for $\tau \neq 0$. Usually, the standard deviations obtained via Barttlet's approximation [69] are used to test the hypothesis, i.e. the whiteness is rejected if the sample $r_\epsilon[\tau]$ falls out of the, for instance, 95% confidence interval. For a selected model, if the whiteness test indicates that $\epsilon[k]$ is correlated, then one needs to reexamine the model and data, and search for a statistically better model.

A close inspection of the ACF for both schedules demonstrate the ability of using BJ models in obtaining white residuals as depicted in Figures 5.11 and 5.12. As well, the confidence interval of the estimated K_d's must be checked to ensure that it does not experience a significant increase, as the order of the filter $H(q)$ increases. For instance, in Schedule 1, the standard deviation of the K_d and K_s for various filter models are depicted in Figure 5.13, showing that the standard deviation of the K_d for the selected model, BJ(1,2), is relatively close to that of the BJ(0,0) or OLS.

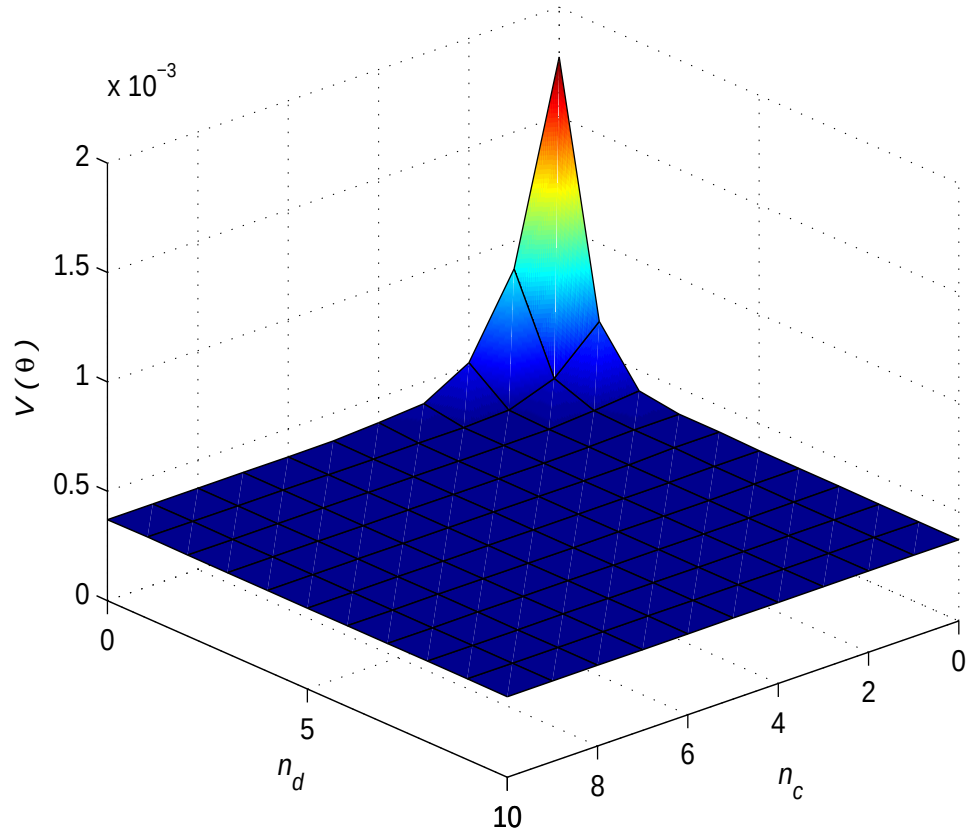

Figure 5.9: Loss function for the BJ(n_c,n_d) model in the 2-area benchmark system; Schedule 1.

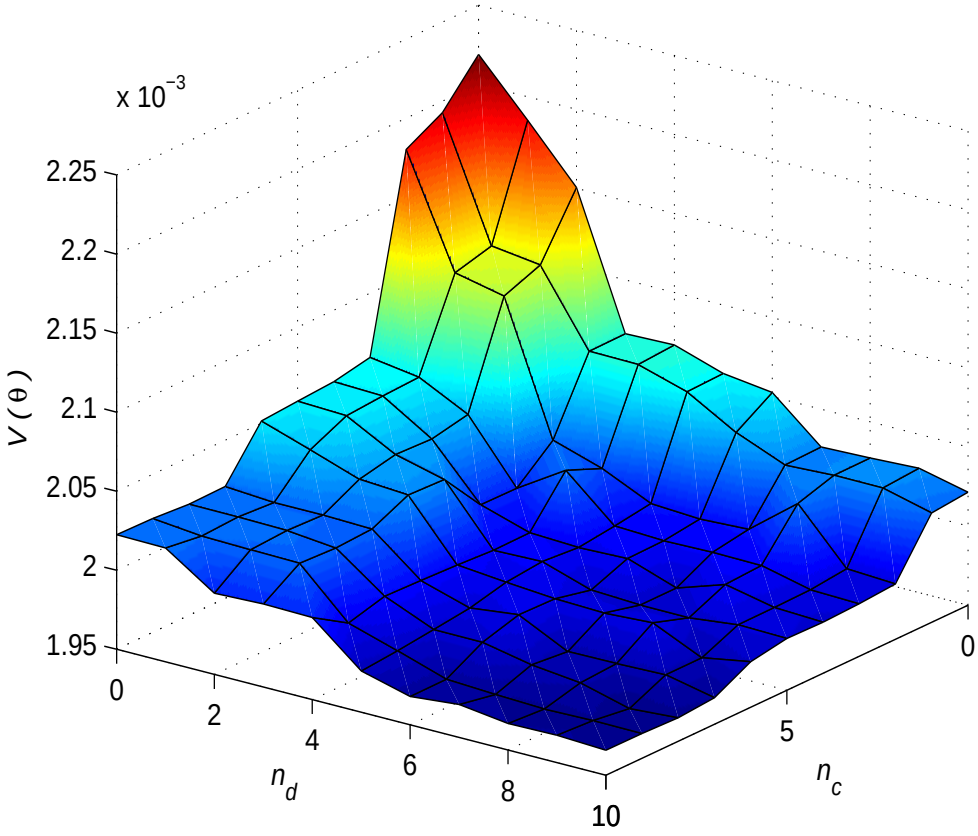

Figure 5.10: Loss function for the BJ(n_c,n_d) in the 2-area benchmark system; Schedule 2.

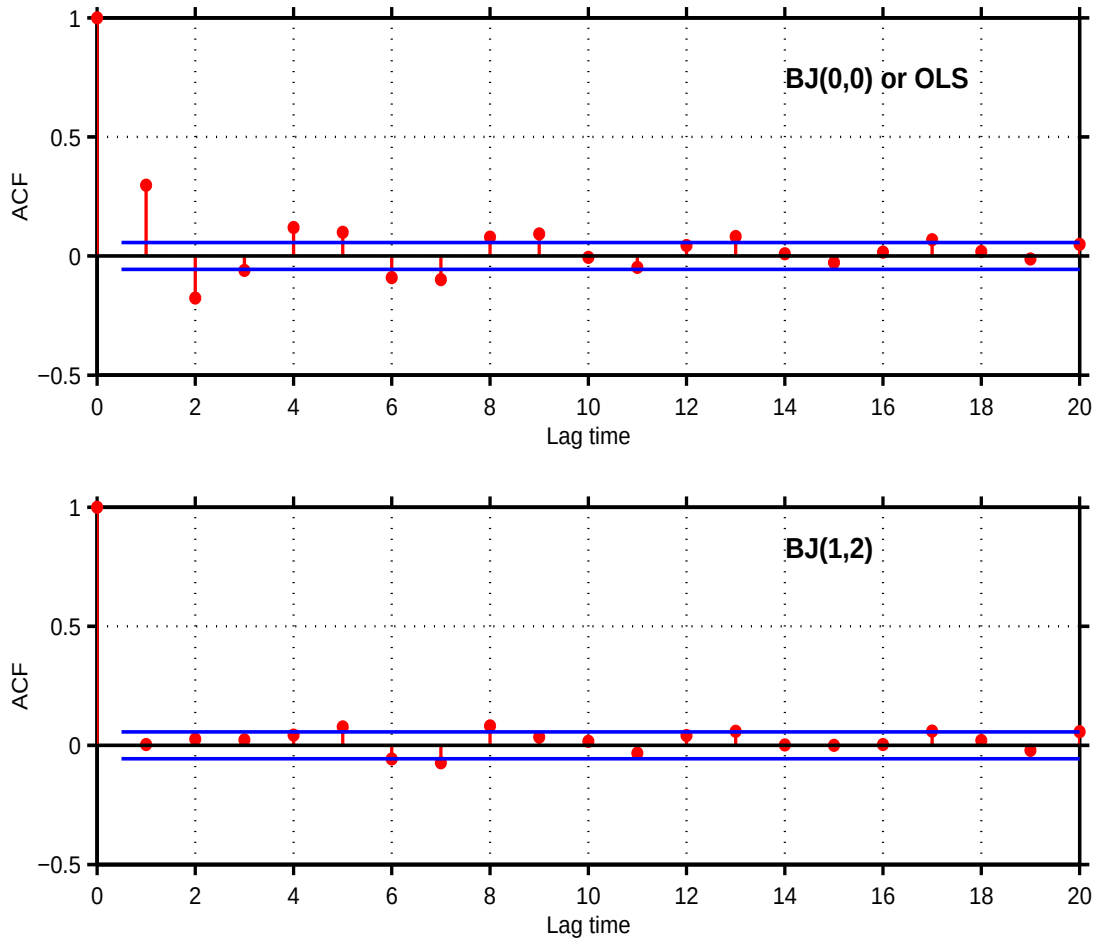

Figure 5.11: Whiteness test for the OLS and BJ(1,2) models using ACF($\epsilon[k]$) in the 2-area benchmark system; Schedule 1. Horizontal bars indicate 95% confidence intervals.

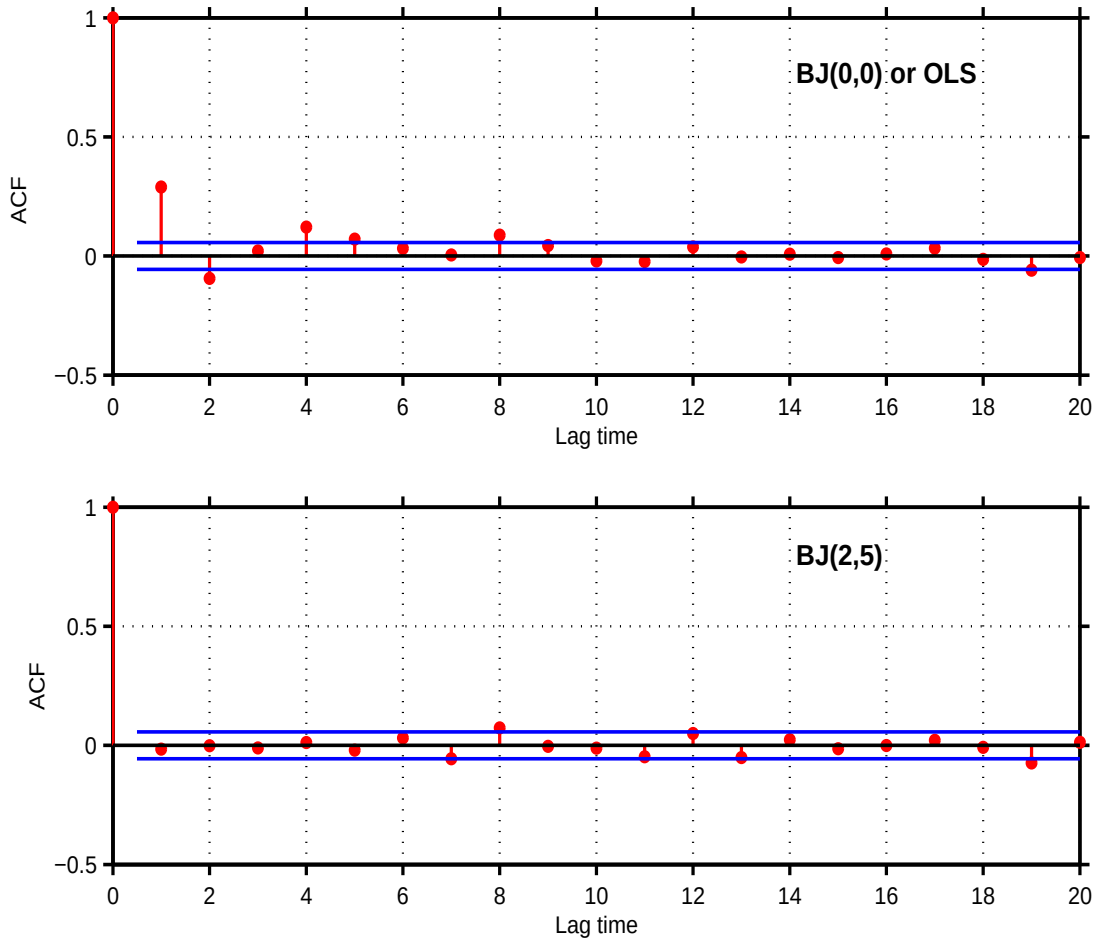

Figure 5.12: Whiteness test for the OLS and BJ(2,5) models using ACF($\epsilon[k]$) in the 2-area benchmark system; Schedule 2. Horizontal bars indicate 95% confidence intervals.

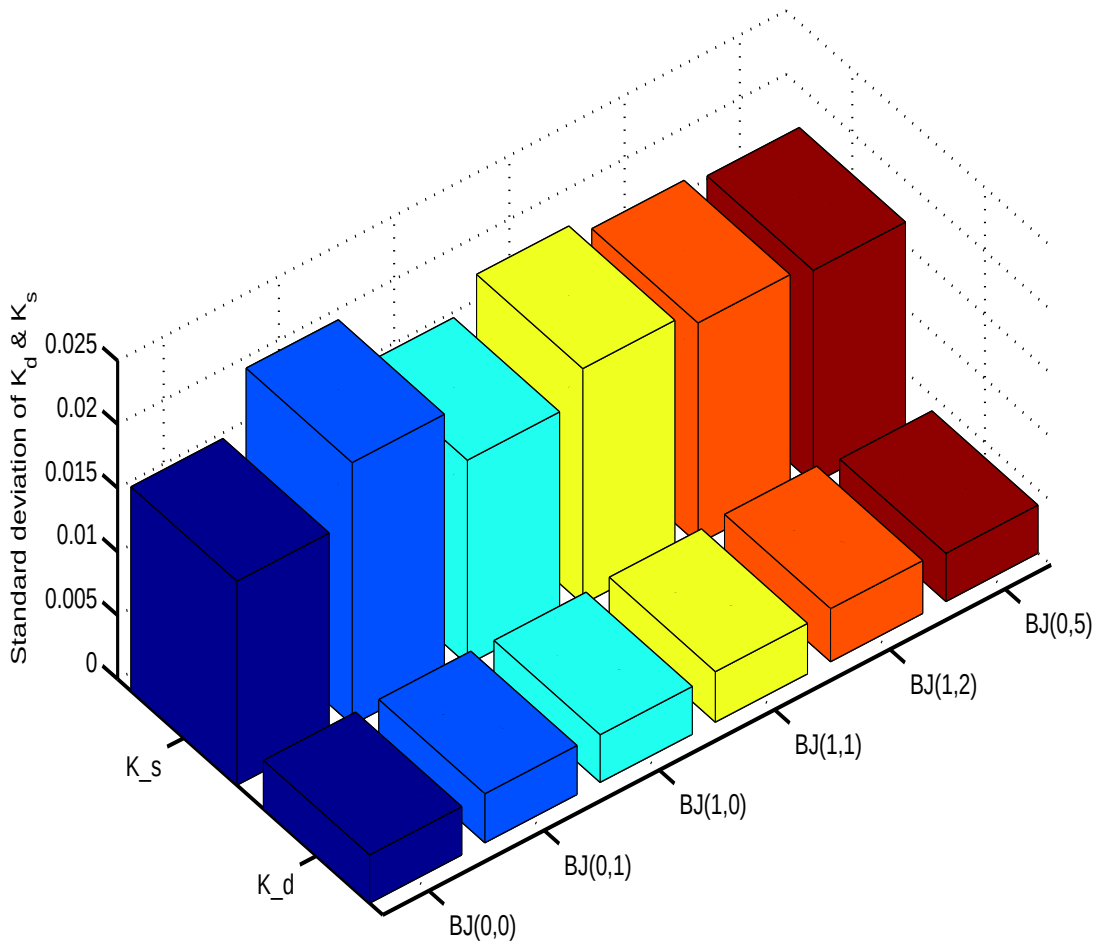

Figure 5.13: The standard deviation of estimated K_d and K_s for the BJ(n_c,n_d) model; Schedule 1.

The estimated K_d's for both schedules are shown in Figures 5.14 and 5.15. A BJ model is employed to estimates the K_d for each generator and is compared to the theoretical and OLS estimates.

Observe that for Schedule 1, all the calculated K_d's tend to zero as the load increases; however, the BJ method offers superior performance in terms of predicting the HB point as well as providing fairly close estimates to the theoretical values, which are denoted as LM in Figure 5.14. Notice that the OLS underestimates the K_d for all the generators, especially at light loading levels.

For Schedule 2, only some of the estimated K_d's are able to predict the instability point. For instance, the trend of the K_d's of generators G_1 and G_2 are giving better prediction of the instability point compared to the K_d's of the Generators G_3 and G_4. Notice that the OLS is providing erroneous K_d's for Generators G_3 and G_4, and that it is unable to predict the instability point, demonstrating the need for using better models such as a BJ model.

The differences observed for generators in Schedule 2 are because of the magnitude of the modes' observability on each generator, i.e. the more observable a mode on a generator, the larger the corresponding oscillations on the generator's response. In Schedule 1, the critical mode is an inter-area mode, and therefore, its observability is almost the same on all the generators; thus, the differences in K_d's are not significant, and all of them can be used to predict the oscillatory stability limit. On the other hand, in Schedule 2, the local mode in Area 2 is not well observed on the generators in Area 1, and therefore, when this mode becomes critical, its effect in not significant on Area 1.

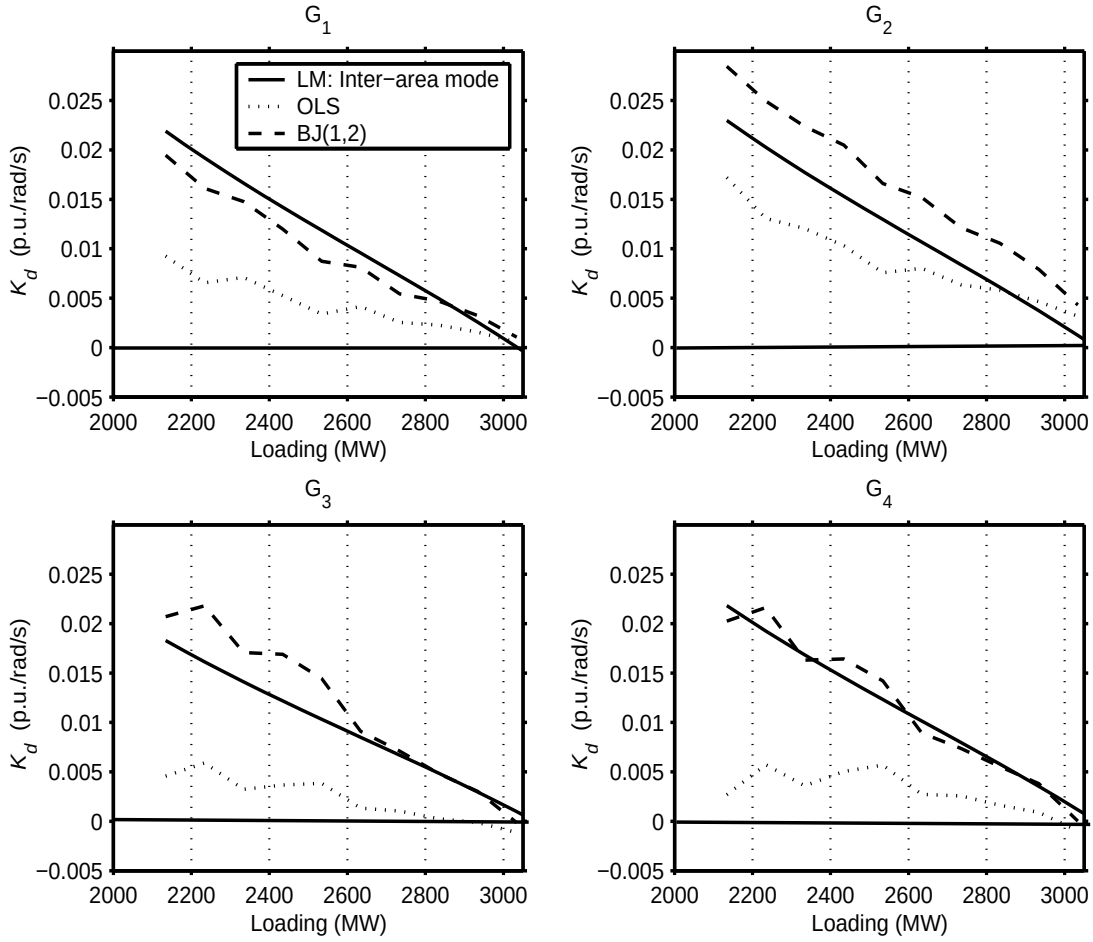

Figure 5.14: Damping coefficients of all generators from ambient data for the 2-area benchmark system; Schedule 1.

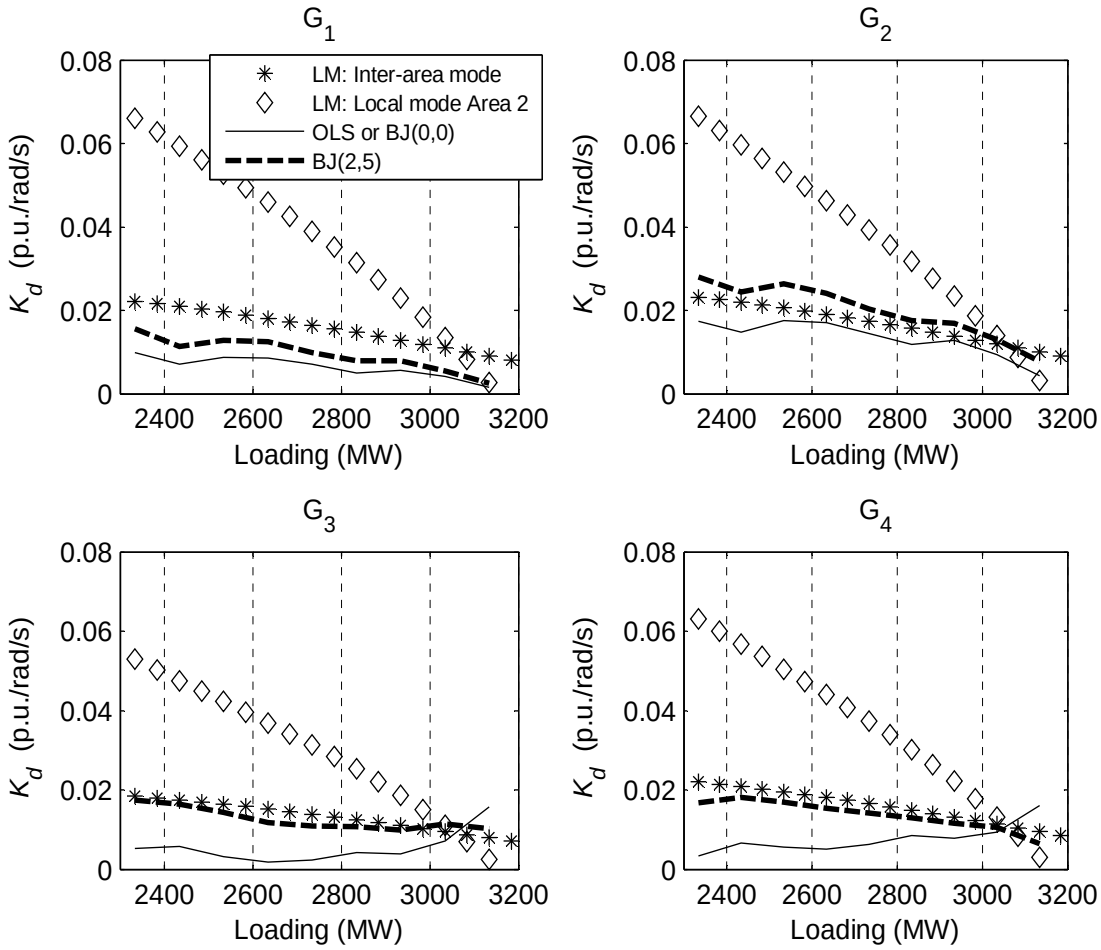

Figure 5.15: Damping coefficients of all generators from ambient data for the 2-area benchmark system; Schedule 2.

5.6 Summary

The procedure to derive the theoretical values of damping and synchronizing coefficients obtained using linearized models of power system is demonstrated. In the systems with single dominant mode, the accuracy of the obtained coefficients using system identification and measured time-domain response of the system is investigated by comparing them with the theoretical values.

The GLS and RFBW identification methods are shown to be better alternatives than the OLS method when the transient response of the power system is available. In particular, it is shown that the OLS method may not be able to accurately estimate the coefficients, because of the nonlinear effects that appear in the measured response of a power system; these effects can be reduced using smaller perturbations. There is a trade off, however, between the magnitude of the perturbation and SNR of the measured signals, i.e. the lower the SNR, the less accurate the estimates.

The damping coefficient is shown to be a useful index to predict the distance to instability points when system loading changes. It is basically a close duplicate of the electromechanical modes behavior; however, it does not require the monitoring of certain modes, which can be an issue in large power systems. Hence, this index may help system operators determine proximity to an oscillatory instability without requiring modeling assumptions and simulations, thus allowing to take proper actions in the case of contingencies and congestion problems.

The Box-Jenkins model is proposed to estimate the damping torque from ambient data, and its effectiveness and superior performance over OLS are illustrated by means of several examples.

Chapter 6

Estimation of Uncertainty

6.1 Introduction

In parameter estimation, second order statistical properties of the estimates, such as confidence intervals, are important when discussing the quality of the estimates, i.e. the tighter the confidence intervals, the better the estimates. For the indices presented in the preceding chapters, the mean value and the confidence interval (standard deviation of the estimates) were studied to ensure that the estimates are both accurate and dependable (e.g. Figures 4.20 and 4.22). The confidence intervals, however, were obtained by means of a Monte-Carlo type of simulation, which requires repeating the simulation for several realizations of the noise; hence, they are computationally expensive and in some cases impractical. For example, in a real power system, the system operating conditions as well as its dynamic characteristics may change over a long time window due to load change, rescheduling, tap changer operation, etc; hence, it is important to quickly conduct the experiment to ensure that the system does not experience significant changes, and that the

stationarity assumption is not violated over the measurement time.

This chapter starts with a background on estimating the covariance of parameters of a linear parametric model. This information is useful in determining the variance of the indices previously proposed.

The index proposed in Chapter 4, the $SISI$, has however a nonlinear relationship with the parameters, and so does its variance. This nonlinear relationship is due to the fact that the $SISI$ is basically related to the eigenvalues of the system that are the roots of the characteristic equation.

A technique that has been used in civil engineering for identification of civil structures to establish a connection between the variance of parameters and the variance of modal parameters is used here [70], and the corresponding equations are explained in detail.

6.2 Covariance of Parameters

A linear model is given by

$$y(k) = G(q)\ u(k) + H(q)\ e(k) \tag{6.1}$$

where $y(k)$ is the output; $u(k)$ is the input; and $e(k)$ models the disturbances. One-step-ahead prediction $\hat{y}(k|\theta)$ uses the observations available up to time $k-1$ to predict $y(k)$, thus:

$$\hat{y}(k|\theta) = H^{-1}(q)\ G(q)\ u(k) + [1 - H^{-1}(q)]\ y(k) \tag{6.2}$$

This notation is adapted from [71] and is used to emphasize its dependence on the parameter vector θ. Rewriting (3.14) using (6.1) and (6.2) results in:

$$\begin{aligned} \hat{\theta} &= \arg\min \quad V(\theta) \\ V(\theta) &= \frac{1}{N}\sum_{k=1}^{N}\frac{1}{2}\epsilon^2(k,\theta) \\ \epsilon(k,\theta) &= y(k) - \hat{y}(k|\theta) \end{aligned} \tag{6.3}$$

where function $V(\theta)$ denotes the loss that results from the model in the fitting process, and "arg min" means the minimization argument of the function $V(\theta)$. Hence, at the solution point, the differentiation of $V(\theta)$ with respect to θ has to be zero, i.e.:

$$V^{'}(\hat{\theta}) = 0 \tag{6.4}$$

Thus, an iterative algorithm, such as Newton, is used to solve for $\hat{\theta}$ by means of the Taylor series expansion of (6.4) around θ^*:

$$0 \approx V^{'}(\theta^*) + V^{''}(\theta^*)(\hat{\theta} - \theta^*) \tag{6.5}$$

or

$$(\hat{\theta} - \theta^*) = -\left[V^{''}(\theta^*)\right]^{-1} V^{'}(\theta^*) \tag{6.6}$$

which requires the first derivative (gradient) and second derivative (Hessian). These derivatives can be expressed as:

$$V^{'}(\theta^*) = -\frac{1}{N}\sum_{k=1}^{N}\psi(k,\theta^*)\ \epsilon(k,\theta^*) \tag{6.7}$$

$$V^{''}(\theta^*) = \frac{1}{N}\sum_{k=1}^{N}\psi(k,\theta^*)\ \psi^T(k,\theta^*) + \frac{1}{N}\sum_{k=1}^{N}\psi^{'}(k,\theta^*)\ \ \epsilon(k,\theta^*) \tag{6.8}$$

$$\psi(k,\theta^*) = -\frac{d}{d\theta}\ \epsilon(k,\theta)|_{\theta=\theta^*} = \frac{d}{d\theta}\ \hat{y}(k|\theta)|_{\theta=\theta^*}$$

Close to the solution $\hat{\theta}$, the predicted errors $\epsilon(k,\theta)$ are independent; thus,

$$V''(\hat{\theta}) \approx \frac{1}{N}\sum_{k=1}^{N} \psi(k,\hat{\theta})\ \psi^T(k,\hat{\theta}) \tag{6.9}$$

It is known that $\sqrt{N}(\hat{\theta}-\theta^*)$ is asymptotically Gaussian distributed with zero mean and a covariance matrix P, i.e. $\mathcal{N}(0,P)$ (for proof refer to [71]). An estimate of P from available data can be obtained as follows:

$$\hat{P} = \hat{\lambda}_0\ \left(V''(\hat{\theta})\right)^{-1} \tag{6.10}$$

$$\hat{\lambda}_0 = \frac{1}{N}\sum_{k=1}^{N} \epsilon^2(k,\hat{\theta}) \tag{6.11}$$

with $\hat{\lambda}_0$ being an estimate of the variance of the errors. Then, the covariance of parameter estimates ($P_{\hat{\theta}} = E[(\hat{\theta}-\theta^*)(\hat{\theta}-\theta^*)^T]$) can be approximated as:

$$P_{\hat{\theta}} \approx \frac{1}{N}\ \hat{P} \tag{6.12}$$

The eigenvalues of a system are the roots of the characteristic equation, and hence are only dependent on the AR part of an ARMA(p,d), as explained in Chapter 3. Thus, the covariance matrix $P_{\hat{\theta}}$ is partitioned so that the rows and columns corresponding to the AR and the MA parts are separate as follows:

$$P_{\hat{\theta}} = \begin{bmatrix} P_{\hat{\theta}_{AR}} & P_{\hat{\theta}_{ARMA}} \\ P_{\hat{\theta}_{ARMA}} & P_{\hat{\theta}_{MA}} \end{bmatrix} \tag{6.13}$$

In the next section, a relationship between $P_{\hat{\theta}_{AR}}$ and the covariance of eigenvalues is established.

6.3 Covariance of Eigenvalues

Eigenvalues are related to the θ_{AR}, which are the coefficients of the characteristic equation. This relationship can be written as:

$$\Phi = \gamma(\theta_{AR}) \tag{6.14}$$

where $\gamma(\theta_{AR})$ is a nonlinear function, and Φ denotes a vector containing the modal parameters; for instance, the real part α and the frequency f of the eigenvalues can be used to define:

$$\Phi = [\alpha_1, f_1, \alpha_2, f_2, \ldots, \alpha_p, f_p]^T \in \Re^{2p} \tag{6.15}$$

In order to obtain the mean and variance of modal parameters, the expected value operator may be applied to a Taylor series expansion of the function γ about an operating point $(\hat{\Phi},\, \hat{\theta}_{AR})$, which may be written as:

$$\Phi \approx \hat{\Phi} + J(\hat{\theta}_{AR}) \left(\theta_{AR} - \hat{\theta}_{AR}\right) \tag{6.16}$$

$$J(\hat{\theta}_{AR}) = \left.\frac{\partial \gamma(\theta_{AR})}{\partial \theta_{AR}}\right|_{\theta_{AR}=\hat{\theta}_{AR}} \tag{6.17}$$

where $J(\hat{\theta}_{AR}) \in \Re^{2p\times p}$.

Thus, rearranging (6.16) and applying the second moment operator (covariance) yields

$$\text{Cov}\ \Phi = E\left[(\Phi - \hat{\Phi})\ (\Phi - \hat{\Phi})^T\right] \ = \ J(\hat{\theta}_{AR})\ P(\hat{\theta}_{AR})\ J^T(\hat{\theta}_{AR}) \tag{6.18}$$

This clearly shows the connection between the covariance of estimates $P(\hat{\theta}_{AR})$ and the covariance of eigenvalues Cov Φ. Hence, in order to obtain Cov Φ, one first needs to calculate the numeric Jacobian $J(\hat{\theta}_{AR})$ as follows:

$$J_{ij}(\hat{\theta}_{AR}) \ = \ \frac{\gamma_i(\hat{\theta}_{AR} + \Delta\theta_j) - \gamma_i(\hat{\theta}_{AR} - \Delta\theta_j)}{2h} \tag{6.19}$$

where

$$\Delta\theta_j = \begin{bmatrix} 0 \\ \vdots \\ 0 \\ h \\ 0 \\ \vdots \\ 0 \end{bmatrix} \longleftarrow j$$

and h is a small number, and $P(\hat{\theta}_{AR})$ can be estimated using (6.12).

6.4 Test case

The proposed method for estimating the standard deviation of the identified modes is tested with the 2-area benchmark system. First, a Monte-Carlo type of simulation with 150 trials is performed by running independent simulations, where 1% of the loads at Buses 7 and 9 are represented as Gaussian noise; 4-minutes data blocks of generator G_1's power output are recorded in each simulation. Then, the preprocessed data blocks along with a PEM are employed to estimate the parameters of an ARMA(10,5) model representing the power system transfer function.

The estimated standard deviation of both the real part and frequency of the inter-area mode obtained using (6.18) is depicted in Figures 6.1 and 6.2, respectively. Observe that the estimates track the results corresponding to the Monte-

Carlos simulation, and that the mean of the estimates depicted in both figures show that it can provide good accuracy with a significantly reduced number of trials. For instance, in Figure 6.1, the convergence speed of the estimates is nearly 3 to 4 times faster than the Monte-Carlo method, which is a significant reduction in the monitoring time.

6.5 Summary

A procedure to calculate the second order statistical properties of the previously proposed is presented and justified. It is based on a technique that employs the Taylor series expansion to establish a connection between the variance of parameters and the variance of eigenvalues. The presented technique can be used to avoid Monte-Carlo type of analyses, thus resulting in a significant reduction in computational time, making the proposed indices and monitoring techniques more appealing for real-time applications.

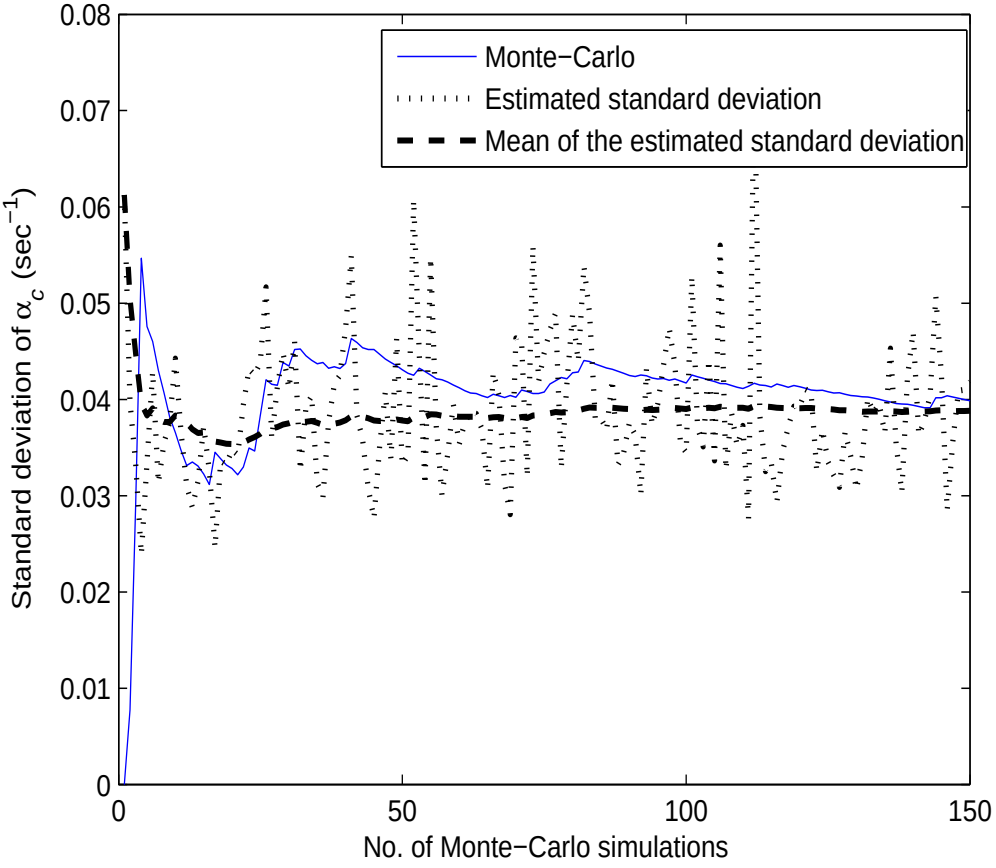

Figure 6.1: Standard deviation of the real part of the identified critical mode $-0.1228 \pm j4.7824$ for the 2-area benchmark system using Monte-Carlo and equation (6.18).

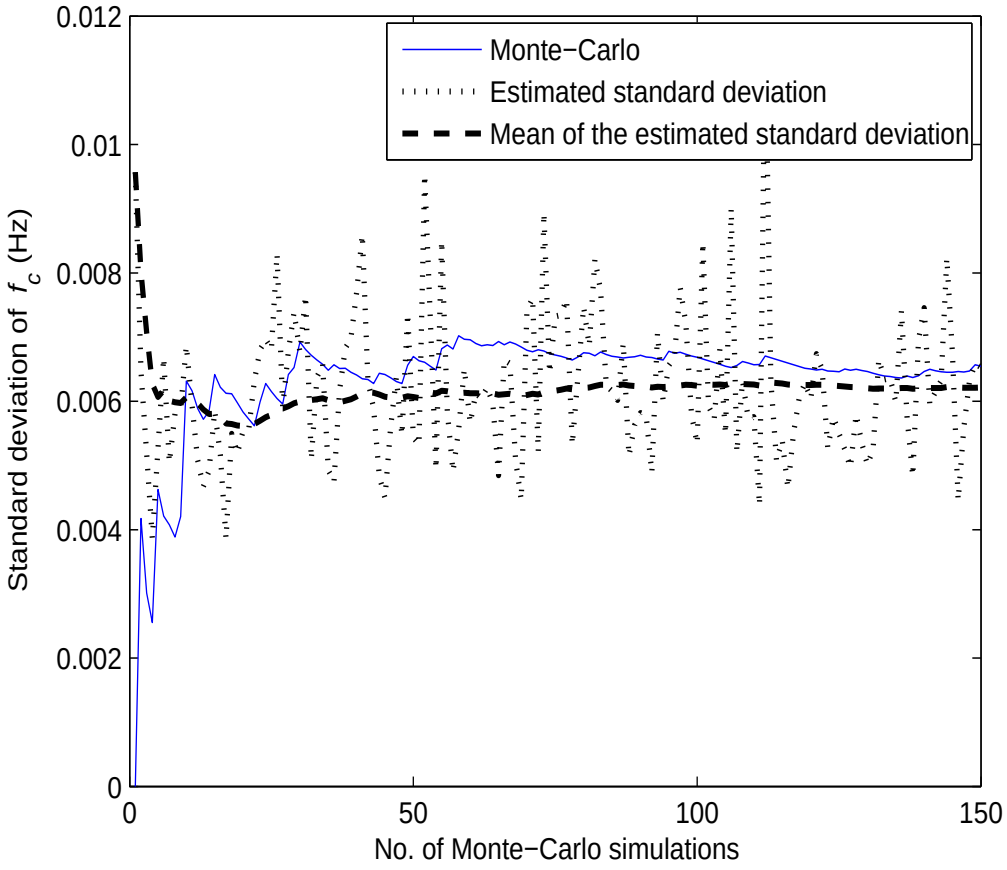

Figure 6.2: Standard deviation of the frequency of the identified critical mode $-0.1228 \pm j4.7824$ for the 2-area benchmark system using Monte-Carlo and equation (6.18).

Chapter 7

System Identification Techniques Applied to Model Validation

7.1 Introduction

This chapter discusses the validation of the simplified models of major power system elements, in particular synchronous generators and STATCOMs. These approximate models, instead of their detailed models, are typically used in power system analysis packages, since power systems normally consist of several thousand buses and machines, which may lead to intractable problem if full device models are used. Thus, TS models are based on simplifications made to enhance computational efficiency.

The validation procedure is performed by means of system identification applied to the time-domain response of the both detailed models and simplified models, so that the identified electromechanical modes can then be compared. The test systems with detailed models was simulated in PSCAD/EMTDC program [72];

since large test cases cannot be handled in this program, the simulations were obtained only for the IEEE 3-bus system.

7.2 Generator Modeling

As explained in Chapter 2, neglecting stator and network transients is the first common step for simplification of the generator detailed model, as it provides a very close approximation of the actual system response; this simplification along with a few other assumptions result in the generator subtransient model [33], and thus permit the use of a much larger step size for integration in transient stability programs. The reason for neglecting stator and network transients is that these transients are fast and damp quickly, as they are related to main frequency transients (50 Hz or 60 Hz), since when these transients are included, there will be a DC offset term in the phase currents, which results in a DC braking torque and a main frequency oscillatory torque, adding a slight degree of stability to the system [33]. Thus, the stability limits obtained using simplified models are conservative when compared to the actual system stability limits. It has been shown that DC offset currents can also develop abnormal oscillatory torques and back swing phenomena [73, 74].

In order to compare generator models by means of system identification techniques, the author has been forced to use signals generated through time-domain simulations of detailed PSCAD/EMTDC [72] models for a small IEEE 3-bus system, so that the resulting signals would be as close to field measurements as possible. To perturb the system in PSCAD, a pseudo-random binary signal (PRBS) [75], which approximates white noise, was used to represent a 1% load modulation at Bus 3. The stochastic subspace technique applied to the generators' output power

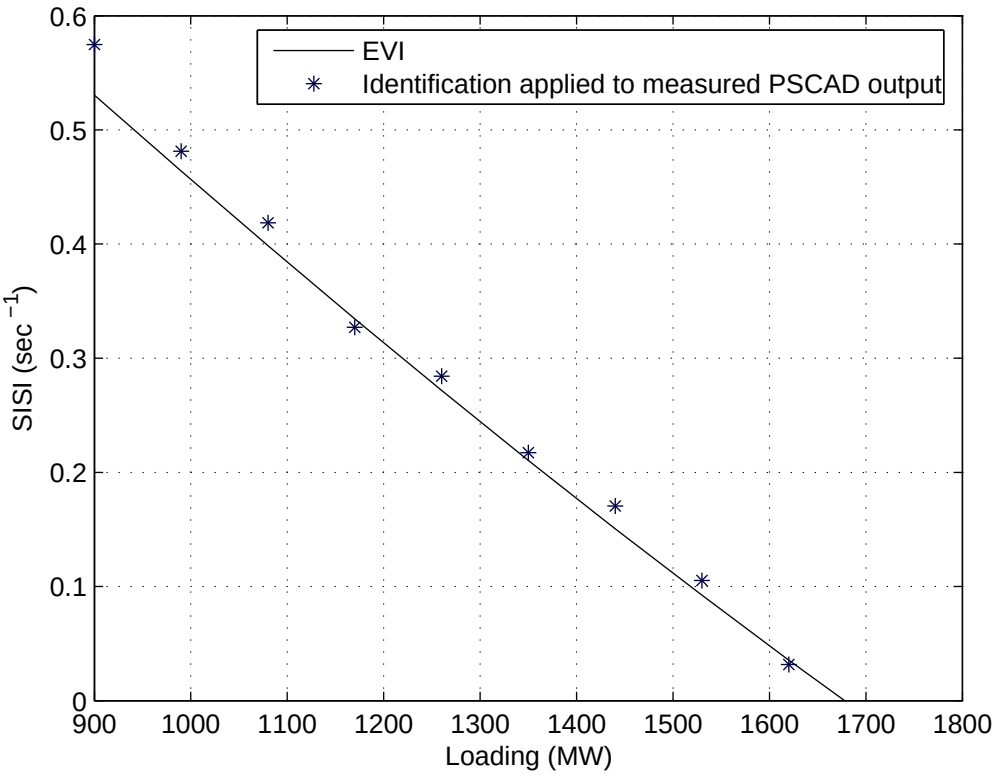

Figure 7.1: SISI for the IEEE 3-bus system; generator detailed model versus its subtransient model.

yielded the results shown in Figure 7.1. Observe that both the generator detailed model and its linearized subtransient model in PST yeild fairly similar results. The maximum error in this case, between the identified and modeled SISI is 0.047 sec^{-1}, which is small.

The effect of including/or neglecting stator and network transients for small-disturbance stability analyses and their impact on rotor angle mode was also studied. A small-disturbance stability program MASS [76], which is capable of performing modal analysis including/neglecting network transients, was used for some test cases and the results were given in Table 7.1. Observe that the corresponding

Table 7.1: Effect of including/neglecting network transients on the critical mode

Network Transients	Included	Neglected
	Mode, Damping	Mode, Damping
IEEE 3-bus	-0.6509 ± j8.09, 8.01%	-0.6298± j8.14, 7.71%
IEEE 14-bus	-0.2502 ± j8.85, 2.82%	-0.2158± j8.83, 2.44%
Two-area 11-bus	-0.0940± j4.61 , 2.04%	-0.0800± j4.61, 1.74%

eigenvalues indicate that network transients add a slight degree of stability to the electromechanical mode, i.e. generator subtransient models are slightly conservative from the point of view of calculating the electromechanical modes.

7.3 STATCOM Modeling

Readily available power system packages employ power flow or TS models to represent FACTS controllers. TS models, however, need to be validated from the small-disturbance analysis point of view prior to using them in TS studies. This can be achieved by means of system identification.

A typical STATCOM TS model is based on a fundamental frequency representation (phasor model) of the power system. In [1, 40], the authors study the accuracy of the proposed TS model with regards to the detailed model only by means of time-domain simulations. However, since these controllers can play a major role in damping electromechanical oscillations [15, 31], one needs to validate these models by means of small-disturbance stability analysis or modal analysis.

In this section, besides time-domain simulation results, a system identification technique is used to investigate the accuracy of a typical STATCOM TS model

Table 7.2: STATCOM static data

R_c (Ω)	$R_{transformer}$ (Ω)	$X_{transformer}$ (Ω)	C (μF)
200	0	0.108	740

Table 7.3: STATCOM controller parameters

K_{p_α}	K_{I_α}	K_{p_m}	K_{I_m}	T_w (s)
0.06	0.6	10	100	10

compared to its detailed model, from the small-disturbance stability analysis point of view.

7.3.1 Test case

Both the STATCOM detailed and TS models are simulated in PSCAD/EMTDC program. Due to the limitations imposed by PSCAD, only the IEEE 3-bus system (Figure 2.8) is studied here. A 200 MVar STATCOM is connected to the Bus 3 through a coupling transformer (Δ-Y, 6 kV/138 kV) to mainly regulate the voltage at Bus 3. By adding a supplementary control loop (Figure 2.3), it could also be used in damping oscillations. The data for the STATCOM are given in Tables 7.2 and 7.3.

The STATCOM detailed PSCAD model includes all the switches and the corresponding snubbers. The PWM control with a carrier frequency of 1260 Hz is used to reduce the harmonics. It should be mentioned that the harmonic content of the output voltage of the converter can be significantly reduced by increasing the carrier frequency f_c. The harmonics with order of $Mf_c \pm Nf_s$ appear in the output

voltage where f_s is power system frequency, M and N are integers, and $M + N$ is an odd integer [77]; however, f_c is limited to the maximum switching frequency that the switches can withstand. A capacitor bank is connected to the Bus 3 to filter high frequency harmonics; it is also providing 140 MVar of reactive power at the fundamental frequency when the loading level is 900 MW.

For TS studies, the converter is replaced in PSCAD with a TS model based on a controlled voltage source with a fixed frequency equal to the fundamental frequency of the power system. The magnitude of the voltage source is determined from the differential equation described in (2.7).

7.3.2 Standard Control Analysis

The detailed model and TS model are studied for several loading conditions. As the load at Bus 3 increases, the electromechanical mode becomes less stable, as shown in Table 7.4. The Prony method is employed to obtain the modal content of the measured generator 1's output power, showing a close agreement between the eigenvalue calculated for the detailed and the TS models. The time-domain simulation results for a line 2-3 outage and reconnection after 2 cycles are depicted in Figure 7.2, showing fairly similar profiles. These results basically validate previous studies of the STATCOM TS model [1, 40].

7.3.3 Supplementary Control Analysis

A supplementary control is added to damp the oscillations and remove the HB point. The auxiliary signal used for this control is usually a local signal such as power or current through the STATCOM adjacent lines. The auxiliary signal used here is

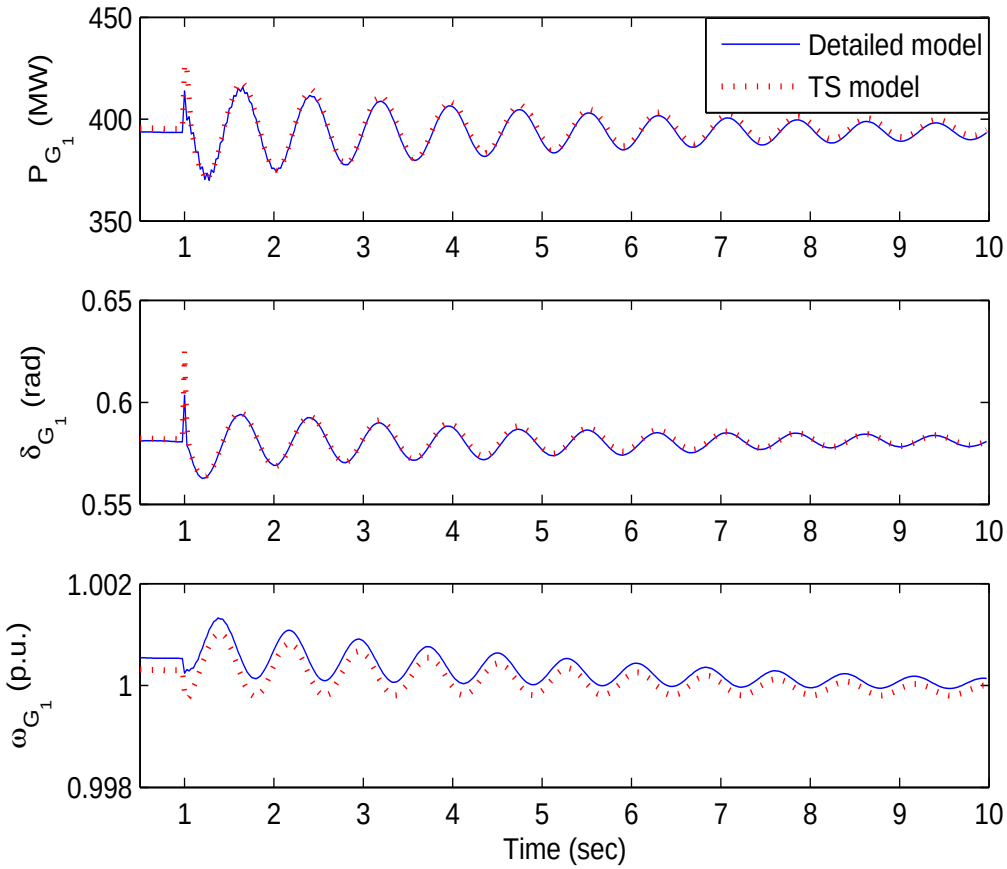

Figure 7.2: The response of the system to a line 2-3 outage in the IEEE 3-bus system; STATCOM at Bus 3 without supplementary control at 160% loading level.

Table 7.4: Critical electromechanical mode for the IEEE 3-bus system with STATCOM detailed and TS models.

Loading Level	Detailed Model	TS Model
	Mode, Damping	Mode, Damping
100% (900 MW)	-0.5600± j8.11, 6.89%	-0.5500± j8.11, 6.77%
130% (1170 MW)	-0.3686 ± j8.12, 4.53%	-0.3698± j8.11, 4.56%
160% (1440 MW)	-0.1993 ± j8.08, 2.47%	-0.2170± j8.07, 2.69%
190% (1710 MW)	-0.0294 ± j8.02, 0.37%	-0.0674± j8.00, 0.84%

the power in line 1-3 due to the better performance of power over other signals as reported in [8]. At the same loading conditions as in the previous case, the critical eigenvalue is calculated by means of the Prony method applied to the time-domain simulation results. Table 7.5 and Figure 7.3 clearly illustrate the effectiveness of the supplementary control in damping electromechanical oscillations when compared to the results in Table 7.4; however, the calculated eigenvalues for the TS model in this case are not as close to the ones related to the detailed model. Observe that the TS model does a better job in damping oscillations, i.e. the TS model provides more optimistic results from the eigenvalue analysis point of view, as depicted in Figure 7.4. This basically results in an overestimation of the real stability margin of the power system, and hence it is a potential risk in power system planning.

The discrepancy between the two models is better illustrated in Figure 7.5, which shows the terminal voltage V_t, the DC bus voltage V_{dc} and converter's delay angle α_{conv}. Observe that the fast transients during and right after clearing the fault are not captured by the TS model. This is due to the fact that the TS model was developed based on the balanced three phase voltages with fundamental fre-

Table 7.5: Critical electromechanical mode for the IEEE 3-bus system; STATCOM with a supplementary control

Loading Level	Detailed Model	TS Model
	Mode, Damping	Mode, Damping
100% (900 MW)	-0.9778± j8.51, 11.41%	-1.0252± j8.44, 12.06%
130% (1170 MW)	-0.7038 ± j8.72, 8.04%	-0.8067± j8.63, 9.31%
160% (1440 MW)	-0.4439 ± j8.76, 5.06%	-0.5952± j8.66, 6.86%
190% (1710 MW)	-0.1766 ± j8.70, 2.03%	-0.3641± j8.60, 4.23%

quency, i.e. phasors, and hence is not able to capture the fast voltage transients. The absorbed active and reactive power from the system to the converter depicted in Figure 7.6 provide additional insights into the functioning of the different models. Notice that the active power, which plays a fundamental role in damping the oscillating power ΔP_{G_1}, is larger in the case of the TS model, hence yielding a more stable system. The main reason for this is that the TS model is based on a controlled voltage source, with its magnitude being controlled by a differential equation, whereas in the detailed model, the voltage is directly affected by fast DC voltage transients.

7.4 Summary

The generator subtransient model and the STATCOM TS model are studied and compared here with respect to their detailed models by means of PSCAD simulations and system identification. From the electromechanical mode point of view, the subtransient model of a generator yields very close results to the those obtained

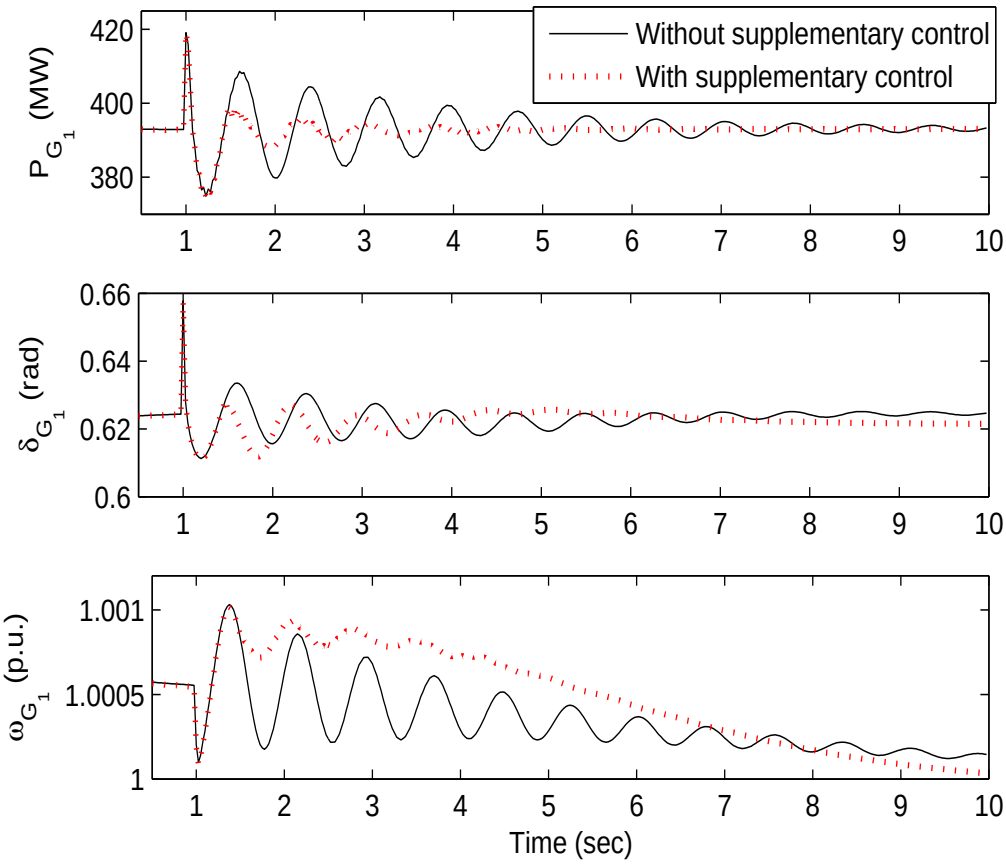

Figure 7.3: Detailed STATCOM model with and without a supplementary control at a 130% loading level.

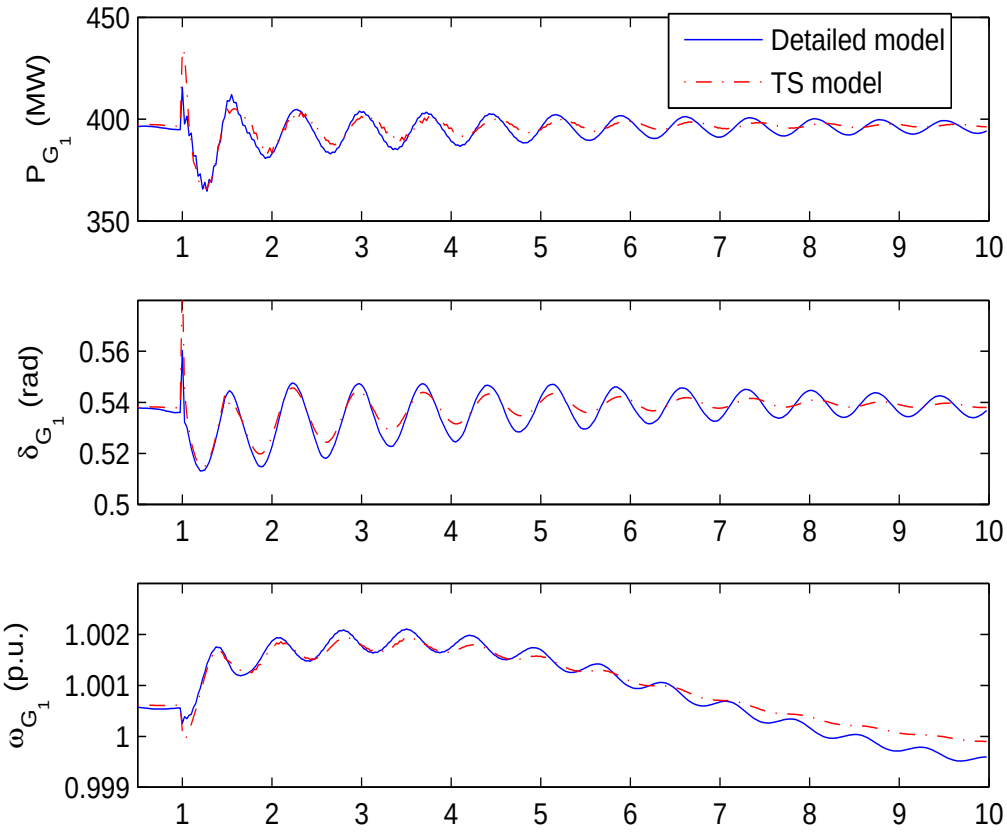

Figure 7.4: IEEE 3-bus system response for a line 2-3 outage for a STATCOM with a supplementary control at 190% loading level.

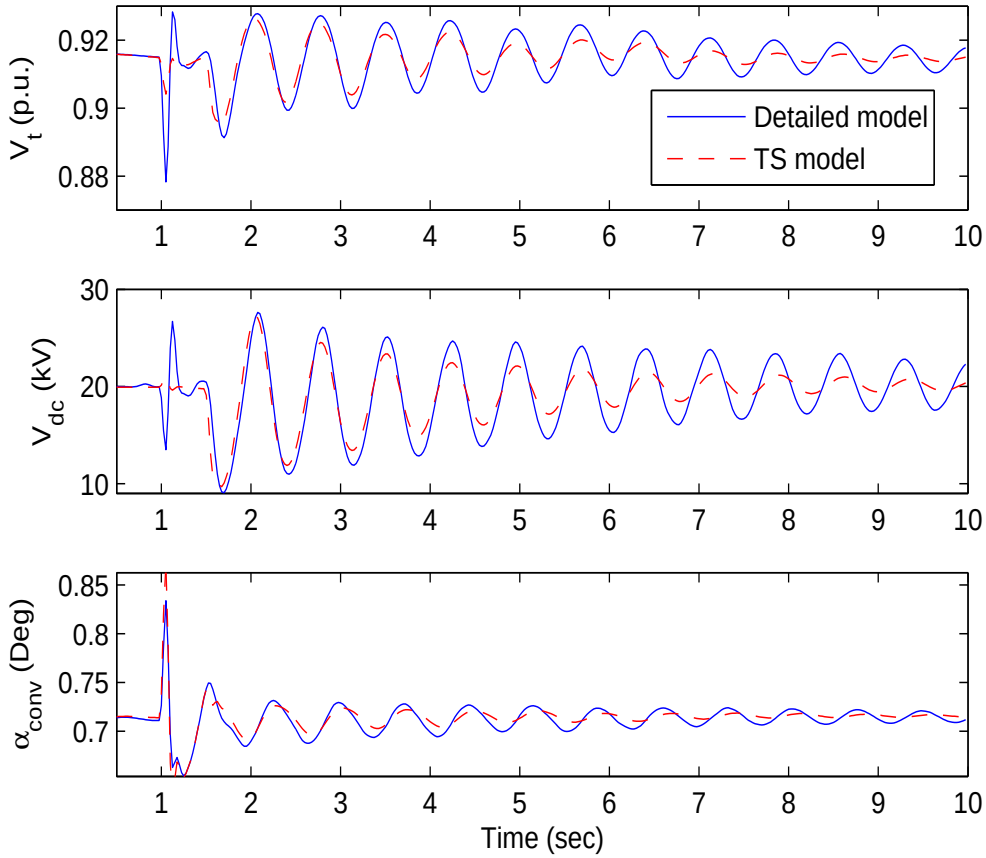

Figure 7.5: IEEE 3-bus system response for a line 2-3 outage for a STATCOM with a supplementary control at a 190% loading level.

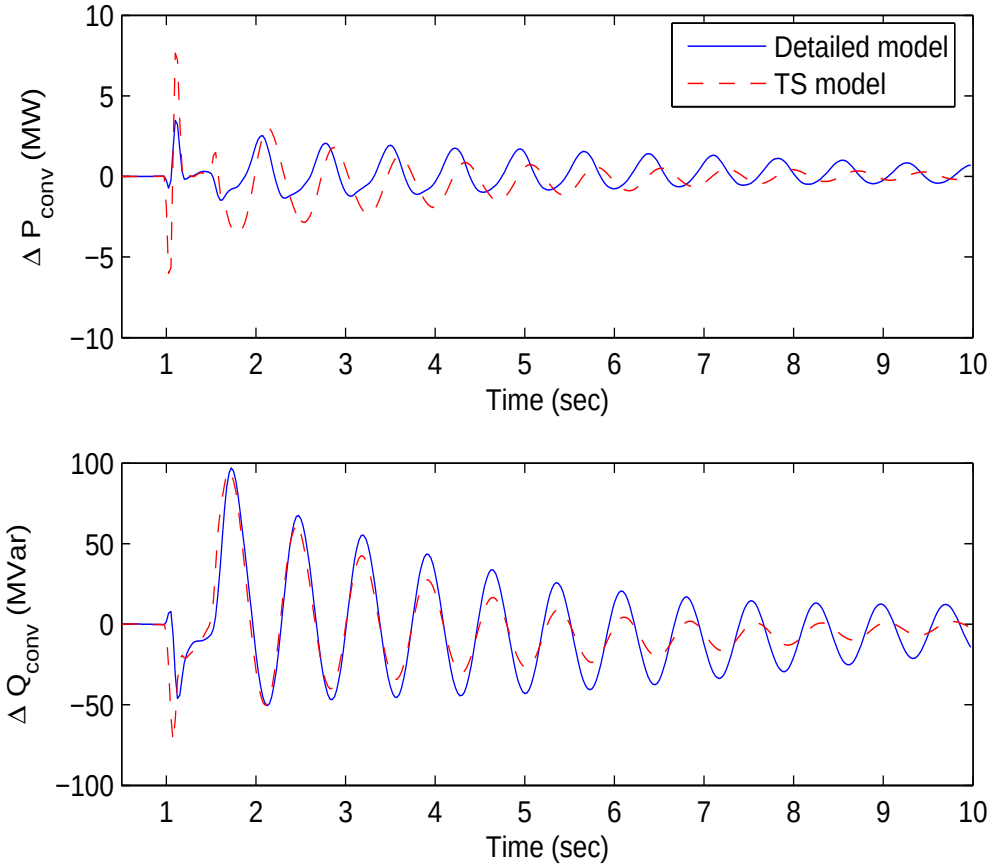

Figure 7.6: The active and reactive power absorbed by the STATCOM with a supplementary control at a 190% loading level.

from the detailed model, while being slightly conservative, which is acceptable from the planning point of view. On the other hand, the STATCOM TS model also yields results fairly close to those of its detailed model for the case when no supplementary control is added to the STATCOM control. However, it is shown that, in the presence of supplementary control, the STATCOM TS model gives optimistic results regarding the electromechanical modes, which could be a problem for power system operators and designers that has not been previously identified.

Chapter 8

Conclusions

8.1 Summary and Conclusions

This thesis concentrates on the study of oscillatory angle stability problems, proposing system identification techniques to detect the electromechanical modes from both power system transient response and ambient noise. Two on-line stability indices, along with several identification methods, are proposed to monitor oscillatory phenomena and to predict stability margins in a power system. Also, a procedure is presented to obtain the confidence intervals of these stability indices from the variance of the parameters. Finally, the generator subtransient model and a typical STATCOM model are compared with respect to their detailed models using system identification tools.

In Chapter 2, the models of some of the key power system components used in this thesis are briefly explained. The importance of selecting the right models for different kinds of power system analyses is also discussed. Power system stability concepts, techniques and tools used throughout this thesis, such as voltage and

angle stability, continuation power flow and system identification are presented here as well.

Chapter 3 describes different types of signals that can be readily measured in a power system, as well as the corresponding techniques to extract the signal modal content. Namely, the Prony method is shown to be suitable for the transient response with high SNR, while the LSMYW and the PEM are shown as proper techniques to analyze ambient noise. A stochastic subspace identification method is proposed to capture the critical modes of a power system from ambient data. The asymptotic behavior of the proposed method is investigated by comparing it with the PEM. It is shown that the methods are asymptotically equivalent; however, the proposed method is easier to implement and is computationally more efficient.

Chapter 4 proposes an eigenvalue based index referred to as SISI to predict the closest stability margin related to the impending oscillatory phenomena. Several test cases along with a 14,000-bus power system are used to illustrate the effectiveness of the index in practice.

In Chapter 5, another stability index based on the damping torque of individual generators is proposed to overcome the shortcomings of the SISI, as it does not require surveillance of certain modes. The drawback of using this index is that the contributing modes to oscillations are not separately identified, as opposed to the SISI which allows to estimate the damping and frequency of each mode. Some identification methods and models, such as GLS method and BJ model, are proposed and studied to estimate the damping torque.

Chapter 6 demonstrates the connection between the second order statistical properties, including confidence intervals, of the estimated modes and the variance of model parameters. These analyses show that Monte-Carlo type of experiments

or simulations can be avoided by using the proposed formulas and procedures.

Chapter 7 investigates the validity of generator subtransient model and a typical STATCOM TS model by means of system identification, illustrating that, under certain conditions, the STATCOM TS model can yield optimistic results regarding damping in the system.

8.2 Contributions

The main contributions of the thesis are the following:

1. Previous research on on-line electromechanical mode detection has been focused on using and developing linear parametric models estimated by means of PEMs, which are computationally demanding, and may run into numerical problems. A new subspace identification method is proposed here to detect the electromechanical mode from ambient noise. It is shown to be asymptotically equivalent to PEMs; however, the proposed method is easier to implement and computationally more efficient, and thus should be useful for on-line monitoring applications in power systems.

2. Currently proposed indices used for prediction of oscillatory stability margins in power systems are based on off-line analyses, which rely on approximate DAE models and data. The proposed new SISI is an on-line index, based on identified critical modes of the system, which allows for the prediction of the distance to the maximum loading condition in practice, as demonstrated here by means of real system studies.

3. A novel damping torque index is also proposed to predict oscillatory stability limits in power systems. This index is shown to offer some complementary

features when compared to the proposed SISI, as it does not need prior knowledge of the critical modes of the system. However, as opposed to the SISI, it cannot correctly reveal the true nature of the poorly damped oscillations, i.e. whether the problematic modes are local modes or inter-area modes, so that appropriate remedial actions can be taken accordingly.

4. The OLS method has been mostly used so far to estimate the damping torque of individual generators; however, it is shown here that for well-damped transient response of power systems and ambient noise, the OLS method cannot accurately estimate the damping torque. Thus, several identification methods are presented and studied for the estimation of the damping torque from power system transient response and ambient noise under various operating conditions. The new techniques are shown to be better than the currently existent methods.

5. In the current technical literature, the most common approach to obtaining the confidence intervals associated with identified electromechanical modes is based on Monte-Carlo type of simulations and experiments. A clear connection is demonstrated here between the confidence intervals of identified modes and the variance of model parameters. This new approach is shown to significantly reduce the number of experiments and recorded data needed to detect critical modes for on-line power system monitoring applications.

6. The TS models of power system components are usually validated only by inspection of the time-domain simulation results and comparing them with those of more detailed models. System identification is employed here to validate the generator subtransient model and the STATCOM TS model from the viewpoint of small-disturbance analysis. These new results show that the

STATCOM TS model, when a supplementary oscillation control is added, can lead to damping levels that are too optimistic, which is a problem that so far has not been identified.

Part of the proposed stability indices, identification methods, and corresponding results presented in this thesis have been published in [78, 79, 80].

8.3 Directions for Future Work

Based on the research work presented and discussed in this thesis, further research may be pursued on the following subjects:

- Application of the proposed SISI and the damping torque index to on-line tuning of power system controllers such as PSSs.
- TS model validation for other FACTS controllers, such as SVC, SSSC and TCSC, from the small-disturbance stability point of view by means of system identification.
- Application of recursive identification methods in mode detection and damping estimation from ambient data to improve computational efficiency.
- Investigate the whiteness of both load switching phenomena and measurement noise in power systems, as well as the "stationarity" hypothesis over a long time monitoring window.

Appendix A

SYSTEM DATA

The dynamic and static data for the test systems used in this thesis are presented here in PST format [36]. The data for teh 14,000-bus real system is confidential.

A.1 IEEE 3-bus System

```
%Bus data
%Column:
%    1   2     3       4      5      6      7       8
%   bus volt angle   p_gen  q_gen  p_load q_load  G_shunt
%     9       10   11    12    13     14    15
% B_shunt type q_max q_min v_rate v_max v_min


bus = [ 1 1.05    0.0   4   1.5  0.0  0.0  0.0  0.0  2   10  -2;
        2 1       0.0   5   1.5  0.0  0.0  0.0  0.0  1  999  -999;
        3 1.0     0     0     0  9   3    0.0  2.0  3    0     0];


% line data format
% line: from bus, to bus, resistance(pu), reactance(pu),
%       line charging(pu), tap ratio, tap phase, tapmax, tapmin, tapsize
```

```
line = [1  3  0.00  0.05    0.  1. 0.;
        2  3  0.00  0.03999 0.  1. 0.;
        2  3  0.00  0.03999 0.  1. 0.];


% Machine data format
% machine:  1. machine number
%           2. bus number
%           3. base mva
%           4. leakage reactance x_l(pu)
%           5. resistance r_a(pu)
%           6. d-axis sychronous reactance x_d(pu)
%           7. d-axis transient reactance x'_d(pu)
%           8. d-axis subtransient reactance x"_d(pu)
%           9. d-axis open-circuit time constant T'_do(sec)
%          10. d-axis open-circuit subtransient time
%                constant T"_do(sec)
%          11. q-axis sychronous reactance x_q(pu)
%          12. q-axis transient reactance x'_q(pu)
%          13. q-axis subtransient reactance x"_q(pu)
%          14. q-axis open-circuit time constant T'_qo(sec)
%          15. q-axis open circuit subtransient time
%                constant T"_qo(sec)
%          16. inertia constant H(sec)
%          17. damping coefficient d_o(pu)
%          18. damping coefficient d_1(pu)
%          19. bus number
%          20. S(1.0) - saturation factor
%          21. S(1.2) - saturation factor


mac_con = [...
1 1 555.5   0.16 0 1.81   0.300 0.217 7.8  0.022 ...
                  1.76   0.610 0.217 0.9  0.074 ...
                  4.53   0     0     1    0.0      0.0;
2 2 700.0   0.16 0 1.81   0.300 0.217 7.8  0.022 ...
                  1.76   0.610 0.217 0.9  0.074 ...
                  6.53   0     0     2    0.0      0.0];
```

```
%Exciter data format
%Column:   1. Exciter type 0 for simple exciter
%          2. Machine number
%          3. Rc compensation resistance
%          4. Xc compensation reactance
%          5. Transuducer time constant
%          6. Voltage regulator gain Kg
%          7. Voltage regulator time constant Ta
%          8. Tb
%          9. Tc
%         10. Maximum voltage regulator output Vmax
%         11. Minimum voltage regulator output Vmin


exc_con = [...
0     1    0.0     100   0.05   0.0   0.0  6.43   -6 ...
0     0    0      0    0     0     0     0       0     0     0     ;
0     2    0.0     100   0.05   0.0   0.0  6.43   -6 ...
0     0    0       0    0     0     0     0       0     0     0
];


%Turbine Governor
%Column
%  1 turbine model number (=1)
%  2 machine number
%  3 speed set point   wf pu
%  4 steady state gain 1/R pu
%  5 maximum power order  Tmax pu on generator base
%  6 servo time constant   Ts sec
%  7 governor time constant  Tc sec
%  8 transient gain time constant T3 sec
%  9 HP section time constant   T4 sec
% 10 reheater time constant    T5 sec


tg_con = [
      1  1 1 5 25 5 0.01 0.01  0.01 0.01;
];
```

A.2 IEEE 14-bus System

```
bus = [
1 1.0600    0.00   2.353 -0.1689  0.0000  0.0000  0.00  0.00 1 10.0  -10.0;
2 1.0450   -4.98   0.40  -0.4240  0.2170  0.1270  0.00  0.00 2   0.5   -0.4;
3 1.0100  -12.72   0.00   0.2815  0.9420  0.1900  0.00  0.00 2   0.4    0.0;
4 1.0107  -10.32   0.00   0.0000  0.4780  0.0390  0.00  0.00 3   0.0    0.0;
5 1.0200   -8.78   0.00   0.0000  0.0760  0.0160  0.00  0.00 3   0.0    0.0;
6 1.0700  -14.22   0.00   0.2400  0.1120  0.0750  0.00  0.00 2   0.24  -1.06;
7 1.0620  -13.37   0.00   0.0000  0.00    0.00    0.00  0.00 3   0.0    0.0;
8 1.0900  -13.37   0.00   0.24    0.00    0.00    0.00  0.00 2   0.24  -1.06;
9 1.0563  -14.95   0.00   0.0000  0.2950  0.1660  0.00  0.00 3   0.0    0.0;
10 1.0513  -15.10   0.00   0.0000  0.0900  0.0580  0.00  0.00 3   0.0    0.0;
11 1.0571  -14.80   0.00   0.0000  0.0350  0.0180  0.00  0.00 3   0.0    0.0;
12 1.0552  -15.08   0.00   0.0000  0.0610  0.0160  0.00  0.00 3   0.0    0.0;
13 1.0504  -15.16   0.00   0.0000  0.1350  0.0580  0.00  0.00 3   0.0    0.0;
14 1.0385  -16.04   0.00   0.0000  0.1490  0.0500  0.00  0.00 3   0.0    0.0];


line = [
1   2   0.01938     0.05917   0.0528    1.     0.;      %1
1   5   0.05403     0.22304   0.0492    1.     0.;      %2
2   3   0.04699     0.19797   0.0438    1.     0.;      %3
2   4   0.05811     0.17632   0.0374    1.     0.;      %4
2   5   0.05695     0.17388   0.0340    1.     0.;      %5
3   4   0.06701     0.17103   0.0346    1.     0.;      %6
4   5   0.01335     0.04211   0.0128    1.     0.;      %7
4   7   0.0         0.20912   0.0       1      0.;      %8
4   9   0.0         0.55618   0.0       1      0.;      %9
5   6   0.0         0.25202   0.0       1      0.;      %10
6  11   0.09498     0.19890   0.0       1.     0.;      %11
6  12   0.12291     0.25581   0.0       1.     0.;      %12
6  13   0.06615     0.13027   0.0       1.     0.;      %13
7   8   0.0         0.17615   0.0       1.     0.;      %14
7   9   0.0         0.11001   0.0       1.     0.;      %15
9  10   0.03181     0.08450   0.0       1.     0.;      %16
9  14   0.12711     0.27038   0.0       1.     0.;      %17
10  11   0.08205     0.19207   0.0       1.     0.;      %18
12  13   0.22092     0.19988   0.0       1.     0.;      %19
```

```
13  14   0.17093     0.34802   0.0       1.     0.];     %20

mac_con = [ ...
1 1 615 0.1725  0.0    0.8979   0.2995  0.23 7.4  0.03 ...
                       0.746   0.646  0.4  0.25   0.033 ...
                       5.548    0.00    0.0     ;
2 2 75 0.00  0.0031  1.0500  0.1850  0.1300 6.10  0.04...
                       0.980  0.36  0.130 0.3  0.099...
                       6.54     0.0      0.0    ;
3 3 75 0.00  0.0031  1.0500  0.1850  0.1300 6.10  0.04...
                       0.98  0.36  0.130 0.3  0.099 ...
                       6.54  0.0     0.0    ;
4 6 25 0.09  0.0014  1.2500  0.2320  0.1200 4.75  0.06 ...
                       1.2200  0.7150  0.1200 1.50  0.21 ...
                         5.06     0.0       0    ;
5 8 25 0.09  0.0014  1.2500  0.2320  0.1200 4.75  0.06...
                       1.2200  0.7150  0.1200 1.50  0.21...
                         5.06     0.0       0];


exc_con = [...
1  1  0.000  190.0  0.05 0.000 0.00  7.32   -1.000 ...
  1.00  0.1900  0.000  0.0000  0.0000  0.0000  0.001  1.0;
1  2  0.000  20.0   0.05 0.000 0.00  7.32   -1.000 ...
  1.00  1.9800  0.000  0.0000  0.0000  0.0000  0.005  1.0;
1  3  0.000  20.0   0.05 0.000 0.00  7.32   -1.000 ...
  1.00  1.9800  0.000  0.0000  0.0000  0.0000  0.005  1.0;
1  4  0.000  20.0   0.05 0.000 0.00  7.32   -1.    ...
  1.00  0.7000  0.000  0.0000  0.0000  0.0000  0.005  1.0;
1  5  0.000  20.0   0.05 0.000 0.00  7.32   -1.    ...
  1.00  0.7000  0.000  0.0000  0.0000  0.0000  0.005  1.0];
```

A.3 Two-area Benchmark System

```
bus = [
1  1.03    26.0   6.84   1.31  0.00  0.00  0.00  0.00 1  990.0  -990.0;
2  1.01    17.0   5.00   1.13  0.00  0.00  0.00  0.00 2  5.0  -300.0;
3  1.03    0.045  9.24   0.67  0.00  0.00  0.00  0.00 2  5.0  -300.0;
```

```
4  1.01    -1.97  7.00   0.43  0.00  0.00  0.00  0.00 2  5.0  -300.0;
5  1.01     20.   0.00   0.00  0.00  0.00  0.00  0.00 3  0.0   0.0;
6  0.98     10.8  0.00   0.00  0.00  0.00  0.00  0.00 3  0.0   0.0;
7  0.97     4.79  0.00   0.00  9.67  1.00  0.00  2.00 3  0.0   0.0;
8  0.9503   0.49  0.00   0.00  0.00  0.00  0.00  0.00 3  0.0   0.0;
9  0.97    -13.14 0.00   0.00 17.67  1.00  0.00  3.50 3  0.0   0.0;
10 0.9862  -8.54  0.00   0.00  0.00  0.00  0.00  0.00 3  0.0   0.0;
11 1.01    -6.52  0.00   0.00  0.00  0.00  0.00  0.00 3  0.0   0.0];

line = [...
1    5  0.0     0.0167   0.00    1.0  0.;
2    6  0.0     0.0167   0.00    1.0  0.;
3   11  0.0     0.0167   0.0     1.0  0.;
4   10  0.0     0.0167   0.0     1.0  0.;
5    6  0.0025  0.025    0.04375 1.0  0.;
6    7  0.001   0.0100   0.0175  1.0  0.;
6    7  0.002   0.0200   0.0170  1.0  0.;
10   9  0.00125 0.0100   0.0175  1.0  0.;
9   10  0.005   0.0125   0.0035  1.0  0.;
7    8  0.0075  0.005    0.12833 1.0  0.;
7    8  0.0075  0.075    0.12833 1.0  0.;
7    8  0.0075  0.075    0.12833 1.0  0.;
7    8  0.0075  0.075    0.12833 1.0  0.;
8    9  0.018   0.180    0.1925  1.0  0.;
8    9  0.018   0.180    0.1925  1.0  0.;
8    9  0.018   0.180    0.1900  1.0  0.;
11  10  0.0025  0.005    0.0140  1.0  0.
];

mac_con = [...
1 1 900 0.200  0.0025  1.8  0.30  0.25 8.00  0.03...
                       1.7  0.55  0.25 0.4   0.05...
  6.5  0  0  1;
2 2 900 0.200  0.0025  1.8  0.30  0.25 8.00  0.03...
                       1.7  0.55  0.25 0.4   0.05...
  6.5  0  0  2;
3 3 900 0.200  0.0025  1.8  0.30  0.25 8.00  0.03...
                       1.7  0.55  0.25 0.4   0.05...
 5.175 0  0   3;
4 4 900 0.200  0.0025  1.8  0.30  0.25 8.00  0.03...
```

```
                    1.7  0.55  0.25 0.4   0.05...
 6.175 0  0   4];

exc_con = [...
0     1    0.0     100   0.02   0.0   0.0  7   -7 ...
0     0     0     0   0     0     0      0       0     0     0     ;
0     2    0.0     100   0.02   0.0   0.0  7   -7 ...
0     0     0     0   0     0     0      0       0     0     0     ;
0     3    0.0      75   0.02   0.0   0.0  7   -7 ...
0     0     0     0   0     0     0      0       0     0     0     ;
0     4    0.0      50   0.02   0.0   0.0  7   -7 ...
0     0     0     0   0     0     0      0       0     0     0     ;
];

tg_con = [
      1  1 1 5 25 5 0.01 0.01  0.01 0.01;
];

%Power System Stabilizer (PSS)
%Column
%1 type
%1 speed input
%2 power input
%2 machine number
%3 gain K
%4 washout time constant T sec
%5 lead time constant T1 sec
%6 lag time constant T2 sec
%7 lead time constant T3 sec
%8 lag time constant T4 sec
%9 maximum output limit pu
%10 minimum output limit pu

pss_con = [...
1 1 6.0  2.0  0.08   0.04  0.08   0.04  10 -10;
1 2 6.0  2.0  0.08   0.04  0.08   0.04  10 -10;
1 3 6.0  2.0  0.08   0.04  0.08   0.04  10 -10;
1 4 6.0  2.0  0.08   0.04  0.08   0.04  10 -10
];
```

Appendix B

SISI Proof

From equation (4.4), the singular values of the matrix Λ_m are defined as:

$$sv_i(\Lambda_m) = \sqrt{\mu_i(Q)} \quad \text{for } i = 1,\ 2,\ \cdots,\ 2n \tag{B.1}$$

$$Q = \Lambda_m^*\,\Lambda_m \in \Re^{2n\times 2n} \tag{B.2}$$

where $\mu_i(Q)$ denotes the i^{th} eigenvalue of Q, and Λ_m^* is the transpose conjugate of Λ_m. Thus,

$$Q = \Lambda_m^*\,\Lambda_m = \begin{bmatrix} \Lambda^*\Lambda + \beta_c^2 I & \beta_c(\Lambda - \Lambda^*) \\ \beta_c(\Lambda^* - \Lambda) & \Lambda^*\Lambda + \beta_c^2 I \end{bmatrix} \tag{B.3}$$

Then, these submatrices can be expressed in terms of the eigenvalues in Λ ($\lambda_i = \alpha_i \pm j\beta_i$) as:

$$\Lambda^*\Lambda + \beta_c I = diag\{|\lambda_1|^2 + \beta_c^2,\ |\lambda_2|^2 + \beta_c^2,\ \cdots, |\lambda_n|^2 + \beta_c^2\} \in \Re^{n\times n} \tag{B.4}$$

$$\beta_c(\Lambda - \Lambda^*) = (2j\ \beta_c)\ diag\{\beta_1,\ \beta_2,\ \cdots, \beta_n\} \in \Re^{n\times n} \tag{B.5}$$

Thus, the characteristic equation of Q can be obtained as:

$$\Delta(s) = det(sI - Q) = [(s - |\lambda_1|^2 - \beta_c^2)^2 - (2\beta_1\beta_c)^2]\,[(s - |\lambda_2|^2 - \beta_c^2)^2 - (2\beta_2\beta_c)^2] \cdots [(s - |\lambda_n|^n - \beta_c^2)^2 - (2\beta_n\beta_c)^2] \tag{B.6}$$

The roots of the characteristic equation are the eigenvalues of Q, which can be written as

$$\mu_i(Q) = \alpha_i^2 + (\beta_c \pm \beta_i)^2 \tag{B.7}$$

Thus, (B.7) and (B.1) yields (4.5). $\diamond$

Appendix C

Alternative Damping Torque Formulation

In order to calculate D_j in (5.5), it is possible to separate the states as $\Delta x = [\Delta\omega_j \ \Delta x_d]^T$, and hence rewrite the linearized state-space model as follows:

$$\Delta\dot{x}_d = A_x \ \Delta x_d + B_\omega \ \Delta\omega_j \tag{C.1}$$

$$\Delta\dot{\omega}_j = A_\omega \ \Delta\omega_j + B_x \ \Delta x_d \tag{C.2}$$

$$\Delta T_{e_j} = C_d \ \Delta x_d + C_{\omega_j} \ \Delta\omega_j \tag{C.3}$$

Replacing d/dt by s in (C.1) would yield $\Delta x_d = (sI - A_x)^{-1} B_\omega \Delta\omega_j$. Thus:

$$D_j(s) = \frac{\Delta T_{e_j}}{\Delta\omega_j} = \left(C_d \ (s \ I - A_x)^{-1} \ B_\omega \ + \ C_{\omega_j}\right) \tag{C.4}$$

Evaluating $D_j(s = \lambda_i)$ would give the same results as (5.5). In [6], the author proposes a method to obtain transfer functions similar to (C.4) by disabling the shaft dynamics in all machines, resulting in various transfer functions. These functions are used to show the inherent damping and interaction between different machines.

However, the procedure shown here is equivalent to disabling only the shaft dynamics for machine j; this means that (C.4) includes the induced damping and synchronizing torques of all machines on the shaft of Machine j.

Bibliography

[1] E. Uzunovic, "Transient Stability and Power Flow Models of VSC FACTS controllers," Ph.D. dissertation, University of Waterloo, Waterloo, ON, Canada, 2001.

[2] "Interim Report: Causes of the August 14th Blackout in the United States and Canada," Tech. Rep., November 2003, available at http://www.nrcan-rncan.gc.ca/media/docs/814BlackoutReport.pdf.

[3] "Report on the events of September 28th, 2003 culminating in the separation of the Italian power system from the other UCTE networks," Tech. Rep., April 2004, available at http://www.autorita.energia.it/docs/04/061-04all.pdf.

[4] "The black-out in southern Sweden and eastern Denmark, 23 September, 2003," Tech. Rep., October 2003, available at http://www.svk.se/upload/3195/Disturbance_Sweden_DenmarkSept23.pdf.

[5] "System Disturbance Stability Studies for Western System Coordinating Council (WSCC)," EPRI Final Report prepared by Powertech Labs Inc., Surrey, BC, Canada, Tech. Rep. TR-108256, September 1997.

[6] M. J. Gibbard, "Co-ordinated design of multimachine power system stabilisers based on damping torque concepts," *IEE Proceedings, Pt. C*, vol. 135, no. 4, pp. 276–284, July 1988.

[7] C. A. Cañizares, editor, "Voltage Stability Assessment: Concepts, Practices and Tools," Special Publication of IEEE Power System Stability Subcommittee, Tech. Rep. SP101PSS, August 2002.

[8] N. Mithulananthan, "Hopf bifurcation control and indices for power system with interacting generator and FACTS controllers," Ph.D. dissertation, University of Waterloo, Waterloo, ON, Canada, 2002.

[9] C. A. Cañizares, N. Mithulananthan, A. Berizzi, and J. Reeve, "On the linear profile of indices for the prediction of saddle-node and limit-induced bifurcation points in power systems," *IEEE Trans. Circuits and Systems*, vol. 50, no. 2, pp. 1588–1595, December 2003.

[10] C. A. Canizares, A. C. Z. de Souza, and V. Quintana, "Comparison of performance indices for detection of proximity to voltage collapse," *IEEE Trans. Power Systems*, vol. 11, no. 3, pp. 1441–1450, August 1996.

[11] V. Ajjarapu and B. Lee, "Bifurcation theory and its application to nonlinear dynamical phenomena in an electrical power system," *IEEE Trans. Power Systems*, vol. 7, no. 1, pp. 424–431, 1992.

[12] W. Zhu, R. Mohler, R. Spee, W. A. Mittelstadt, and D. Maratukulam, "Hopf bifurcation in a SMIB power system with SSR," *IEEE Trans. Power Systems*, vol. 11, no. 7, pp. 1579–1584, 1996.

[13] C. A. Cañizares, N. Mithulananthan, F. Milano, and J. Reeve, "Linear performance indices to predict oscillatory stability problems in power systems," *IEEE Trans. Power Systems*, vol. 19, no. 2, pp. 1104–1114, May 2004.

[14] T. Kim and E. H. Abed, "Closed-loop monitoring system for detecting impending instability," *IEEE Trans. Circuits and Systems*, vol. 47, no. 10, pp. 1479–1493, October 2000.

[15] N. Mithulananthan, C. A. Cañizares, J. Reeve, and G. J. Rogers, "Comparison of PSS, SVC and STATCOM controllers for damping power system oscillations," *IEEE Trans. Power Systems*, vol. 18, no. 2, pp. 786–792, May 2003.

[16] "Power Dynamics Management (PDM)," Psymetrix Limited, Scotland, UK, Tech. Rep., available at www.psymetrix.com.

[17] D. H. Wilson, "Managing oscillatory stability using on-line dynamics measurements," in *Power System Conference & Exposition*, New York, October 2004.

[18] I. Fernando, L. Chung, L. Midford, A. Silk, R. Coish, A. Golder, K. Hay, and D. Wilson, "Real time online evaluation of small signal system damping applied to power system stabilizer commissioning and testing," in *International Conference on Power Systems Transients - IPST*, New Orleans, 2003.

[19] J. F. Hauer, "The use of Prony analysis to determine modal content and equivalent models for measured power system response," in *IEEE/PES Symposium on Application of Eigenanalysis and Frequency Domain Methods for System Dynamic Performance*, July 1989, pp. 105–115.

[20] J. R. Smith, F. Fatehi, C. S. Woods, J. F. Hauer, and D. J. Trudnowski, "Transfer function identification in power system applications," *IEEE Trans. Power Systems*, vol. 8, no. 3, pp. 1282–1290, August 1993.

[21] J. F. Hauer, "Application of Prony analysis to the determination of modal content and equivalent models for measured power system response," *IEEE Trans. Power Systems*, vol. 6, no. 3, pp. 1062–1068, August 1991.

[22] B. J. Bujanowski, J. W. Pierre, S. M. Hietpas, T. L. Sharp, and D. A. Pierre, "A comparison of several system identification methods with application to power systems," in *IEEE Proceedings of the 36th Midwest Symposium on Circuits and Systems*, vol. 1, August 1993, pp. 64–67.

[23] R. W. Wies, J. W. Pierre, and D. J. Trudnowski, "Use of ARMA block processing for estimating stationary low-frequency electromechanical modes of power systems," *IEEE Trans. Power Systems*, vol. 18, no. 1, pp. 167–173, 2003.

[24] J. W. Peirre, D. J. Trudnowski, and M. Donnelly, "Initial results in electromechanical mode identification from ambient data," *IEEE Trans. Power Systems*, vol. 12, no. 3, pp. 1245–1251, August 1997.

[25] M. K. Pal, "Voltage stability conditions considering load characteristics," *IEEE Trans. Power Systems*, vol. 7, pp. 243–247, February 1992.

[26] W. S. Kao, "The effect of load models on unstable low-frequency oscillation damping in taipower system experience w/wo power system stabilizers," *IEEE Trans. Power Systems*, vol. 16, pp. 463–472, August 2001.

[27] C. A. Canizares, "On bifurcations, voltage collapse and load modeling," *IEEE Trans. Power Systems*, vol. 10, pp. 512–522, February 1995.

[28] M. H. J. Bollen, G. Yalcinkaya, and G. Hazza, "The use of electromagnetic transient program for voltage sag analysis," in *Proc. 8th International Conference on Harmonics And Quality of Power*, vol. 1, October 1998, pp. 598–603.

[29] G. Rogers, *Power Sysem Oscillations*. Boston/London/Dordrecht: Kluwer Academic Publishers, 2000.

[30] M. Klein, G. J. Rogers, and P. Kundur, "A fundamental study of inter-area oscillation in power systems," *IEEE Trans. Power Systems*, vol. 6, no. 3, pp. 914–921, 1991.

[31] N. Mithulananthan, C. A. Cañizares, and J. Reeve, "Hopf bifurcation control in power system using power system stabilizers and static var compensators," in *Proc. of NAPS'99*, San Luis Obispo, California, October 1999, pp. 155–163.

[32] Y. Ni and L. Snider, "STATCOM power frequency model with VSC charging dynamics and its application in power system stability analysis," in *Proceedings of APSCOM'97*, Hong Kong, November 1997, pp. 119–125.

[33] P. Kundur, *Power System Stability and Control*. New York: McGraw-Hill, 1994.

[34] F. Milano, *Power System Analysis Toolbox (PSAT), Version 1.3.4, User Manual*, 2005, available at http://www.power.uwaterloo.ca/∼fmilano.

[35] F. P. Demello and C. Concordia, "Concepts of synchronous machine stability as affected by excitation control," *IEEE Trans. Power Apparatus and Systems*, vol. PAS-88, no. 4, pp. 316 – 329, April 1969.

[36] *Power System Toolbox (PST) Version 2.0: Dynamics Tutorial and Functions*, Cherry Tree Scientific Software, 2002.

[37] G. Hingrani, *Understanding FACTS*. New York: IEEE Press, 2000.

[38] A. E. Hammad, "Comparing the voltage control capabilities of present and future var compensating techniques in transmission systems," *IEEE Trans. Power Delivery*, vol. 11, no. 1, pp. 475–484, January 1996.

[39] E. Larsen, S. Nilsson, N. Miller, and S. Lindgren, "Benefits of gto-based compensation systems for electric utility applications," *IEEE Trans. Power Delivery*, vol. 7, no. 4, pp. 2056–2062, October 1992.

[40] C. A. Cañizares, M. Pozzi, and E. Uzunovic, "STATCOM modeling for voltage and angle stability studies," *International Journal of Electrical Power & Energy Systems*, vol. 25, no. 6, pp. 431–441, June 2003.

[41] V. Venkatasubramanian, H. Schattler, and J. Zaborsky, "Dynamics of large constrained nonlinear systems-a taxonomy theory [power system stability]," in *Proceedings of the IEEE*, vol. 83, no. 11, November 1995, pp. 1530–1561.

[42] N. Mithulananthan and S. C. Sirvastava, "Investigation of a voltage collapse incident in Sri Lanka's power system network," in *EMPD'98*, Singapore, March 1998, pp. 47–52.

[43] C. A. Caizares and F. L. Alvarado, "Point of collapse and continuation methods for large ac/dc systems," *IEEE Trans. Power Systems*, vol. 8, no. 1, pp. 1–8, February 1993.

[44] *Transient Security Assessment Tool (TSAT), User Manual*, Powertech Labs Inc., Surrey, BC, Canada, V3W 7R7, 2002.

[45] *System Identification Toolbox Version 5.0.1*. www.Mathworks.com, 18-May-2001.

[46] S. K. M. Kodsi and C. A. Cañizares, "Modeling and simulation of IEEE 14-bus system with FACTS controllers," University of Waterloo, Canada, Tech. Rep., March 2003, available at www.power.uwaterloo.ca.

[47] *Power Flow and Short-circuit Analysis Tool (PSAT), Version 5.1, User Manual*, Powertech Labs Inc., Surrey, BC, Canada, V3W 7R7, 2002.

[48] *Voltage Security Assessment Tool (VSAT), Version 5.2, User Manual*, Powertech Labs Inc., Surrey, BC, Canada, V3W 7R7, 2002.

[49] *Small Signal Analysis Tool (SSAT), User Manual*, Powertech Labs Inc., Surrey, BC, Canada, V3W 7R7, 2002.

[50] S. L. Marple, *Digital Spectral Analysis*. Englewood Cliffs, N.J.: Prentice Hall, 1987.

[51] Y. Hua and T. K. Sarkar, "Generalized pencil-of-function method for extracting poles of an EM system from its transient response," *IEEE Trans. Antenna and Propagation*, vol. 37, no. 2, pp. 229–234, February 1989.

[52] J. F. Hauer, C. J. Demeure, and L. L. Scharf, "Initial results in Prony analysis of power system response signals," *IEEE Trans. Power Systems*, vol. 5, no. 1, pp. 80–89, February 1990.

[53] D. J. Trudnowski, J. M. Johnson, and J. F. Hauer, "Making Prony analysis more accurate using multiple signals," *IEEE Trans. Power Systems*, vol. 14, no. 1, pp. 226–231, February 1998.

[54] D. J. Trudnowski, J. R. Smith, T. A. Short, and D. A. Pierre, "An application of Prony methods in PSS design for multimachine systems," *IEEE Trans. Power Systems*, vol. 6, no. 1, pp. 118–126, February 1991.

[55] D. W. Tufts and R. Kumaresan, "Singular value decompsition and improved frequency estimation using linear prediction," *IEEE Trans. Acoustics, Speech, and Signal Processing*, vol. ASSP-30, no. 4, pp. 671–675, August 1982.

[56] S. M. Kay, *Modern Spectral Estimation: Theory and Application*. Englewood Cliffs, N.J.: Prentice Hall, 1988.

[57] M. L. VanBlaricum and R. Mittra, "Problems and solutions associated with prony's method for processing transient data," *IEEE Trans. Antennas and Propagation*, vol. AP-26, no. 1, pp. 174–182, January 1978.

[58] L. Ljung, *System Identification: Theory for the User*, 2nd ed. Englewood Cliffs, N.J.: Prentice-Hall, 1999.

[59] R. Söderström, *System Identification*. Cambridge, UK: Prentice Hall International (UK) Ltd., 1989.

[60] B. Friedlander, "Instrumental variable methods for ARMA spectral estimation," *IEEE Trans. Acoustics, Speech, and Signal Processing*, vol. ASSP-31, no. 2, pp. 404–415, April 1983.

[61] P. V. Overshee and B. D. Moor, *Subspace Identification for Linear Systems: Theory-Implementation-Applications*. Kluwer Academic Publishers, 1996.

[62] D. Bauer, "Subspace Algorithms," 2003, seminar notes, available at http://cowles.econ.yale.edu/seminars/ecm03/bauer-031022.pdf.

[63] B. Dietmar, "Asymptotic efficiency of CCA subspace methods in the case of no exogenous inputs," Department of Electrical and Computer Engineering, Linkoping University, SE-581 83, Linkoping, Sweden, Tech. Rep. LiTH-ISY-R-2262, 2000.

[64] R. T. H. Alden and A. A. Shaltout, "Analysis of damping and synchronous torques: Part I - A general calculation method," *IEEE Trans. Power Systems*, vol. PAS-98, no. 5, pp. 1696–1700, Sept/Oct 1979.

[65] A. A. Shaltout and B. A. Abu Al-Feilat, "Damping and synchronous torque computation in multimachine power systems," *IEEE Trans. Power Systems*, vol. 7, no. 1, pp. 280–286, February 1992.

[66] P. Pourbeik and M. J. Gibbard, "Damping and synchronizing torques induced on generators by facts stabilizers in multimachine power systems," *IEEE Trans. Power Systems*, vol. 11, no. 4, pp. 1920–1925, November 1996.

[67] T. C. Hsia, *System Identification: Least-Square Methods.* Lexington, MA: Lexington Books, D.C. Health and Company, 1977.

[68] *Statistic Toolbox 1.1 in MATLAB*, The Mathworks, 2000.

[69] A. Pankratz, *Forecasting with Univariate Box-Jenkins Models: Concepts and Cases*, 1st ed. New York: Wiley, 1983.

[70] P. Andersen, "Identification of civil engineering structures using vector ARMA models," Ph.D. dissertation, Aalborg University, Aalborg, Denmark, 1997.

[71] L. Ljung, *System Identification Theory for the User.* Englewood Cliffs, N.J.: Prentice Hall, 1999.

[72] *On the Use of Power System Computer Aided Design (PSCAD) Version 4.0.3, User's Guide*, Manitoba HVDC Research Centre, 244 Cree Crescent, Winnipeg, Manitoba, Canada R3J 3W1, 2003.

[73] T. J. Hammons et al., "Effect of damper modelling and the fault clearing process on response torque and stressing of turbine generator rotors," *IEEE Trans. Energy Conversion*, vol. EC-1, no. 9, p. 113, 1986.

[74] T. Kumano et al., "Effect of back swing phenomena upon transient stability," *Trans. IEE of Japan*, vol. 109-B, no. 9, p. 403, 1989.

[75] I. D. Landau, *System Identification and Control Design.* Englewood Cliffs, N.J.: Prentice Hall, 1990.

[76] *Small Signal Stability Program (SSSP) Version 3.1, User's Manual*, Ontario Hydro, 1994.

[77] N. Mohan, T. M. Undeland, and W. P. Robbins, *Power Electronics : Converters, Applications, and Design*, 2nd ed. NJ: Wiley, 1994.

[78] H. Ghasemi, C. A. Cañizares, and A. Moshred, "Oscillatory stability limit prediction using stochastic subspace identification," *IEEE Trans. Power Systems*, vol. 21, no. 2, pp. 736–745, May 2006.

[79] H. Ghasemi, C. A. Cañizares, and J. Reeve, "Prediction of instability points using system identification," in *Proc. Bulk Power System Dynamics and Control - VI*, Cortina D′Ampezzo, Italy, August 2004, 6 pages.

[80] H. Ghasemi and C. A. Cañizares, "Damping torque estimation and oscillatory stability margin prediction," accepted to *IEEE Power Engineering Summer Meeting*, Montreal, Canada, June 2006, 6 pages.